NASA/TM–20220000562
NESC-RP-20-01576

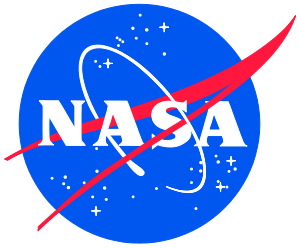

Review of the MeMoSeE Lunar Meteoroid Ejecta Model

Joseph Minow/NESC
Langley Research Center, Hampton, Virginia

Mark Matney
Johnson Space Center, Houston, Texas

Michael Bjorkman
Jacobs Technology, Inc., Houston, Texas

Jordan Kendall
University of Maryland, Baltimore County, Maryland

Althea Moorhead
Marshall Space Flight Center, Huntsville, Alabama

Menelaos Sarantos
Goddard Space Flight Center, Greenbelt, Maryland

Emerson Speyerer
Arizona State University, Tempe, Arizona

Michael Squire
Langley Research Center, Hampton, Virginia

Jamey Szalay
Princeton University, Princeton, New Jersey

January 2022

NASA STI Program Report Series

Since its founding, NASA has been dedicated to the advancement of aeronautics and space science. The NASA scientific and technical information (STI) program plays a key part in helping NASA maintain this important role.

The NASA STI program operates under the auspices of the Agency Chief Information Officer. It collects, organizes, provides for archiving, and disseminates NASA's STI. The NASA STI program provides access to the NTRS Registered and its public interface, the NASA Technical Reports Server, thus providing one of the largest collections of aeronautical and space science STI in the world. Results are published in both non-NASA channels and by NASA in the NASA STI Report Series, which includes the following report types:

- TECHNICAL PUBLICATION. Reports of completed research or a major significant phase of research that present the results of NASA Programs and include extensive data or theoretical analysis. Includes compilations of significant scientific and technical data and information deemed to be of continuing reference value. NASA counterpart of peer-reviewed formal professional papers but has less stringent limitations on manuscript length and extent of graphic presentations.

- TECHNICAL MEMORANDUM. Scientific and technical findings that are preliminary or of specialized interest, e.g., quick release reports, working papers, and bibliographies that contain minimal annotation. Does not contain extensive analysis.

- CONTRACTOR REPORT. Scientific and technical findings by NASA-sponsored contractors and grantees.

- CONFERENCE PUBLICATION. Collected papers from scientific and technical conferences, symposia, seminars, or other meetings sponsored or co-sponsored by NASA.

- SPECIAL PUBLICATION. Scientific, technical, or historical information from NASA programs, projects, and missions, often concerned with subjects having substantial public interest.

- TECHNICAL TRANSLATION. English-language translations of foreign scientific and technical material pertinent to NASA's mission.

Specialized services also include organizing and publishing research results, distributing specialized research announcements and feeds, providing information desk and personal search support, and enabling data exchange services.

For more information about the NASA STI program, see the following:

- Access the NASA STI program home page at http://www.sti.nasa.gov

- Help desk contact information:

https://www.sti.nasa.gov/sti-contact-form/
and select the "General" help request type.

NASA/TM–20220000562
NESC-RP-20-01576

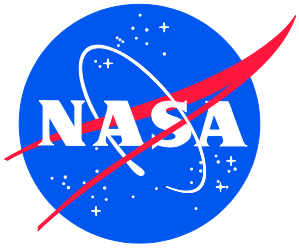

Review of the MeMoSeE Lunar Meteoroid Ejecta Model

Joseph Minow/NESC
Langley Research Center, Hampton, Virginia

Mark Matney
Johnson Space Center, Houston, Texas

Michael Bjorkman
Jacobs Technology, Inc., Houston, Texas

Jordan Kendall
University of Maryland, Baltimore County, Maryland

Althea Moorhead
Marshall Space Flight Center, Huntsville, Alabama

Menelaos Sarantos
Goddard Space Flight Center, Greenbelt, Maryland

Emerson Speyerer
Arizona State University, Tempe, Arizona

Michael Squire
Langley Research Center, Hampton, Virginia

Jamey Szalay
Princeton University, Princeton, New Jersey

National Aeronautics and
Space Administration

Langley Research Center
Hampton, Virginia 23681-2199

January 2022

Acknowledgments

The assessment team thanks Sam Lawrence, Diego Janches, Eric Christiansen, William Cooke, Dan Dorney, Steve Gentz, and Mark Terrone for their time and expertise in providing a peer review of this work.

Available from:

NASA STI Program / Mail Stop 148
NASA Langley Research Center
Hampton, VA 23681-2199
Fax: 757-864-6500

NASA Engineering and Safety Center
Technical Assessment Report

Review of the MeMoSeE Lunar Meteoroid Ejecta Model Review

NESC-TI-20-01576

NESC Lead, Joseph Minow

Technical Lead, Mark Matney

December 14, 2021

Report Approval and Revision History

NOTE: This document was approved at the December 14, 2021, NRB. This document was submitted to the NESC Director on December 17, 2021, for configuration control.

Approved:	*Original signature on file.*	
	NESC Director	Date

Version	Description of Revision	Office of Primary Responsibility	Effective Date
1.0	Initial Release	Joe Minow, NASA Technical Fellow for Space Environments, MSFC	12/14/2021

Table of Contents

Technical Assessment Report

List of Figures

List of Tables

1.0 Notification and Authorization

Dr. Robert Suggs, Human Landing System (HLS) Natural Environments Discipline Lead, requested the NASA Engineering and Safety Center (NESC) perform an independent review of a new lunar meteoroid ejecta model developed by the Natural Environments Branch at Marshall Space Flight Center (MSFC). MSFC has proposed to use the new model to replace the Apollo-era lunar ejecta environments in the SLS-SPEC-159 Cross-Program Design Specification for Natural Environments (DSNE) document [ref. 1] that specifies engineering design environments for NASA's Exploration Systems Development (ESD) and Artemis Programs. The NESC assessment team reviewed the physical basis of the new lunar ejecta model, identified issues with the model, and provided recommendations for improvements before the model results are incorporated into a DSNE update.

2.0 Signature Page

Submitted by: NESC Lead

Original signatures on file.

Dr. Joseph Minow

Significant Contributors:

Dr. Mark Matney	Dr. Michael Bjorkman
Dr. Jordan Kendall	Dr. Althea Moorhead
Dr. Menelaos Sarantos	Dr. Emerson Speyerer
Mr. Michael Squire	Dr. Jamey Szalay

Signatories declare the findings, observations, and NESC recommendations compiled in the report are factually based from data extracted from program/project documents, contractor reports, and open literature, and/or generated from independently conducted tests, analyses, and inspections.

3.0 Team Members

Name	Discipline	Organization
Core Team		
Joseph Minow	NESC Lead, Space Environments Subject Matter Expert (SME)	LaRC
Mark Matney	Technical Lead, Meteoroids and Orbital Debris SME	JSC
Michael Bjorkman	Meteoroid and Orbital Debris Impact Risk SME	JSC/Jacobs
Jordan Kendall	Impact and Cratering SME	GSFC/University of Maryland-Baltimore County
Althea Moorhead	Meteoroid Environment SME	MSFC
Menelaos Sarantos	Meteoroid and Dust Environment SME	GSFC
Emerson Speyerer	Impact and Cratering SME	Arizona State University
Michael Squire	Hypervelocity Impact SME	LaRC
Jamey Szalay	Impact and Cratering SME	Princeton University
Business Management		
Theresa Bardusch	Program Analyst	LaRC/MTSO
Assessment Support		
Missy Strickland	Project Coordinator	LaRC/AMA
Linda Burgess	Planning and Control Analyst	LaRC/AMA
Leanna S. Bullock	Technical Editor	LaRC/AMA

3.1 Acknowledgments

The assessment team thanks Sam Lawrence, Diego Janches, Eric Christiansen, William Cooke, Dan Dorney, Steve Gentz, and Mark Terrone for their time and expertise in providing a peer review of this work.

4.0 Executive Summary

The NASA Engineering and Safety Center (NESC) Lunar Meteoroid Ejecta Model Review assessment team was tasked with reviewing the proposed lunar ejecta model Meteoroid Model of Secondary Ejecta (MeMoSeE), developed at Marshall Space Flight Center (MSFC), and to review the model inputs to the SLS-SPEC-159 Cross-Program Design Specification for Natural Environments (DSNE) document [ref. 1] to be used by NASA's Exploration Systems Development (ESD) and Artemis Programs for future lunar surface system design. The proposed model is intended to update the Apollo-era model contained in the DSNE in order to provide a better understanding of the impact risk to lunar surface operations.

The NESC assessment team looked at several aspects of the model, focusing on questions related to the physical basis of the model. These questions included:

> Were the direction, velocity, and distributions in time, geography, and size/mass assumed for the primary impactors modeled appropriately?
>
> Were the direction, velocity, and distributions size/mass/density of the ejecta from the cratering phenomena modeled appropriately?
>
> Did the debris transport equations from cratering events adequately compute the flux on an asset some distance away?
>
> Were the DSNE inputs adequate to compute the risks to vehicles, habitats, and other objects on the lunar surface?

Overall, the MeMoSeE model was found to incorporate the appropriate phenomenology for a DSNE inputs environment, but with a number of critical caveats. The review identifies a number of specific sensitivity studies to compare how various sets of assumptions, mostly concerning the physics of the ejecta creation, would affect the flux calculations. The review also found an unmodeled portion of the flux from ejecta particles ascending from the surface due to nearby primary impacts close by the asset that roughly match in magnitude the NASA SP-8013 Meteoroid Environment Model – 1969 [Near Earth to Lunar Surface] [ref. 2] flux through a flat sheet lying on the lunar surface. This phenomenon will need to be added to adequately assess the total risk from ejecta.

One important NESC assessment team finding is that the ejecta flux is highly stochastic, and perhaps a "traditional" average flux may not be adequate to capture some of this highly variable behavior. This could have important implications on how the statistics of risks to surface missions on airless planetary bodies are computed.

The NESC assessment team identified key findings and observations and, when appropriate, associated NESC recommendations. The assessment identified many aspects of the MeMoSeE model that are technically correct. However, there are a number of technical aspects of this model that either do not reproduce satellite measurements of lunar ejecta and surface changes due to impacts or could be improved.

In addition, the NESC assessment team used a Monte Carlo test of the MeMoSeE flux algorithms to determine an ascending flux generated by primary impacts close to a target could be important but are not considered in the model. The team found the model as developed is focused on mean environments while rare, large impacts could be important drivers to design of

lunar surface systems. Finally, a number of issues with the software implementation of the MeMoSeE model were identified and documented in a series of findings.

While the MeMoSeE is the appropriate type of model to use in computing the ejecta risk and computing the tables used in the DSNE update, there are significant findings in this report that need to be addressed before the model is ready for use. Detailed results from the completed set of 36 Findings, 9 Observations, and 24 NESC Recommendations are described in the text of the report.

5.0 Introduction and Assessment Plan

The lunar meteoroid ejecta environment is a potential threat to spacecraft and crew operating on and near the lunar surface. The lunar ejecta model used for engineering design by NASA's Artemis Program including the HLS and Exploration Extravehicular Mobility Unit (xEMU) System dates to 1969. The SLS-SPEC-159 Cross-Program DSNE document applicable for engineering design of all elements of the Artemis Program specifies the Apollo-era lunar meteoroid ejecta model. MSFC's Natural Environments Branch developed a new lunar meteoroid ejecta model based on improvements since the Apollo days in the knowledge of the primary meteoroid flux at the Moon and impact processes responsible for generating the ejecta environment. MSFC is proposing the new model, named the "Meteoroid Model of Secondary Ejecta" and abbreviated as MeMoSeE (pronounced "mimosa"), to replace the 1969 ejecta model in an upcoming DSNE revision scheduled for release in late 2021. MeMoSeE was developed by Dr. Anthony DeStefano of MSFC, hereafter referred to as the "developer." HLS, as one of the lunar surface systems primarily impacted by the ejecta environment, requested an independent NESC assessment to review the new lunar ejecta model and proposed update to the DSNE.

The NESC established an assessment team with expertise on lunar impacts and cratering, hypervelocity impacts, and space environmental effects to review the physical basis of the proposed MeMoSeE model and the model inputs to the DSNE document to be used by NASA's ESD and Artemis Programs for future lunar surface system design. The model is intended to update the Apollo-era model contained in the DSNE providing a better understanding of the impact risk to lunar surface operations.

The NESC assessment team looked at several aspects of the model, focusing on the physical basis of the model. This review summarizes the physical basis of the MeMoSeE model, its applicability to NASA lunar programs, and provides NESC recommendations to improve the model.

6.0 Problem Description

6.1 Prior Work

Prior work on the lunar ejecta environment can be divided into two groups. The first consists of engineering environments for evaluating the spacecraft impact risk. The second is the vastly larger literature considering the ejecta environment as an important geologic process modifying the lunar surface, and as a mechanism for lofting dust from the surfaces of airless bodies into solar orbit. The Lunar Source Book [ref. 3] is an entrance to the literature on impact as a geologic process and Szalay et al, 2018 [ref. 4] to the literature on lofting dust.

Lunar ejecta engineering models begin with a BELLCOMM study performed for the Apollo Program during 1963. Orrok [ref. 5] concluded in the BELLCOMM study that crater ejecta could no more than double the threat of puncture by meteoroids. He argued that the meteoroid could transfer no more than 100% of its kinetic energy to the lunar ejecta. Because the spacecraft skin thickness that will stop an ejecta particle is proportional to the kinetic energy of the ejecta particle, Orrok thought that the penetration rate at the surface of the Moon would at most be double the penetration rate in lunar orbit. This result was widely circulated at the time as evidenced by the following quote from a NASA history of Apollo.

> *"NASA issued a technical note reporting that scientists at Ames Research Center (ARC) Hypervelocity Ballistic Range, Moffett Field, Calif., were conducting experiments simulating the impact of micrometeoroids on the lunar surface. The experimenters examined the threat of surface debris, called secondary ejecta, that would be thrown from resultant craters. Data indicated that secondary particles capable of penetrating an astronaut's space suit nearly equaled the number of primary micrometeoroids. Thus, the danger of micrometeoroid impact to astronauts on the moon may be almost double what was previously thought." (Morse and Bays [ref.;6]; see also Miller [ref. 7])*

NASA engineers quickly recognized that an estimate of a factor-of-two larger risk was overly conservative because the average speed of ejecta particles is much less than the average meteoroid speed. The Manned Spacecraft Center[1] EC-1 meteoroid environment technical report [ref. 8] included a lunar ejecta environment that reduced the risk from ejecta to a factor two orders of magnitude smaller than the risk from sporadic meteoroids. The results from Gault's impact tests [ref. 9] indicated that the ejecta flux was three to four orders of magnitude larger than the meteoroid flux. The writers of the EC-1 technical report chose the ejecta flux to be an intermediate value of 6,800 times larger than the incident meteoroid flux. The ratio of ejecta flux to incident flux coupled with the Whipple [ref. 10] sporadic meteoroid flux relation (i.e., $F \propto m^{-1.34}$), an average sporadic meteoroid speed of 30 km/s and an average lunar ejecta particle speed of 200 m/s gave a factor of 100 between the incident penetrating meteoroid flux and the penetrating lunar ejecta flux.

Zook [ref. 11] extended the EC-1 ejecta environment analysis by considering a distribution of ejecta speeds, binned into three ranges of speed: 0 to 100 m/s, 100 to 250 m/s, and 250 m/s to 1 km/s. Figure 6.1-1 is a plot of the flux curves for each of the three speed bins. Like the EC-1 environment technical report, Zook based his analysis on Gault's basalt cratering results. Zook's lunar ejecta environment gives a comparable ratio between the ejecta flux and the incident flux (i.e., ~100). However, Zook based the incident meteoroid flux on the smaller DS-21 REV A (January 1967) environment specification. This environment specification revised the sporadic meteoroid flux down by a factor of 12.

[1] Subsequently becoming the Johnston Space Center (JSC)

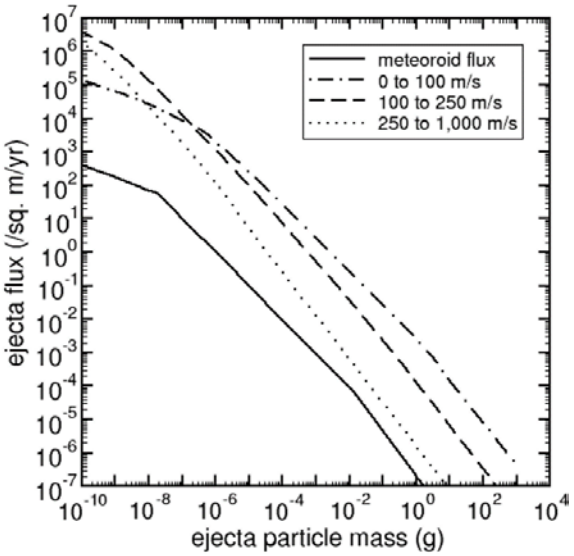

Figure 6.1-1. Zook's Cumulative Ejecta Flux Environment

The NASA SP-8013 [ref. 2] meteoroid environment released in 1969 separated the ejecta flux into three speed bins, similar to Zook, but took the same approach as EC-1 and used a fixed ratio of penetrating sporadic flux to penetrating ejecta flux. NASA SP-8013 contains a model of the flux of ejecta particles for particles with speeds from 0 to 100 m/s, 100 to 250 m/s, and 250 m/s to 1 km/s. NASA SP-8013 specifies a 100-m/s average ejecta speed for preliminary risk assessments, but detailed risk assessments should be based on the distributed velocity model. Figure 6.1-2 is a plot of the NASA SP-8013 ejecta fluxes. NASA SP-8013 does not specify the upper size limit of ejecta particles, but plots the flux for masses up to 100 g.

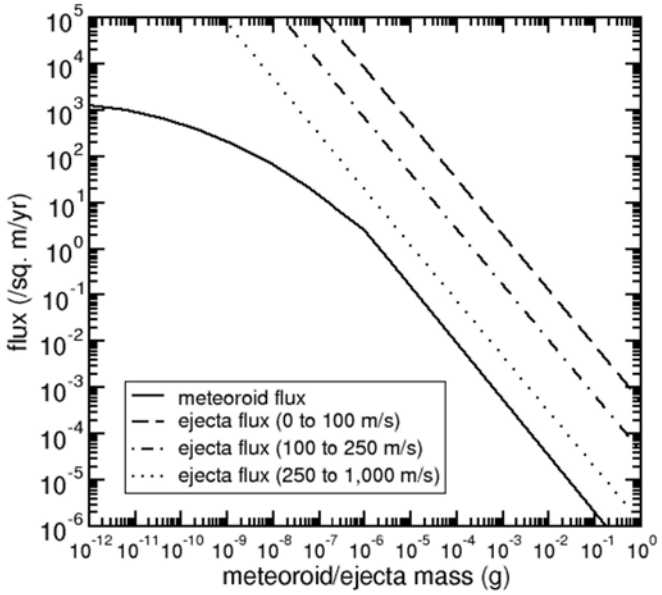

Figure 6.1-2. NASA SP-8013 Cumulative Ejecta Flux Environment

The NASA SP-8013 is the last released lunar ejecta environment for design and is the environment specified in the DSNE.

The four engineering environment models described have trended towards smaller and smaller impact risk as the modelers reduced conservatism. MeMoSeE continues this trend, but the lunar ejecta impact risk is not ignorable for all spacecraft components as described in Section 10.5.2.

6.2 Summary of MeMoSeE Model

MeMoSeE combines models of impacting particles from meteoroids, asteroids, or comets with cratering relations and regolith properties to generate a description of lunar ejecta particles.

6.2.1 Input Models

MeMoSeE relies on two separate models of incoming particles to compute the impact rate. These models are the Meteoroid Engineering Model, version 3 (MEM 3) [refs. 12, 13] and a simple near-Earth object (NEO) model [refs. 14, 15]

MEM is a mature model that has been in use since 2004 to compute the flux of hazardous meteoroids for spacecraft risk assessments. It contains a physics-based, dynamical model of the meteoroid complex [refs. 16, 17] that has been recently updated to include meteoroid density information derived from ablation modeling [refs. 18, 19]. MEM 3 has been validated against spacecraft impact rates measured by the Pegasus and the Long Duration Exposure Facility satellites [ref. 13]. It reports the flux of meteoroids and its breakdown by mass, speed, angle, and density, providing the quantities needed by MeMoSeE to compute the ejected mass.

Unlike MEM, the NEO model used by MeMoSeE is simplistic. It is constructed by combining the estimated flux of large objects (comets and asteroids) onto the Earth's atmosphere [ref. 14] with the speed distribution of bolides reported on the Center for Near Earth Object Studies (CNEOS) website. The directionality of NEOs is not modeled; instead, the impact angle distribution is assumed to be the same as that of the high-density meteoroid population in MEM.

6.2.2 Cratering Relations

The MeMoSeE model uses a relation given in Housen and Holsapple [ref. 20] to compute the mass ejected from an impact as a function of: secondary ejecta speed, target density, impactor mass, impactor density, impactor speed, and impact angle from the surface normal. This framework uses scaling laws to extend the range of experimentally determined ejecta properties given in 16 separate references and is utilized to compute lunar impact ejecta properties. Equation 2.18 in reference 21 summarizes the scaling laws used in the model. The MeMoSeE does not use the empirical relations in Koschny and Grün [ref. 22], which were applicable to solid ice-silicate mixtures.

Once the total ejected mass as a function of speed is computed following the Housen and Holsapple scaling relations [ref. 20], the MeMoSeE model incorporates additional assumptions on the ejecta mass and angular distributions. The model assumes the angular distribution is independent of speed and particle size and adopts the zenith and azimuth distributions from Rival and Mandeville [ref. 23]

6.2.3 Assumptions

As with any physical model, there are several simplifying assumptions in the model to make the calculations simpler and are summarized in this section.

6.2.3.1 Flux Calculation Assumptions

The MeMoSeE flux is calculated assuming a flat disc on the surface of the Moon. To avoid computation difficulties with particles "ascending" from nearby impacts MeMoSeE neglects primary impacts within a 1-km radius of the target disc. The ejecta population is assumed to be only from those particles that have passed their apoapsis and are starting to descend onto the lunar surface. Note that particles are assumed to be on elliptical Kepler orbit paths until they re-encounter the lunar surface, so secondary perturbation effects (e.g., Earth gravity) are ignored.

The flux is calculated as an average where impacts around the Moon are integrated over time and geography.

6.2.3.2 Cratering Assumptions

There are a number of assumptions in the MeMoSeE model about how the particles are ejected from an impact event in zenith angle (i.e., the angle from the local normal), in azimuth due to the direction of the primary impactor hitting at oblique angles, in size distribution, and in ejection speed. There are also assumptions about the composition (i.e., primarily material density) of the ejecta particles, based on assumptions of the lunar surface composition where the impact occurs. All of these assumptions are identified in the documentation.

One assumption that may affect ejection directions is that the MeMoSeE model assumes the surface of the Moon to be a smooth sphere. While this assumption is probably valid for large impacts, local structure (e.g., hills, rocks) may influence the ejection physics of small impacts.

MeMoSeE uses a radius of this smooth lunar sphere that differs from the one used by the lunar science community [ref. 24](https://nssdc.gsfc.nasa.gov/planetary/factsheet/moonfact.html).

Observation 1: The radius of the Moon used in MeMoSeE when calculating the escape velocity is 1737.1 km versus the traditionally accepted mean lunar radius of 1737.4 km.

Recommendation 1: Use 1737.4 km for the geometrically averaged lunar radius.

6.2.4 Model Name and Acronym

The model name and acronym are likely to be troublesome for a number of reasons, which include:

1. It contains the words "meteoroid model" but does not describe meteoroids (Ejected particles that remain gravitationally bound to the Moon do not meet the International Astronomical Union's definition of a meteoroid: https://www.iau.org/static/science/scientific_bodies/commissions/f1/meteordefinitions_approved.pdf).
2. It does not contain the words "lunar" or "Moon" even though the model is specific to the Moon (for instance, the size distribution of the ejecta particles is taken from that of the lunar regolith).
3. The term "secondary ejecta" is somewhat ambiguous. Some researchers use the term to describe particles ejected from primary impact craters, but others describe such particles simply as "ejecta."
4. The acronym is long and alternates between uppercase and lowercase letters. This impairs reading [ref. 25], is tedious to type, and is unlikely to be rendered correctly by anyone other than the model creator.

5. The pronunciation chosen by the model creator, which resembles “mimosa,” will not be apparent to those encountering the acronym in print. Native English speakers are most likely to pronounce it as “memo-see.” The differences in both stress pattern and vowel sounds could produce confusion in meetings and presentations; listeners may not even realize that “mimosa” refers to MeMoSeE.

Observation 2: The model name “Meteoroid Model of Secondary Ejecta” does not accurately and unambiguously describe the environment modeled and the acronym (MeMoSeE, pronounced “mimosa”) is difficult to type and unclear how to pronounce.

Recommendation 2: Consider changing the model name and acronym to those that emphasize accuracy and ease of use (e.g., Lunar Ejecta Engineering Model (LEEM)).

Observation 3: The documentation uses the term “secondary ejecta.” This term can be ambiguous, as it can be confused with other phenomena on the Moon.

Recommendation 3: Use the terms “secondaries,” “secondary environment,” or “ejecta” in place of “secondary ejecta.”

6.3 Model Use

Spacecraft can be damaged in a number of ways, and one source of risk is penetration by particle impacts. These particles can be man-made (e.g., orbital debris) or natural (e.g., meteoroids). The risk of penetration by these particles can be assessed by combining up-to-date models of the environment, a spacecraft description and trajectory, and damage equations using a risk assessment code (see Figure 6.3-1). NASA’s primary risk assessment code is Bumper, which is operated by the Johnson Space Center (JSC) Hypervelocity Impact Technology (HVIT) team.

The risk of damage from impacts is governed by the number and properties of particles striking a spacecraft, and the spacecraft or asset configuration location and motion. For instance, a sheet of mylar may be vulnerable to small impacts and penetrated many times compared to a plate of mm-thick aluminum. A simple Whipple shield is effective at protecting a surface from high-speed meteoroid impacts, but less effective at blocking slower particles. For this reason, it is customary to use a stuffed Whipple shield to protect against orbital debris impacts, which are slower than meteoroids. Furthermore, a spacecraft’s motion can increase (or decrease) the relative speed of some impacts, changing the risk they pose. Thus, the outputs from models such as MeMoSeE must be combined with a spacecraft or asset description and trajectory with the risk of failure or penetration computed according to ballistic limit or damage equations that are specific to the materials in question. This combination of information and analysis flow is depicted in Figure 6.3-1.

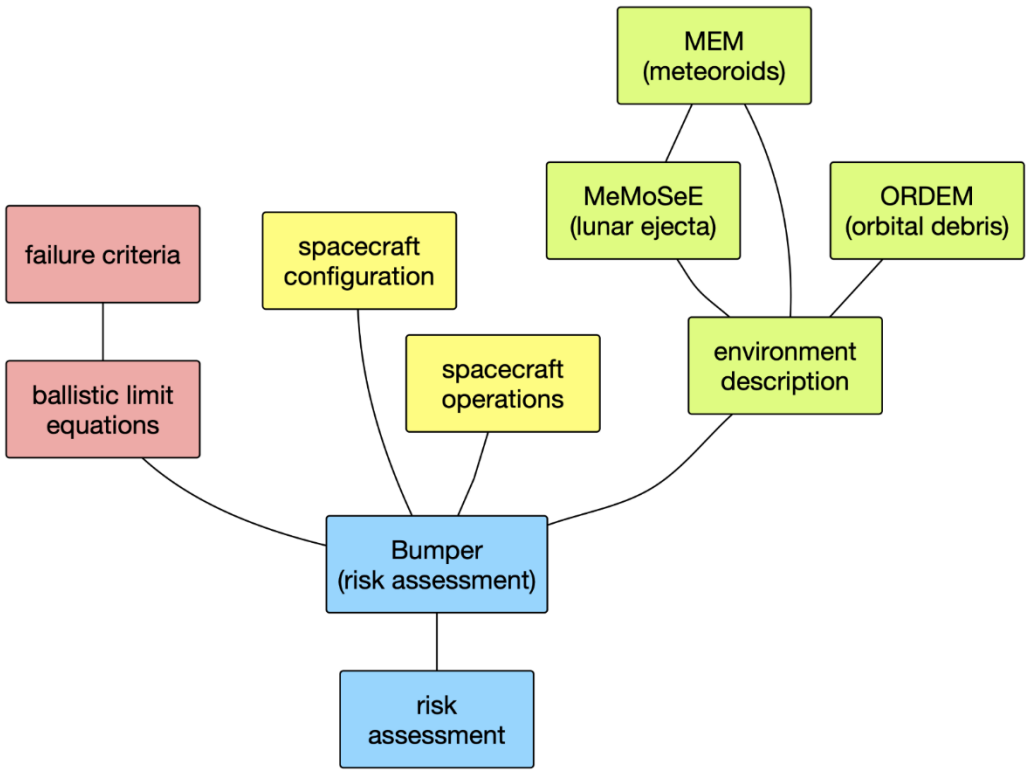

Figure 6.3-1. Risk Assessment Model Flow Chart

MeMoSeE will be one of three environment models that is integrated into the Bumper risk assessment code. The other two are the MEM and the Orbital Debris Engineering Model (ORDEM). MEM contains a dynamical model of the meteoroid environment and uses this model to compute the flux, speed, impact direction, and bulk density of meteoroids striking a spacecraft on a given trajectory. Users may attempt to interpret the MEM's outputs directly, or they can use an established risk assessment code. Similarly, users can use ORDEM to generate descriptions of the debris environment near Earth, or they can rely on Bumper. However, ORDEM is not relevant for lunar-orbiting spacecraft, where the amount of debris generated in cislunar space is lower and their lunar orbits are unstable.

Unlike MEM and ORDEM, the MeMoSeE model is not intended for public distribution nor for direct incorporation into Bumper. Instead, the developers plan to use MeMoSeE to generate location-specific descriptions of lunar ejecta in the form of tables that can then be incorporated into risk analyses. The main output are tables of flux that will be provided via the DSNE document (see reference 1).

While MeMoSeE relies on MEM to calculate the rate of ejecta-generating meteoroid impacts, it is not responsible for generating a description of the meteoroid environment for incorporation into Bumper. MEM continues to provide that information for risk assessments. MEM describes the meteoroid flux, which includes natural particles traveling through interplanetary space. However, MEM does not include particles liberated from the surface of the Moon by meteoroid or asteroid impacts. These ejected particles largely remain gravitationally bound to the Moon and do not contribute to the meteoroid environment as a whole but may be able to significantly increase the particle flux near the lunar surface. MeMoSeE fills this gap by modeling these lunar ejecta.

6.3.1 DSNE Inputs

The primary use of MeMoSeE is to generate tables of the flux of ejected particles that can be incorporated into the DSNE document [ref. 1]. The DSNE describes a wide variety of environmental hazards and is referenced during the design phase of a mission.

The MeMoSeE model developer has drafted a new proposed section of the DSNE on lunar ejecta that briefly describes the model and contains three flux tables, a single particle density value, and a size-scaling relation. Each table corresponds to a different selenographic latitude or pair of latitudes (i.e., 0°, ±45°, and ±90°) and reports the flux in three velocity bins and nine elevation angle bins. The fluxes are those of particles between 1 μm and 1 cm in "size," although it is not specified whether this size is radius, diameter, or some other debris characteristics (e.g., circumference).

The damage done by a particle impact is typically expressed as a function of impactor diameter, bulk density, speed, and impact angle. Thus, some description of these four quantities must be provided. The proposed DSNE inputs break the flux down by impact speed and elevation angle. It is stated that the variation with azimuth is "small" [ref. 26], implying that readers should assume axisymmetry about the zenith. The size distribution is handled by providing an equation that can be used to scale the flux values to the desired minimum "size," and readers are advised to use a particle density of 3,100 kg m^{-3}.

6.3.2 Bumper Integration

MeMoSeE output is an input to the micrometeoroid impact risk codes used to verify spacecraft meet the impact risk system-requirements. The Bumper program is the NASA product used to evaluate NASA spacecraft (see, Section 10.5.2). The MeMoSeE and Bumper developers concurred on the format of the MeMoSeE output tables included in a DSNE draft during the third quarter of 2020. Subsequently, the Bumper developers implemented the MeMoSeE environment tables in a developmental version of Bumper. The MeMoSeE environment is not available in versions of Bumper released to NASA partners and contractors.

Finding 1: The DSNE tables provide the information necessary for Bumper micrometeoroid and orbital debris (MMOD) risk assessments.

7.0 Primary Impact Flux

MeMoSeE models the flux, speed, and elevation angle of particles produced by impacts of meteoroids and asteroids on the lunar surface. These primary impactors range in mass from 1 μg to 1.6×10^{15} g in size, where the upper bound is the mass of a 1 km sphere with a density of 3,000 kg m^{-3}.

7.1 Meteoroids

Small primary impactors (< 10 g) are modeled as meteoroids using MEM 3 [ref. 12, 13]. For each selenographic latitude of interest, the modeler generated a series of state vectors corresponding to a point on and rotating with the Moon's surface at that latitude. These state vectors spanned a Metonic cycle (i.e., 19 years) and represent an average meteoroid environment seen at that latitude. The resulting fluxes, speeds, and impact angles generated by MEM were used as inputs to the chosen cratering relation.

MEM specifically describes the sporadic meteoroid complex, and the particles it models arise from different families of comets. It does not describe the directionality of NEOs. Thus, above a certain size threshold, it becomes necessary to switch to an asteroid dynamical model. MEM's upper mass limit is 10 g, and so the modeler uses this as the dividing line between meteoroids and asteroids.

MEM 3 is a mature, peer-reviewed model of the meteoroid environment in the inner solar system, complete with gravitational focusing and shielding by planetary bodies. MEM 3 is currently the preferred NASA model for describing meteoroid impacts in the inner solar system, and it provides the flux, speed, density, and directionality of meteoroids impacting the Moon in the 1-μg to 10-g mass range.

7.2 Near-Earth Objects (NEOs)

7.2.1 Flux

Above the 10-g threshold, the modelers use the Brown et al. [ref. 14] relation for the NEO flux, adjusted for the difference in gravitational focusing at the Moon versus the Earth, and converted to a mass-limited flux [ref. 15]. The flux per unit lunar surface area is:

$$g_{lun} = 2.89 \times 10^{-11}\ \text{meter}^{-2}\ \text{year}^{-1} \cdot m^{-0.9} \tag{7-1}$$

where m is the mass of the impactor in kilograms. Above the 10-g threshold, MeMoSeE rescales the high-density component of the MEM outputs such that its total matches that of Eq. 7-1, after multiplying by 4 to convert to a flux per unit cross-sectional area. However, this rescaling appears to be done incorrectly.

Equation 7-1 gives the large impactor flux averaged over the entire surface of the Moon. This is most analogous to the flux computed for MEM on an outward-facing plate. It is not analogous to the "total cross-sectional flux" listed at the top of the MEM output files, which is analogous to the flux on a sphere hovering just above the lunar surface. Furthermore, the total flux computed by MEM may vary per location.

Finding 2: The NEO flux appears to be implemented incorrectly in the MeMoSeE model (e.g., a meteoroid flux that is partially shielded by the Moon is rescaled using a NEO flux that contains no such shielding).

Recommendation 4: Calculate the meteoroid-to-NEO flux scaling using the meteoroid flux on a flat plate sitting on the lunar surface and facing local zenith as compared to the NEO flux onto the lunar surface per unit surface area.

One possible approach to calculate the meteoroid-to-NEO flux ratio is the following:

1. Select a large number of random points on the Moon's surface and a corresponding number of random Julian dates within a single Metonic cycle.
2. Generate a "trajectory" file that corresponds to these points and dates, where the velocity vectors reflect the rotation of the lunar surface.
3. Perform a MEM run using this trajectory file, a limiting mass of 10 g, and a body-fixed coordinate system for outputs (so that the +z direction will point directly outward from the lunar surface).
4. Extract the total flux for the appropriate population (low- or high-density) on a space-facing surface: this will correspond to the $\hat{z}$ direction.

5. Divide Eq. 7-1 by this quantity to obtain a flux scaling term as a function of limiting NEO mass that can be applied to MEM flux elements.

MeMoSeE uses MEM's upper mass limit of 10 grams as the boundary between the meteoroid/asteroidal flux. The 10-gram upper limit for MEM was an arbitrary choice, based on the realization that the meteoroid flux at this and larger masses was too small to be of any consequence in spacecraft design or hazard assessments. There was no physical reason for this limit, and the reason the MeMoSeE developers chose this as the boundary between meteoroid and asteroid impactors is not clear, other than it was the MEM limit.

Some evidence exists to suggest that a mass several orders of magnitude higher may be a better point to transition between the two populations. For example, Figure 7.2-1, adapted from Zolensky et al. (2006) [ref. 27] has a green band to indicate the comet/asteroid particle transition region, where there is a gradual transitioning to fragments from the NEO population starting around a kilogram. The NEO population should accurately depict the environment at masses larger than a hundred kilograms or so [ref. 28] – several orders of magnitude higher than 10 grams.

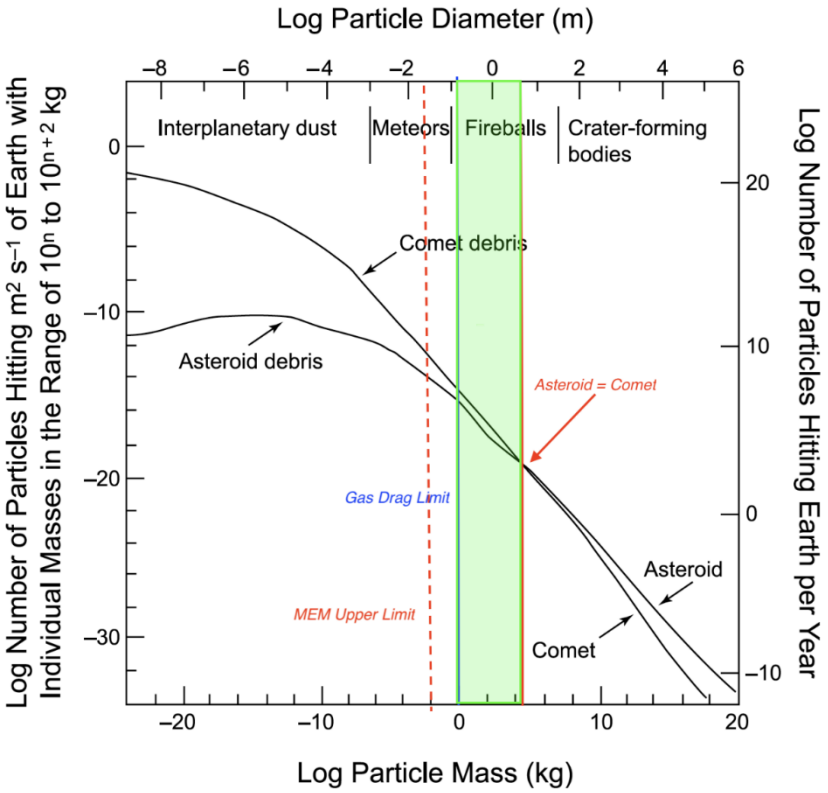

Figure 7.2-1. Cometary and asteroidal contribution to near-Earth flux.

Finding 3: It is not clear that the 10-gram boundary between the cometary and asteroid populations used in MeMoSeE is an appropriate boundary. Observations and research indicate that the transition occurs at masses between 2 and 4 orders of magnitudes larger (1 to 100 kilograms).

Recommendation 5: Developer should work with experts from NASA's Meteoroid Environment Office to identify an appropriate mass boundary between the cometary and asteroidal populations.

7.2.2 Speed Distribution

MeMoSeE adopts a NEO speed distribution that is derived from speeds of kiloton-or-larger impacts on the Earth's atmosphere, taken from the CNEOS website (https://cneos.jpl.nasa.gov/fireballs/) and converted to a mass-limited lunar speed distribution [ref. 15]. This is a global average; it is unknown whether the speed distribution varies substantially from location to location on the lunar surface. However, this question cannot be easily answered without implementing a full dynamical model of the NEO population.

Observation 4: The NEO input population is not modeled to the same level of detail as the meteoroid population and is instead a global average.

7.2.3 Directionality of Larger Objects

A geocentric radiant distribution is not available from the CNEOS data. MeMoSeE therefore assumes that the orbital inclinations of NEOs are concentrated near the ecliptic, and on that basis, assumes that their zenith angles relative to the lunar surface will be distributed similarly to that of helion/antihelion meteoroids in MEM (i.e., the "high density population" in MEM 3), which are also concentrated near the ecliptic.

To test the validity of this assumption, a crude model of the NEO population was constructed by replacing MEM's distributions of meteoroid orbits with those of near-Earth asteroids (NEAs) taken from the Jet Propulsion Laboratory's Small-Body Database (https://ssd.jpl.nasa.gov/sb/). The NEA population was chosen by using a cumulative magnitude distribution and finding the point where the cumulative curve "turned over," which would mark the brightness below which the population was starting to be incomplete. While this sub-population is more likely to be complete, it is not fully corrected for observing biases, and thus may differ from that encountering the Moon. However, this simple test reveals that the angles at which NEOs encounter the Moon do not resemble those of helion meteoroids. Instead, these angles are more similar to those of the "low-density population," which consists of apex and toroidal meteoroids.

Figure 7.2-2 presents the elevation angles of NEAs impacting the lunar surface for three locations: a point near the lunar equator (top left), a point near 45° S (top right), and a point near the lunar south pole (bottom left). In each case, the NEA zenith angle distribution was compared with that of the high-density and low-density populations from the MEM. The low-density meteoroid population more closely matches the NEAs in its distribution of elevation angles. At bottom right, the speed distribution of NEAs impacting the lunar surface, averaged over all locations, was compared with that derived from CNEOS data [ref. 15]. The NEA-MEM speed distribution appears faster than that derived from the CNEOS data. However, this result may be due to detection biases.

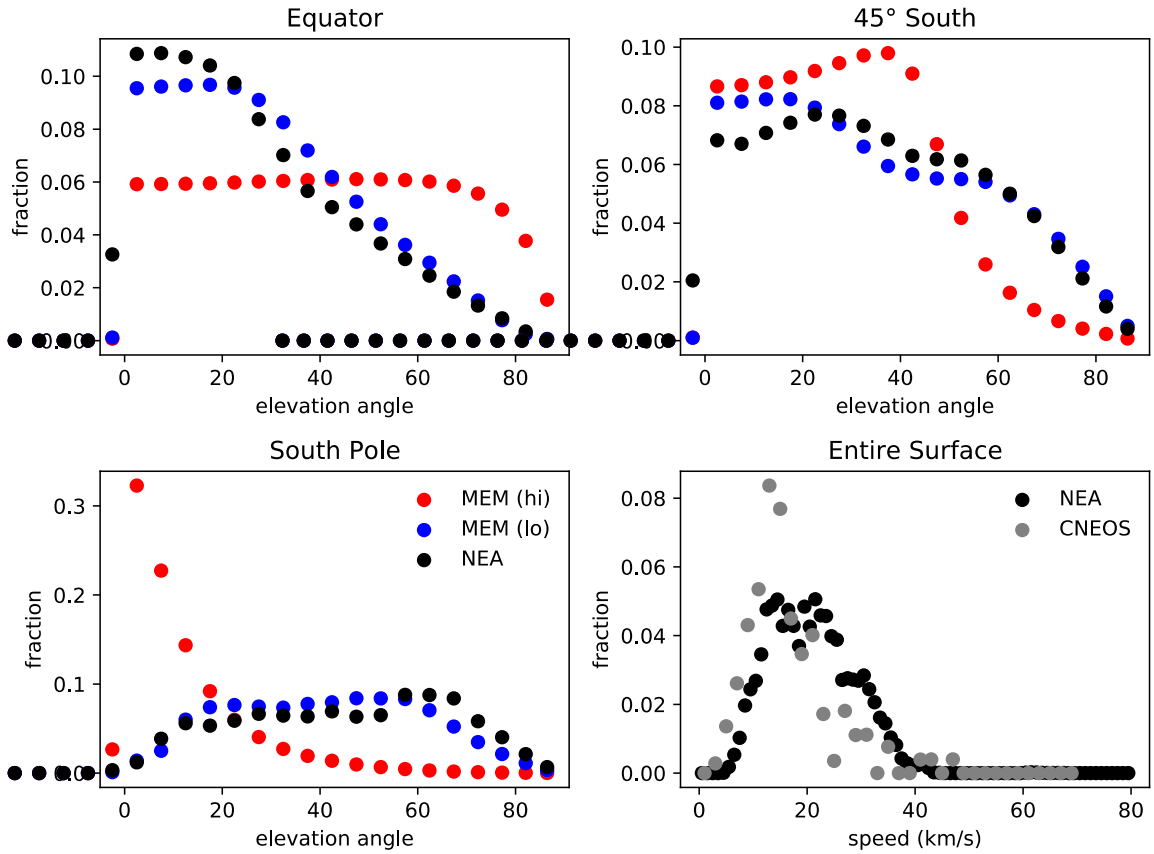

Figure 7.2-2. Elevation Angle and Speed Distributions of NEAs Impacting Lunar Surface

Figure 7.2-3 presents the directionality of NEAs relative to an object orbiting the Sun at 1 au, modeled using the framework of the MEM. Angular coordinates are in a Sun-centered ecliptic frame in which the center of the plot (i.e., 270°, 0°) points in the direction of the reference object's orbital motion (i.e., "ram"). Again, the directionality does not resemble that of the high-density population in MEM. This difference in behavior is likely because NEOs are on more circular orbits than most meteoroids, which originate primarily from comets. A relatively small inclination can correspond to a fairly inclined selenocentric trajectory (i.e., a small out-of-ecliptic velocity component will be proportionally larger to the in-ecliptic velocity component after subtracting the Moon's velocity vector).

Ideally, the NEO angular distribution could be corrected by extracting impact angles from an appropriate dynamical model of asteroids and comets. If this is not feasible, then at a minimum the authors should replace the NEO angular distribution with that of the low-density meteoroid population in MEM.

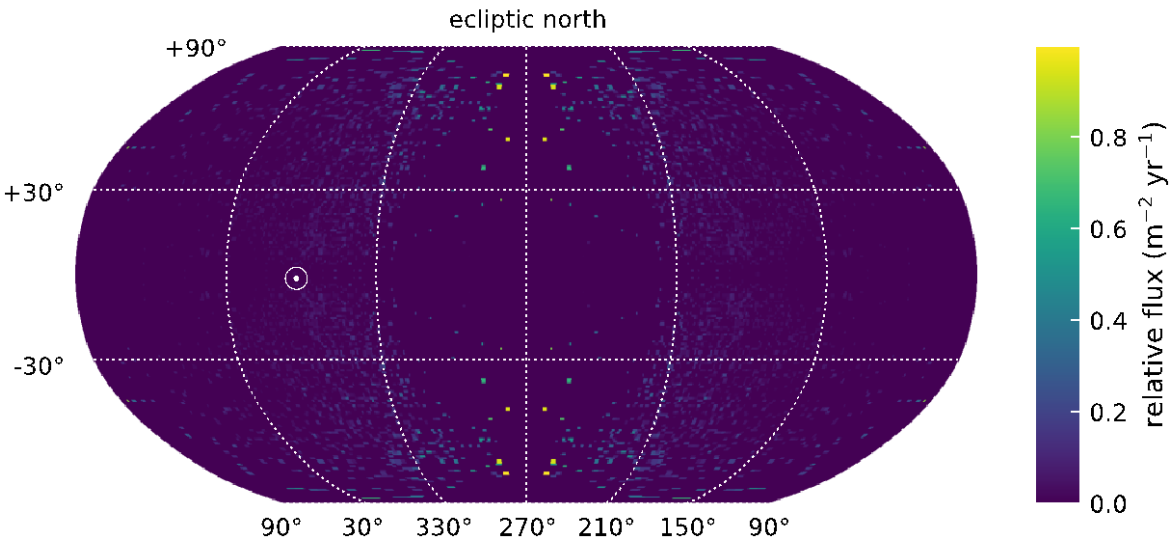

Figure 7.2-3. Directionality of NEAs Relative to an Object Orbiting Sun at 1 au

Finding 4: The MeMoSeE model's assumed NEO impact angles of incidence with respect to the Moon's surface resemble the MEM high-density population but should more closely resemble the low-density meteoroid population in MEM.

Recommendation 6: The NEO angular distribution should be corrected by extracting impact angles from an appropriate dynamical model of asteroids and comets.

8.0 Ejection Process

This section will compare the MeMoSeE model crater ejection phenomena and corresponding output to observations acquired by the Lunar Atmosphere Dust and Environment Explorer (LADEE) and the Lunar Reconnaissance Orbiter (LRO). The LADEE mission launched in September 2013 and entered lunar orbit on October 6, 2013. During the 100-day science mission, the Lunar Dust Experiment (LDEX) recorded more than 140,000 impacts from dust cloud particles. The LRO spacecraft launched in June 2009 and has been orbiting the Moon for nearly 12 years. The spacecraft is equipped with two Narrow Angle Cameras (NACs) and a Wide-Angle Camera (WAC) packaged together as the Lunar Reconnaissance Orbiter Camera (LROC).

8.1 LADEE Comparison

8.1.1 Size Distribution

The discussion and last two paragraphs of Section 2.5.1 in reference 21discusses how the size distribution is modified to account for the LADEE-observed power-law cumulative size index of –2.7 [ref. 29] for grains with radii below ~5 μm (see Figure 8.1-1). Figure 8.1-1 shows the exponent of the power-law distributions fitted to Lunar Dust Experiment (LDEX) measurements as functions of altitude (i.e., 15-km bins) and time (i.e., 10-day bins). The color indicates the value of the differential mass distribution index (1+α), where α is the cumulative mass index, and the size of a circle is inversely proportional to its absolute uncertainty. The inset shows the impact charge distribution for all heights for the entire mission, resulting in a χ^2 minimizing fit of $\alpha = 0.910 \pm 0.003$ [ref. 29]. The model adequately accounts for the LADEE size distribution measurements in the triple power-law distribution given in Eq. 2.16 in reference 21.

Because of the nature of the ejecta environment, it extends some distance above the lunar surface (LADEE orbited tens of km above the surface), where it can affect the risk to objects in lunar orbit.

Finding 5: The MeMoSeE model adequately accounts for the LADEE ejecta particle size distribution measured from lunar orbit.

Recommendation 7: The presence of ejecta detected at altitudes above the lunar surface suggests that it might be appropriate to consider extending MeMoSeE to also cover objects in low lunar orbit and provide an appropriate altitude limit where the model is applicable.

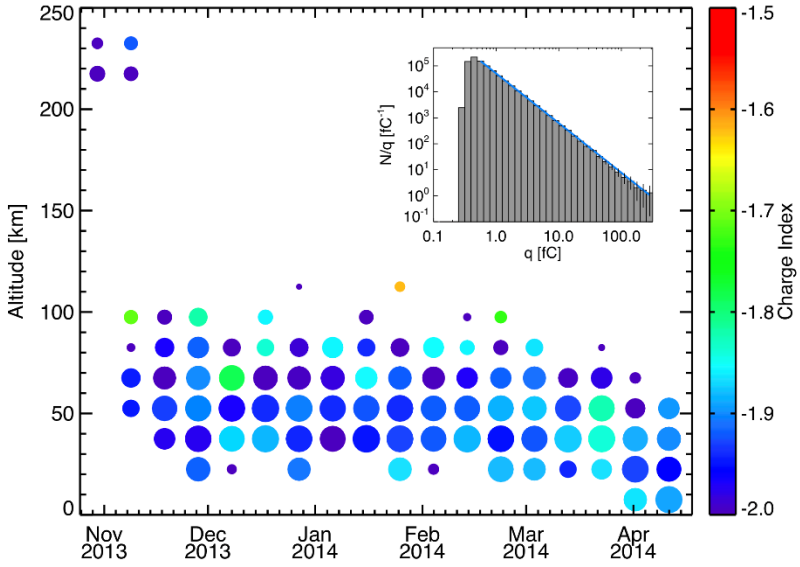

Figure 8.1-1. Slope of Charge and Mass Distributions

8.1.2 Ejecta Yield

The ejecta yield is the ratio of total ejecta mass produced to the total impacting mass. For example, an ejecta yield of 100 means that 100 times more mass is produced as secondary impact ejecta than the total sum of primary impacting meteoroid masses. The ejecta yield for MeMoSeE was estimated to be on the order of 10 to 20 for impactors in the 1-microgram to 10-g range, which are commensurate with those observed by LADEE. LADEE observed ejecta yields ~10 for the Moon's fine regolith surface [refs. 30, 31]. This is in contrast to ejecta yields ~10^3 to 10^4 at the icy Galilean moons of Jupiter (Table 3 in reference 32). To explain the low ejecta yield measured by LADEE compared to the Galilean moons, reference 30 suggested that "the ejecta observed by LDEX may have been launched from the surface under an entirely different regime of impact ejecta physics, where a much larger fraction of the energy is available to be partitioned into local heating of the regolith instead of into the kinetic energy of launched particles".

In the other limit (i.e., Galilean moon surface), an impact into a solid surface gives significantly larger yields. As this model includes impactors producing the ejecta observed by LADEE and larger impactors, it is perhaps reasonable to expect a larger yield. The fact that the yield of 10 to 20 used in MeMoSeE agrees with that for the fine regolith LADEE-derived yield of 10 suggests the total ejecta production is well estimated in this model.

Finding 6: The MeMoSeE model and the LADEE data are both consistent with a lunar impact ejecta yield of ~10.

8.1.3 Angular Distribution

The MeMoSeE model is not fully consistent with LADEE results for the ejecta angle distribution, but this may not mean the model is unrealistic. For background, LADEE typically detected a single ejecta particle per lunar impact event. However, occasionally it observed dense ejecta plumes when a large number of LADEE detections were attributed to a single lunar impact. In these cases, the LADEE data allowed for estimates of the impact ejecta plume properties, notably the exterior angle, which should be analogous with the Zenith Angle. For the dense plume detections by LADEE, angles were found to be 8° ± 3° [ref. 33] as shown in Figure 8.1-2. In this figure, the left shows the assumed plume parameters for simulation to compare to LADEE/LDEX plume observations. The right panel shows a histogram of fitted outer plume angles. Plumes with outer angle 8° ± 3° were consistent with LADEE/LDEX observations [ref. 33].

This angle is notably narrower than any of the zenith angles given in Table 2 of reference 21, and could have bearing in the ejecta distance estimates. The LADEE data does not give any information on the impact zenith angle, so the values it determines represent an average over a range of impact zenith angles for LADEE's latitudinal range of approximately ±20° selenographic latitude. It was posited that the LADEE-observed plume detections were "reverse plumes," which are "narrow high-velocity plumes produced shortly after the initial plume cone is generated due to the swift collapse of the crater or impactor breakdown [ref. 33]." Hence, the LADEE observations may not represent the bulk of the ejecta distribution and therefore the discrepancy between the MeMoSeE model's assumptions and the narrow LADEE plumes is not in direct contradiction.

Finding 7: The MeMoSeE model ejecta angular distribution does not reproduce LADEE measurements.

Recommendation 8: Include LADEE ejecta angular distributions inferred from plume measurements into the MeMoSeE model.

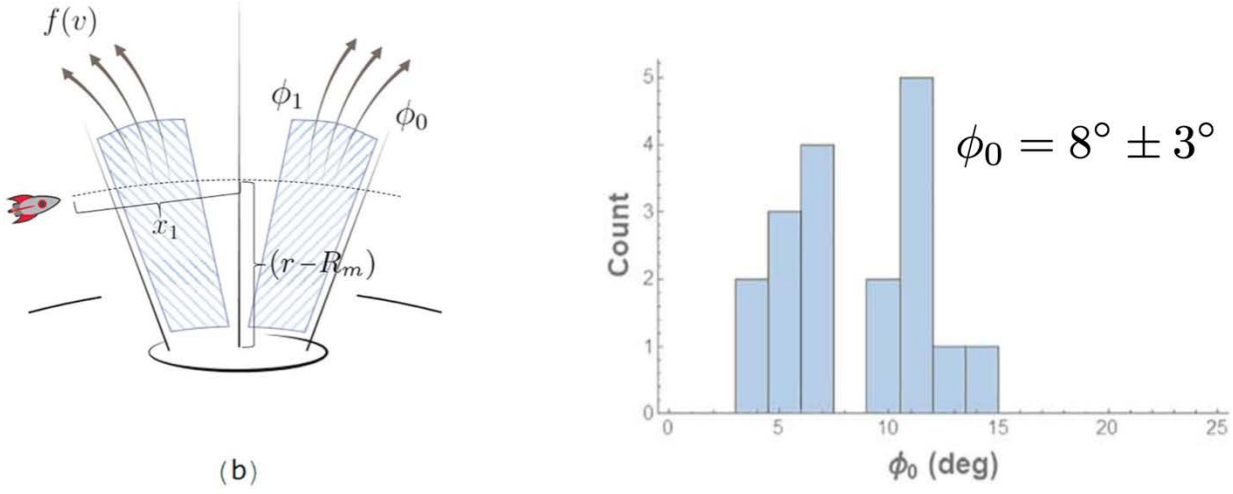

Figure 8.1-2. Angular Ejecta Distribution from LADEE/LDEX

8.1.4 Velocity Distribution

Combining Eqs. 2.18 and 2.68 from reference 21, the MeMoSeE model includes a complex speed dependence. This dependence appears fundamentally to be related to a power-law

distribution, which is different than the one derived from LADEE data. The LADEE distribution was derived with certain assumptions. First, LADEE/LDEX measured impact rates, not densities. To convert rates into densities, knowledge or assumptions about the impact velocity vector must be incorporated. The following assumptions were made: 1) all grains detected by LADEE had no horizontal velocity component (i.e., ejected purely normal from a reference lunar spheroid), and 2) grains were detected at their vertical turning points, such that they had zero relative speed with respect to the Moon.

After these assumptions were made, the impact rates were converted into impact ejecta densities. It was found that the density as a function of altitude was well-represented by an exponential, such that $n(h) = n_0 \exp(-h/h_0)$, where a scale height of $h_0 = 200$ km best fit the data [ref. 34]. From conservation of energy, this density distribution was then inverted to derive an initial impact ejecta speed distribution:

$$f(\hat{v}) = \frac{\delta \hat{v}}{(1-\hat{v}^2)^2} e^{-\frac{\beta \hat{v}^2}{1-\hat{v}^2}} \quad (8\text{-}1)$$

where $\hat{v} = v/v_{esc}$ is the speed normalized by the Moon's escape speed, and the fitted parameters $\beta = 8.69$ and $\delta = 7.2 \times 10^{-3}$ seconds per meter (note this equation appears in different form as Eq. 1 in Szalay and Horányi, 2016 [ref. 34], and Eq. 19 in Szalay et al. 2018 [ref. 4]). Figure 8.1-3 (right panel) shows this inferred speed distribution from LADEE/LDEX data, calculated using ~140,000 impacts averaged over LADEE's 6 months of operations in lunar orbit. White regions indicate locations LADEE did not visit or could not take measurements due to sun pointing constraints. Altitude bands are not to scale. The right panel shows the inferred surface ejecta velocity distribution from the altitude density fit. The dotted line indicates the maximum altitude explored by LADEE, above which the distribution function is an extrapolation [ref. 4]. Notably, the lunar speed distribution derived from LADEE/LDEX avoids the artificial cutoff speed required for purely power-law distributions that are not defined at $v = 0$. However, the derived lunar speed distribution has intrinsic assumptions that limit it to purely bound ejecta, as it was derived assuming all detected impacts were bound at their vertical turning points. Hence, it is an approximation of the impact ejecta speed distribution.

The power-law ejecta speed distribution function is used extensively throughout the literature and provides a common framework to cross-compare measurements. However, this distribution is not consistent with the impact ejecta distribution observed at the Moon for grains with radii below ~5 μm.

Finding 8: The MeMoSeE model's ejecta speed distribution shape differs from the exponential distribution determined from LADEE observations.

Recommendation 9: Incorporate LADEE ejecta speed distributions into the MeMoSeE model and compare with current speed distribution assumptions.

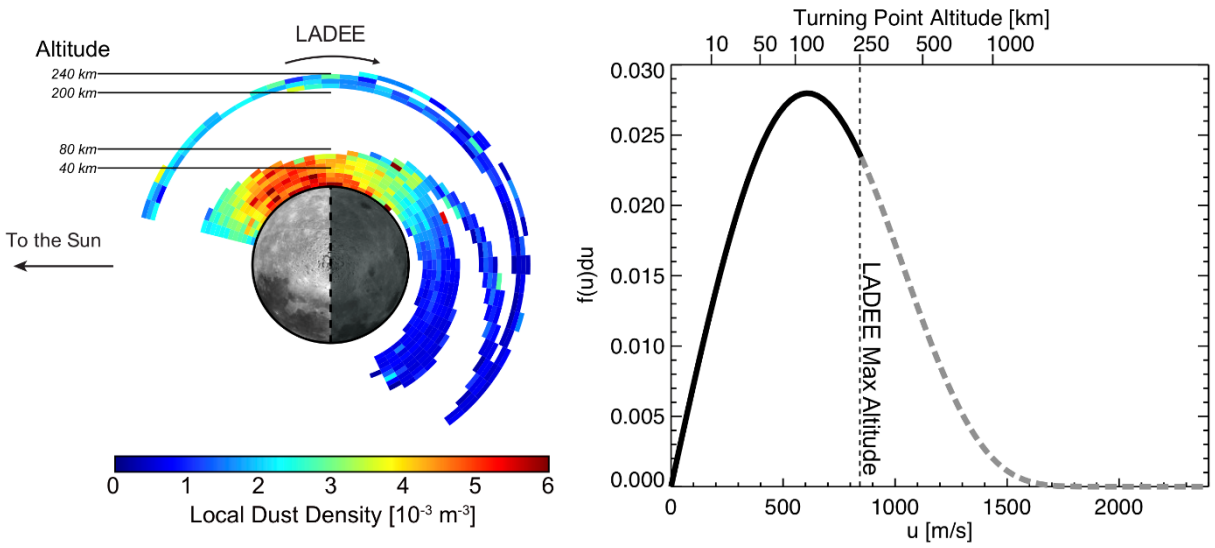

Figure 8.1-3. Left: Dust Density Distribution About the Moon.; Right: Inferred Speed Distribution from LADEE/LDEX Data

8.1.5 Ejected Mass

The projectile and the target density are used in the ejecta rate calculation. Whereas the meteoroid density of 2.5 g cm^{-3} is frequently assumed as the standard projectile density [ref. 35]. The MeMoSeE model accounts for the expected variation of densities between the different populations of meteoroids (Figure 9, Section 2.9 of reference 21), which are dependent on their origin [ref.19].

The density of the target can be taken as the specific gravity or the bulk density of lunar regolith. The concept of bulk density includes porosity and is always smaller than the density of individual regolith particles. Thus, a representative value of density for individual regolith grains is $\rho \approx 3$ g cm^{-3}, which is used for all calculations, whereas representative values for regolith bulk density are 1.30 g cm^{-3} at the surface, and 1.52 g cm^{-3} at a depth of 10 cm [ref. 36]. However, the precise value of the target density adopted in the MeMoSeE model seems to have only a small effect (i.e., ~10%) in the output as the total ejected mass falls off as the density $\rho^{-0.2}$ (Eq. 4.5 of reference 21).

The MeMoSeE model approximates the ejecta size distribution as that of the lunar regolith particles (Section 2.5 in reference 21). The model further extends the results from lunar samples to particles < 5 μm by using LADEE measurements.

The ejecta model for total mass is based upon Housen and Holsapple [ref. 20]. Comparison to the Zook [ref. 11] formula was provided (Section 3.1 in reference 21). Comparison to other formulas frequently used for the calculation of ejecta rates were not provided.

According to the formula adopted, the total mass ejected by an impactor is given by Eqs. 2.18 and 4.1 of reference 21:

$$M_{>v} = C_4 m_p \left(\frac{v}{v_p \sin\alpha}\right)^{-3\mu} \left(\frac{\rho}{\rho_p}\right)^{1-3\nu} \tag{8-2}$$

$$C_4 = \frac{3k}{4\pi} C_1^{3\mu} \tag{8-3}$$

where in these equations, v is the ejecta speed (with a minimum of 0.1 km/s), m_p is the mass of the primary impactor/projectile, v_p is its speed, and ρ_p is its density. The quantity α is the impact angle, measured from the local horizon, and ρ is the density of the regolith and ejected particles, which is assumed to be 3,100 kg m^{-3}. The quantities $\mu = 0.4$, $\nu = 0.4$, $k = 0.3$, and $C_1 = 0.55$ are material-specific constants for sand-fly ash (see Table 3 of reference 20). With the values adopted, $M \propto m_p v_p^{1.2}$.

Another popular formula for the mass production rate is that of Koschny and Grun [ref. 22]:

$$M = C\ cos^2 a\ m_p^{\gamma 1} v_p^{2\gamma 2} = C\ cos^2 a\ m_p^{1.23} v_p^{2.46} \quad (8\text{-}4)$$

where $\gamma 1$ and $\gamma 2$ are empirical power law parameters. This formula was derived in laboratory experiments for impacts $v_p < 10$ km/s, which are smaller than experienced on the lunar surface. It is evident that the Koschny and Grun formula is a more sensitive function of the projectile speed and will tend to accentuate the ejecta production from high-speed impactors at the apex. Importantly, there is an additional dependence on projectile mass in the Koschny and Grun formulation that, albeit weak, $m_p^{0.23}$ provides a way to assess which formula should be used. Using a similar dynamical model to MEM, Pokorny et al. [ref. 31] found that the ejecta production rate should be described as proportional to the mass of the projectile, $M \propto m_p v_p^{2.46}$ (i.e., $\gamma_1 = 1$ in the Koschny and Grun 2001 formula), in order for LADEE measurements to be consistent with the current constraints on the relative ratios of Jupiter-family comets (JFC), Halley-type comets (HTC), and Oort-cloud comets (OCC) particles as measured from radar at Earth. This finding follows from a segregation in the mass indices of the different populations arriving at Earth according to Pokorny et al. [ref. 31]. The velocity index was found to be uncertain and was studied only in the range 2 to 2.6. With the Kochny and Grun formula, the total ejection rate seems to have exceeded LADEE by four orders of magnitude.

Finding 9: The LADEE data are more consistent with the Housen and Holsapple [ref. 20] formula over the Koschny and Grun [ref. 22] formula. This provides confidence in the modeling approach adopted for MeMoSeE.

8.2 LROC Comparison

The LROC instrument has collected nearly half a million WAC images at 100 meters per pixel, and 1 million NAC observations at meter-scale pixels over illuminated terrain. With this extensive image library and additional observations collected during a series of extended science missions, LROC has a large catalog of temporal image pairs. These before and after image pairs have nearly identical lighting and viewing geometries and are separated in time by 6 months to almost the length of the mission (currently 12 years). By systematically scanning these observations, newly formed surface features can be mapped and classified. To date, LROC has identified over 500 newly formed craters and 150,000 other surface changes. Many of these other surface changes are thought to be distal secondary impacts due to their proximity to newly formed craters.

In 2015, the LROC team published a manuscript documenting a newly formed 18-meter crater located with the help of an impact flash observed on March 17, 2013, by the Automated Lunar and Meteor Observatory (ALaMO) [ref. 37]. Robinson and coauthors [ref. 38] identified four distinct reflectance zones around the impact site: Proximal High Reflectance Zone (PHRZ), Proximal Low Reflectance Zone (PLRZ), Distal High Reflectance Zone (DHRZ), and Distal

Low Reflectance Zone (DLRZ). Figure 8.2-1 highlights shows the extent of each zone by computing a ratio image of the after image (M1129645568L) and the before image (M183689789L). The blue outline in Figure 8.2-1a shows the outer extent of DLRZ, red line delimits outer boundary of DHRZ, orange polygon defines the outer limit of the PLRZ, and the PHRZ extends from the crater rim out to the green boundary. An enlargement of the top panel is shown in Figure 8.2-1b detailing the zones closer to the impact site. This work documented 248 distal ejecta impacts creating a series of splotches that surrounded the impact site. Figure 8.2-2 displays a subset of these splotches (white arrows) exhibited herringbone patterns that pointed toward the impact site (direction of the black arrows).

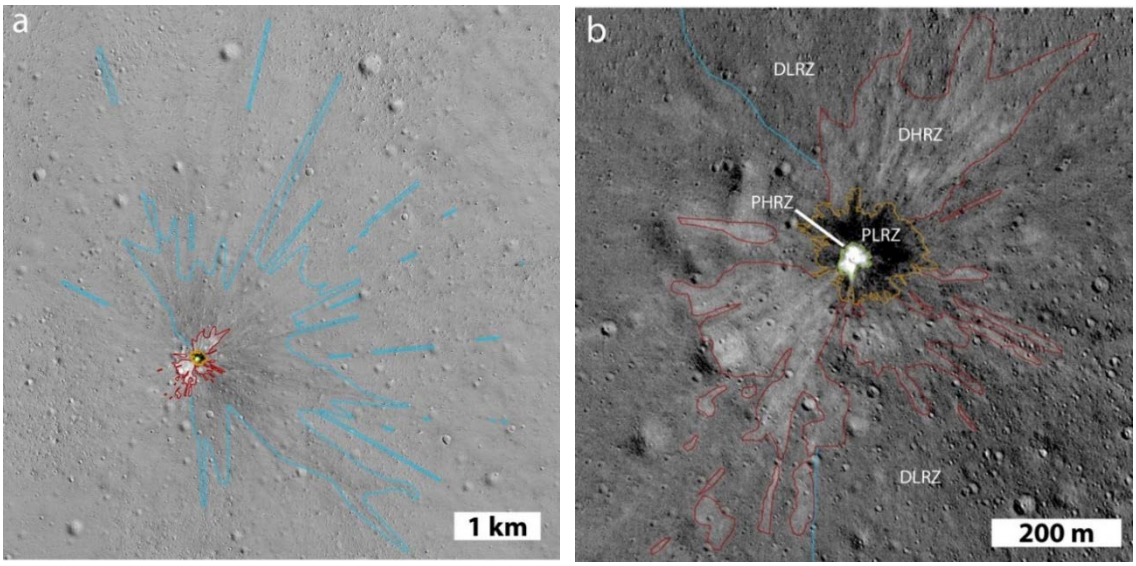

Figure 8.2-1. Temporal Ratio Image of an 18 m Lunar Impact that Formed on March 17, 2013 [ref. 38]

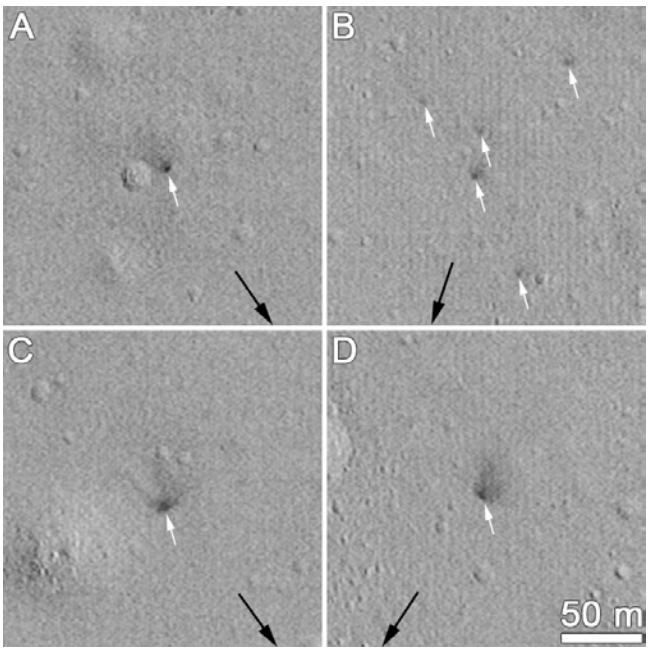

Figure 8.2-2. Secondary Splotches (highlighted with white arrows) Observed in Temporal Ratio Images Around the March 17, 2013 Lunar Impact Site

Speyerer and coauthors [ref. 39] examined 222 newly formed impact craters and 120,000 splotch-like features in a follow-on study. With these additional craters, the study expanded upon the existence of the reflectance zones and proposed that the two distal zones result from impact jetting. Jetting occurs in the contact and compression phase of the impact process. This process occurs before the projectile is fully compressed and ends with the projectile halfway into the target (i.e., t = D/2v; D = projectile diameter, v = projectile velocity) [ref. 40]. While the mass ejected during jetting is small compared to the material removed during the excavation phase, the velocity profile is on the same order or even faster than the original projectile velocity [ref. 41]. Previous work indicates that this jetting phenomenon is more pronounced in oblique impacts [refs. 41, 42, 43]. Jetted material is composed of a mixture of melted and vaporized rock – primarily from the impactor – that travels along the surface. Figure 8.2-3A-C shows temporal ratio images highlighting distal zones around a newly formed 19.5, 12, and 11 m crater, respectively. Image ratios (Figure 8.2-3D and 3E) show the distal zones flowing around topographic features (i.e., small crater), which indicates that the jet indeed has a low ejection angle. Additionally, it was found that these disturbances can cover large distances from the primary impact; up to 100 km for a 70-m crater (Figure 8.2-3F) when the surrounding surface exhibits few topographic obstacles (i.e., lunar maria).

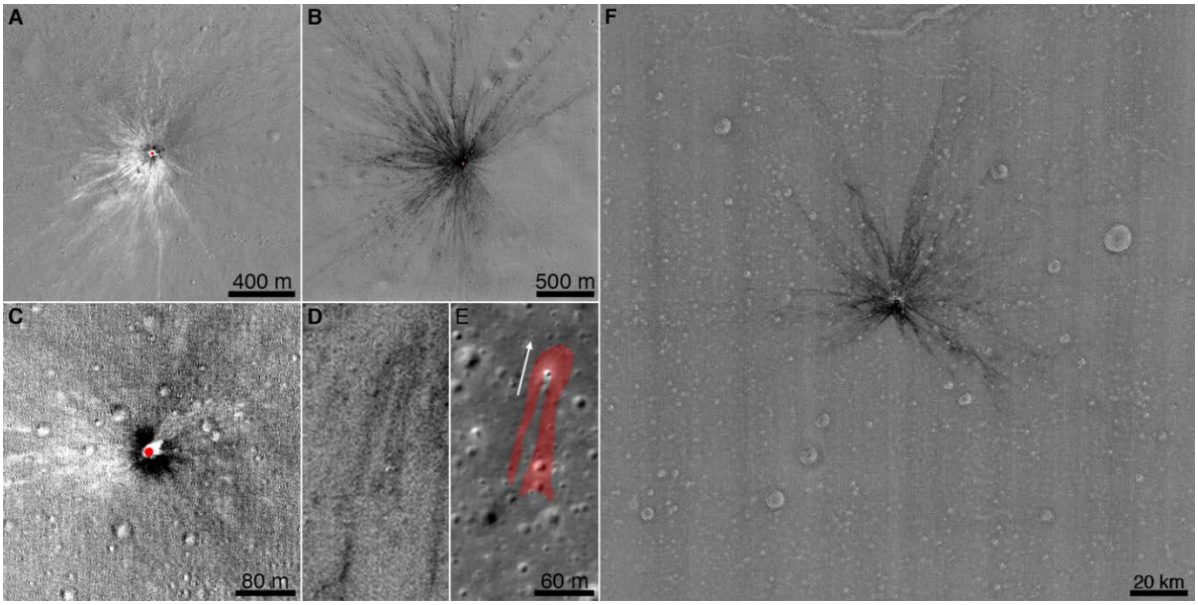

Figure 8.2-3. Series of Temporal Ratio Image Showing Extent of Distal Zones Around Newly Formed Lunar Craters

The MeMoSeE model is a convenient tool to assess the average ejecta distribution during the excavation phase of the impact process. When modeling oblique impacts, the model accurately portrays the impact process by ejecting more material in the impact site downrange direction and leaving an exclusion zone in the up-range direction. Modification to the code could enable the modeling of an individual or a handful of impacts to further study the ejecta distribution around newly formed craters observed with LROC, and help constrain the impactor's properties (e.g., impact angle).

The MeMoSeE model estimates the number of particles impacting a surface as a function of impact angle (i.e., eight bins) and speed (i.e., three bins). The table for the secondary statistics gathered for the nearside equatorial region (0° N, 0° E) is reproduced in Table 8.2-1. Using the

median particle size as 0.072 mm (see Section 3.4.2.2.1 of reference 1) along with speed and impact angle information, the crater size created by the ejected particles was estimated using the Holsapple scaling model and approximations [refs. 20, 44]. While these models typically are not used to assess impacts caused by low-speed projectiles, the equations provide a rough approximation of the secondary crater size (Table 8.2-2).

Table 8.2-1. Primary Ejecta Flux Versus Elevation and Speed for 0° N and 0° E

Elevation			Speed		
PHI1	PHI2	PHIavg	0.1-0.3 km/s avg=170 m/s	0.3-1 km/s avg=535 m/s	1-2.4 km/s avg=1.53 km/s
Degrees			Number Flux [#/m^2/yr]		
0	10	4.98	2.75E-12	1.97E-12	3.32E-13
10	20	14.94	3.21E-07	1.57E-07	2.95E-08
20	30	24.90	2.02E-04	8.20E-05	1.10E-05
30	40	34.85	1.35E-02	5.10E-03	6.56E-04
40	50	44.78	2.35E-01	8.70E-02	1.13E-02
50	60	54.69	1.53E+00	6.00E-01	7.73E-02
60	70	64.54	4.37E+00	1.87E+00	2.70E-01
70	80	74.21	5.03E+00	2.78E+00	4.78E-01
80	90	82.93	1.25E+00	1.17E+00	2.55E-01

Table 8.2-2. Crater Size Estimated for Each Bin Assuming a Secondary Particle Size of 0.072 mm and Average Impact Elevation (PHIavg) and Average Speed Associated with Each Bin

Elevation			Speed		
PHI1	PHI2	PHIavg	0.1-0.3 km/s avg=170 m/s	0.3-1 km/s avg=535 m/s	1-2.4 km/s avg=1.53 km/s
Degrees			Diameter of Secondary Crater [cm]		
0	10	4.98	0.11	0.17	0.26
10	20	14.94	0.17	0.27	0.41
20	30	24.90	0.21	0.33	0.50
30	40	34.85	0.23	0.37	0.56
40	50	44.78	0.25	0.40	0.61
50	60	54.69	0.27	0.42	0.65
60	70	64.54	0.28	0.44	0.67
70	80	74.21	0.29	0.45	0.69
80	90	82.93	0.29	0.46	0.70

Suppose each of these secondary impacts from Table 8.2-2 creates an ejecta blanket that extends two crater diameters away from the rim. In that case, a Monte Carlo model can be executed to estimate the resurfacing rate of the Moon and compare it to observations made by LROC and the secondary splotches observed in the temporal images. Speyerer et al. [ref. 39] found that splotches down to 1 m in diameter had the potential to cover 99% of the Moon in 81,000 years. Using the secondary crater size estimates in Table 8.2-2 and the assumption that each impact modifies the surface within two crater diameters, a resurfacing rate of 78,000 ±1400 years is estimated, within 4% of the resurfacing estimates computed from LROC observations.

While these estimates are comparable, it should be noted that LROC observed secondary splotches that were 1.5 m to as large as 30 m in diameter. None of the ejecta particles described in the MeMoSeE model could account for creating these significant disturbances. Speyerer et al. [ref. 39] proposed that these splotches could be formed by a grouping of poorly consolidated regolith ejected in clumps. This method would imply that the splotches are created by many dozens to thousands of small particles modifying the surface and increasing the roughness of the top regolith layer and reducing the overall observed reflectance. This scenario would not create a

crater visible in LROC images consistent with what was observed in temporal pairs. However, it is possible that small craters (e.g., < 3 pixels across) form during these secondary impacts but are not observable by LROC or any other remote imager.

Finding 10: The MeMoSeE model focuses on particles ejected during the impact excavation phase and does not account for jetted material expelled at low angles to the target's surface and high velocities during the contact/compression phase.

Recommendation 10: Incorporate jetted material expelled during the impact contact/compression phase into the MeMoSeE model.

Finding 11: The lunar resurfacing rate of ~80,000 years modeled with MeMoSeE is comparable with statistics derived from LROC NAC temporal observations.

Finding 12: The LROC temporal image pairs (before/after observations) reveal secondary surface disturbances that are significantly larger (i.e., 1 m to 30 m in diameter) than the secondary impacts modeled in MeMoSeE (<0.01 m).

Recommendation 11: Consider modifying the MeMoSeE model to account for the clustering of secondary particles impacting the surface.

9.0 Propagation of the Ejecta to the Asset

One of the important aspects of the MeMoSeE model is how the various ejecta models are put together to generate the flux at a position on the Moon. As this is a particularly important component of MeMoSeE, and it is difficult to isolate the mathematics of the flux calculations from the numerous other calculations, a tool is needed to isolate these calculations and to compare with some sort of "truth."

9.1 Monte Carlo Approach

The easiest way to do this is to come up with a simplified version of the ejecta model, and to use a Monte Carlo technique to compute the fluxes on a lunar target. One simplification is to have the primary impactor flux isotropic over the Moon, and have the ejecta only have a single particle size that leave the crater isotropic in azimuth and a simple function for speed and zenith angle distributions.

The target on the Moon's surface must be carefully considered to compute accurate and usable flux values. MeMoSeE uses the equivalent of a hemispherical target for flux calculations, but the simplest Monte Carlo target is a sphere with a given radius sitting on the Moon's surface (Figure 9.1-1). It presents its πr^2 cross-sectional area to particles from any direction. That way, the cross-sectional flux is easy to assess from any given ejecta direction as the number of particles that penetrate the sphere per unit time divided by its cross-sectional area.

Note that cross-sectional area of a target hemisphere (i.e., $A_{\text{hemisphere}}$) useful for computing the flux is a function of the zenith angle of the impactor γ:

$$A_{hemisphere} = \frac{\pi}{2} r^2 (1 + \cos\gamma) \tag{9-1}$$

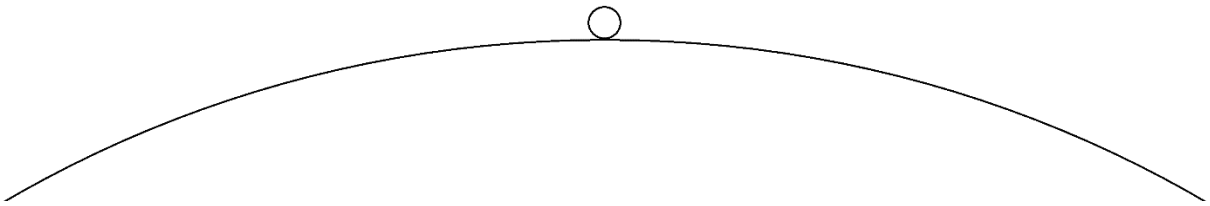

Figure 9.1-1. Monte Carlo Target – a Sphere of Known Radius Sitting on the Lunar Surface

The idealized flux is computed for the limit when the sphere on the Moon's surface has a vanishingly small radius. However, for practical reasons, the sphere needs to be of sufficient size to record a nontrivial number of impacts. Ideally, as long as the radius of the sphere is much smaller than the radius of the Moon, the Monte Carlo flux should be accurate.

The Monte Carlo procedure used was:

1. The sphere with radius 500 m is placed on the Moon's surface.
2. A primary impact site is randomly chosen on the Moon's surface.
3. A single ejecta particle is created, with randomized azimuth, zenith angle, and speed based on the distribution to be tested.
4. The Kepler orbit for that ejecta particle is computed, and it is determined whether a particle intersects the sphere before it re-encounters the Moon's surface.
5. The conditions of that impactor are written to a file.
6. The process is repeated at step 2 until a sufficient number of Monte Carlo runs have been completed.

The total number of particles created is recorded for use in determining flux. Note that the initial velocities of all particles created from a cratering event will be ascending from the Moon's surface, but the zenith angle γ of a particle hitting the sphere can be any value between 0° and 180°; with angles between 0° and 90° representing "descending from above" (Case I), and those from 90° to 180° "ascending from below" (Case II), as shown in Figure 9.1-2.

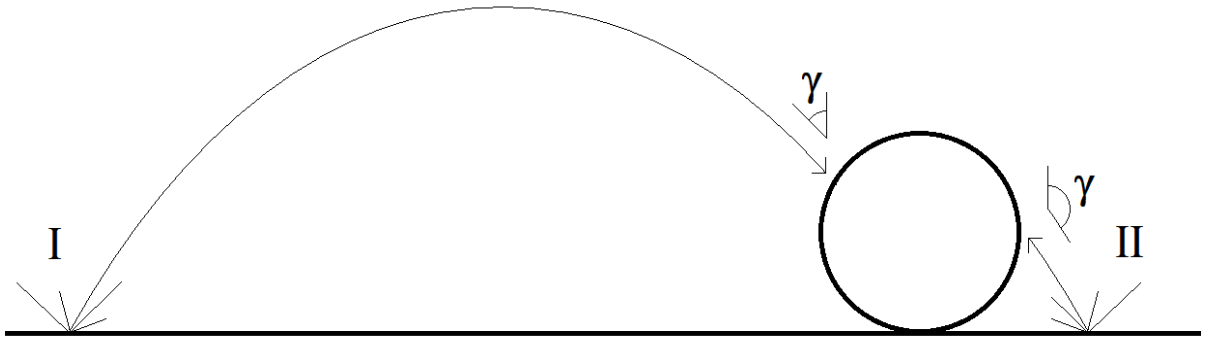

Figure 9.1-2. Two General Cases of Objects that Hit the Sphere
Case I "Descending" and Case II "Ascending"

For the cases studied, the velocity distribution was that used in MeMoSeE, with the speed distribution given by:

$$D(v)dv \propto \left(\frac{v}{v_{min}}\right)^{-2.2} dv \tag{9-2}$$

with a maximum velocity equal to the Moon's escape velocity, and a minimum velocity set at 100 m/s.

As stated, the azimuth distribution was randomized, but for the zenith angle γ distribution several different distributions were used.

Case A was a simple distribution that sheds light on the physics of this process:

$$D(\gamma) \propto \sin\gamma \cos\gamma \tag{9-3}$$

The sine term is due to the solid angle, but the cosine term is to avoid large numbers of particles created horizontally.

The second test zenith angle distribution is the one used in the MeMoSeE model:

$$D(\gamma) \propto \sin\gamma \, (\cos\gamma)^{\alpha}(1-\cos\gamma)^{1/\alpha} \tag{9-4}$$

Again, the sine term is due to the solid angle. The α term determines the peak zenith angle: $\alpha = 1$ corresponds to peak zenith angles near 60° (Case B60), and $\alpha = \sqrt{1+\sqrt{2}} \approx 1.554$ corresponds to peak zenith angles near 45° (Case B45).

Figure 9.1-3 shows a histogram of the distribution in zenith angle hitting the 500-m radius target sphere from Case A, where the directional distribution looks similar to an isotropic distribution. The histogram represents the fraction of the 2×10^{11} total ejecta particles created. Note that a large number of impacts (i.e., roughly half) are ascending from the lunar surface (i.e., zenith angles >90°). Figure 9.1-4 is a scatter plot of the relationship of the ejecta zenith angle to the range and shows that most of the ascending ejecta impacts (zenith angles > 90°) are due to nearby primary impacts. Note that the descending impacts have contributions from primary impacts distributed over the entire surface of the Moon; some from the antipode or that travel more than halfway around the Moon before striking the sphere. But those that hit ascending from the lunar surface are from primary impacts near the target sphere (i.e., within a few km).

Some primary impacts that contribute to the ejecta flux occur "beneath" the sphere. While some of these are problematical (i.e., how can there be a primary impact if the sphere blocks it?), it does show the considerable contribution of near-field ejecta relative to the more conventional descending ejecta from primary impacts far away.

Figure 9.1-5 shows the normalized distribution of these distances, broken out by whether the impacts are ascending or descending. ~15% of the total ejecta striking the sphere originate from primary impacts "beneath" the sphere, and ~70% originate from within a 10-km radius. The figure shows that most of the ejecta originate within a few tens of km of the target. Of the population that strike the target sphere "from below," virtually all are from primary impacts close to the target sphere (i.e., the simulation shows <10 km, but that precise distance is a function of the shape and size of the target). Of the population that strike the target sphere "from above," 40% come from the near field (i.e., <10 km), and most (i.e., >85%) are from distances within 100 km. Only a small fraction come from distant parts of the Moon. There are probably some geometry effects from the finite size and shape of the 500-m diameter target sphere used in the calculations that determine these precise ranges, but the general trend should be correct and should be considered illustrative of the phenomenon.

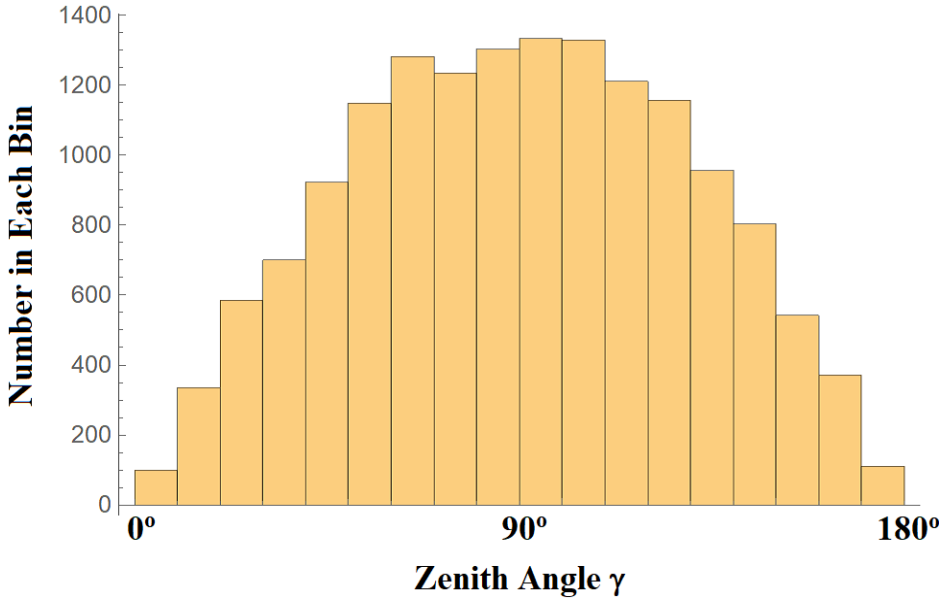

Figure 9.1-3. Histogram of Distribution in Zenith Angle Hitting 500-m Radius Target Sphere from Case A

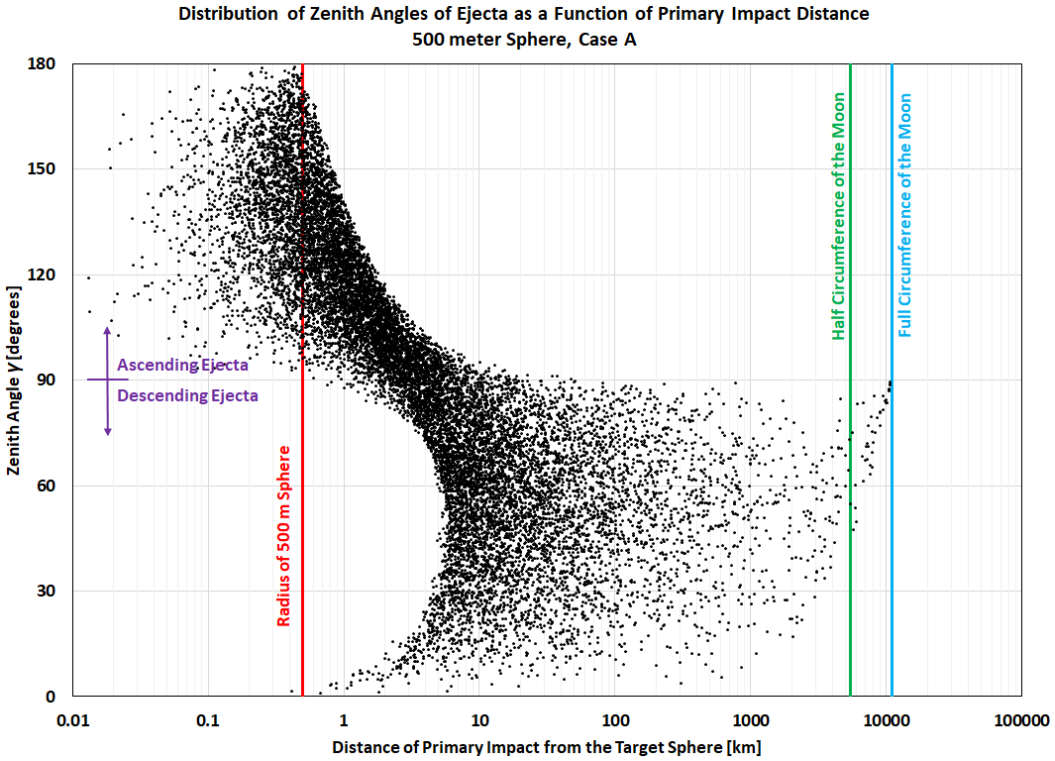

Figure 9.1-4. Computed Distribution of Zenith Angle of Ejecta as a Function of Range of Parent Impact

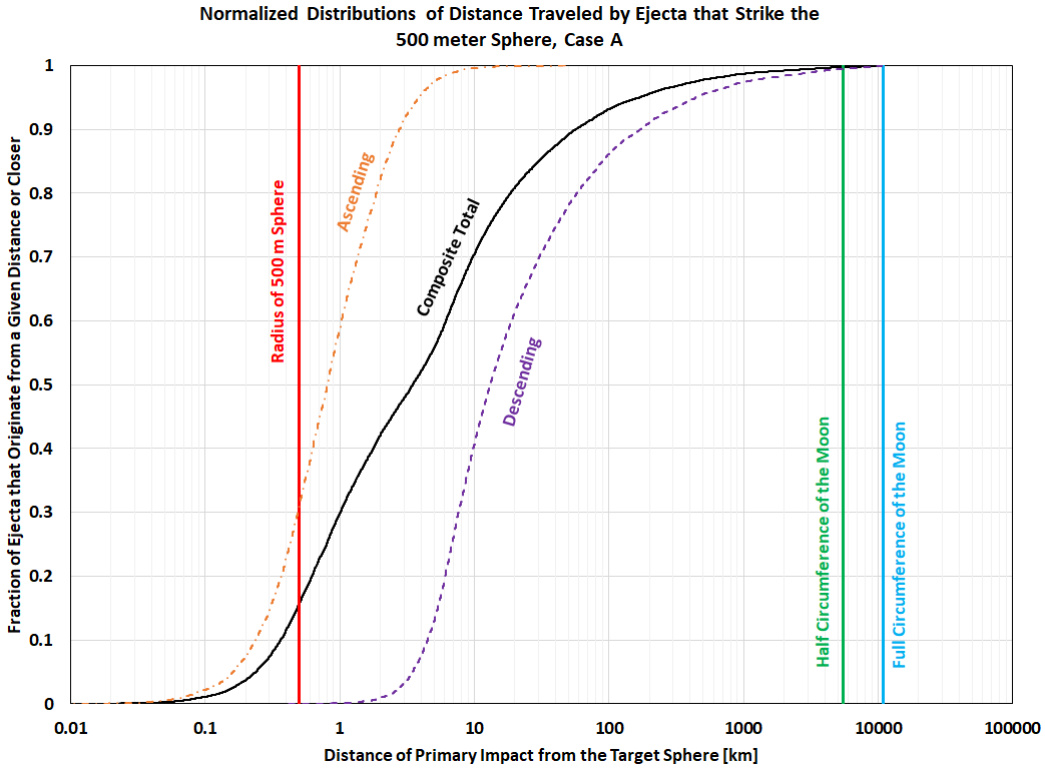

Figure 9.1-5. Normalized Cumulative Distribution of Distance to Primary Impact Location

The total number of ejecta simulated for this calculation was 2×10^{11}. Of these, 7610 hit the target from descending trajectories, which means for every ejecta particle created the probability of striking a target "from above" is approximately 4.8×10^{-14} per square meter of target. There were 7812 that hit the target sphere on ascending trajectories, with a probability of striking the targe "from below" of 5.0×10^{-14} per square meter.

The ejecta numbers are dependent on the details of the simulation. To demonstrate this, Figure 9.1-6 shows the zenith angle histogram of Case B60. Note that the shape of the distribution changes, but the fraction of descending and ascending ejecta hitting the target are of similar magnitude. The distribution in zenith angle of simulated ejecta hitting the 500-m sphere using the Case B60 direction distribution shows similar ascending/descending symmetry as in Case A. Of a total of 10^{11} total ejecta particles created, 4936 hit the target sphere on descending trajectories for a probability of 6.3×10^{-14}, and 5210 hit the target sphere on ascending trajectories for a probability of 6.6×10^{-14}. Note these numbers are slightly higher than for Case A.

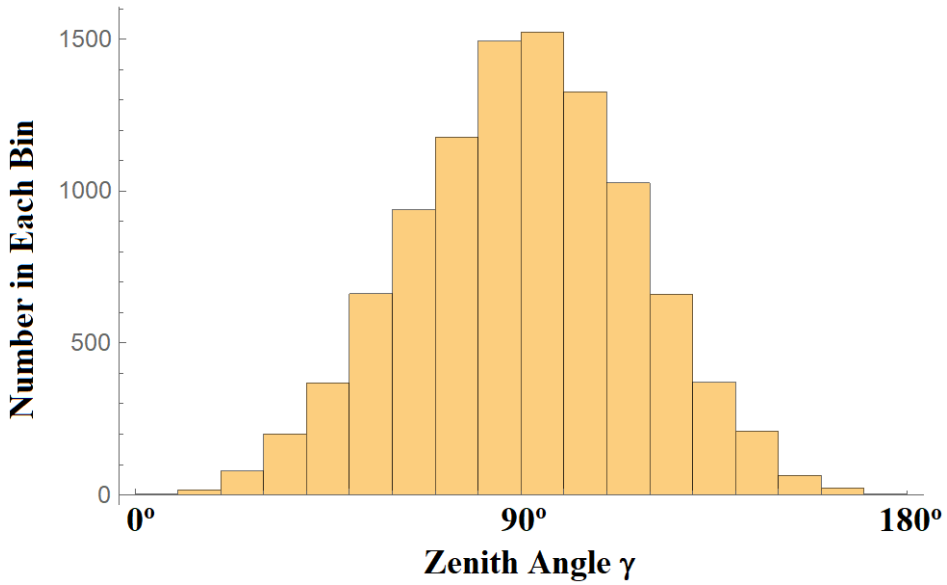

Figure 9.1-6. Zenith Angle Histogram of Case B60

For Case B45, Figure 9.1-7 shows similar symmetry for ascending and descending ejecta as the other cases, though the shape of the zenith angle distribution is different. The distribution in zenith angle of simulated ejecta hitting the 500-m sphere using the Case B45 direction distribution shows similar ascending/descending symmetry as in Case A and Case B60. Of a total of 10^{11} total ejecta particles created, 4311 hit the target sphere on descending trajectories for a probability of 5.5×10^{-14} per square meter, and 4243 hit the target sphere on ascending trajectories, for a probability of 5.4×10^{-14} per square meter.

While there are some differences depending on the detailed ejecta model chosen, the trend is the same, with similar probabilities of each ejecta particle hitting the target sphere, and approximately equivalent flux from ascending and descending trajectories.

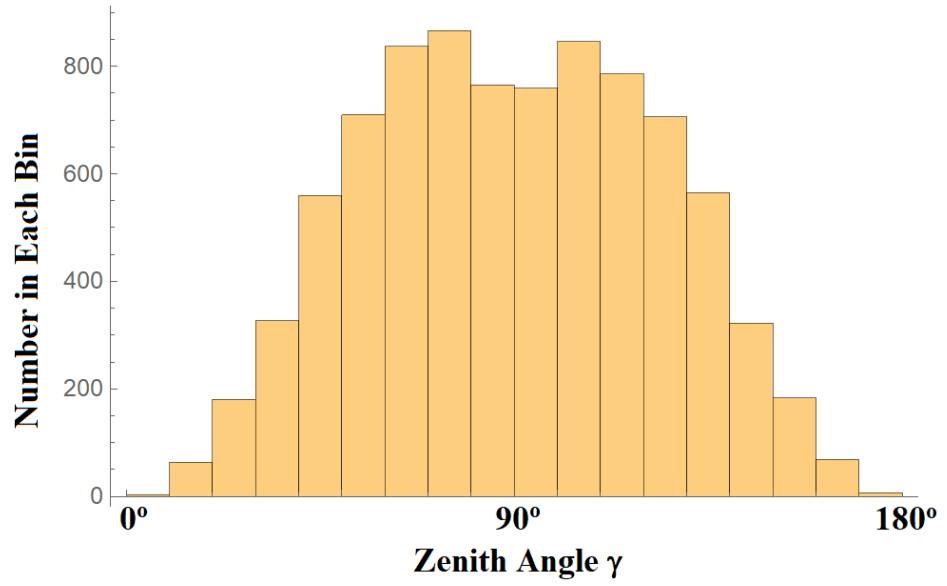

Figure 9.1-7. Zenith Angle Histogram of Case B45

One other parameter to consider is that some ejecta may leave the impact crater with velocities exceeding the Moon's escape speed. These are typically ignored for descending ejecta, as they will not re-encounter the lunar surface. However, secondaries from the near field that exceed the escape velocity can impact the target while on ascending trajectories, so limiting to speeds below the lunar escape velocity may undercount that population hitting the target "from below."

As MeMoSeE only computes ejecta from impacts at least a minimum distance away, the ascending contribution is not taken into account. While the details of primary impacts that occur "below" the asset are not clear, it is apparent that the ascending ejecta component can be of the same order of magnitude as the contribution from the more familiar long-distance descending ejecta. This means any complete ejecta model will ultimately need to include this ascending component from primary impacts near the asset.

Note that the nature of the "long-range" ejecta allows the MeMoSeE model to treat the asset in a simple manner much like orbital debris or meteoroids; only taking into account the generic projected area of the surfaces. However, if the "short-range" component is computed, then the detailed geometry of the asset may become important; especially how the asset "shadows" primary impacts from "below" it. This may mean the assumption of a sphere may not be good for a particular flux calculation for a specific asset. Therefore, the results presented are intended to show the general effects, not to be definitive computations of the relative contribution of the different types of ejecta. A thorough analysis should be based upon the size and shape of the actual asset being studied.

Finding 13: Monte Carlo techniques have been used to compute fluxes for reference cases that can be compared with the MeMoSeE algorithm for consistency.

Recommendation 12: Use the Monte Carlo flux calculation results provided to verify MeMoSeE flux calculations.

Finding 14: The flux of ascending ejecta (i.e., striking the asset "from below") is not included in the MeMoSeE model.

Finding 15: The detailed effect of the ascending component of the ejecta on an asset is dependent on the detailed shape and size of that asset.

Recommendation 13: Include ascending ejecta flux in the MEMoSeE model.

Finding 16: Ascending ejecta particles from nearby primary impacts can strike an asset with speeds greater than escape velocity, adding to the overall MMOD risk.

Recommendation 14: Include high-velocity (i.e., ≥ escape velocity) particle flux in the DSNE tables if ascending ejecta are added to the model.

9.2 Stochastic Behavior of Primaries

This Monte Carlo method of simulating average numbers of impacts may help reveal the effects of another phenomenon. Primary impacts by larger impactors are rare, but primary impacts by smaller impactors are more common and behave more like a constant "rain" over the lunar surface. Primary impacts that contribute a large probability to impact risk are those close to the asset. For very large impactors, the probability of hitting within a short distance of the asset during a finite time is low, but the risk contribution of such rare events is high. Using the distribution in Figure 9.1-5 for the descending population, it is possible to simulate a number of finite time intervals and see the variability of the flux. Figures 9.2-1 through 9.2-3 show the

results of such a simulation. Each case uses a different expectation value of the number of primary impacts.

The Monte Carlo procedure used was:

1. An integer number of primary impacts is generated from a Poisson sample of the expectation value (e.g., 10.0, 100.0, and 1,000.0).
2. Those primary impacts are distributed randomly around the Moon.
3. For each primary impact, the probability of an ejecta impact on the sphere is computed using the curve in Figure 9.1-5.
4. The probability is summed and compared to the average value.
5. The process is repeated at step 1 until a sufficient number of Monte Carlo runs have been completed.

Figures 9.2-1 through 9.2-3 show the distributions in these fluxes for each random pattern of primary impacts scaled to the mean value, considering only the descending component of the flux.

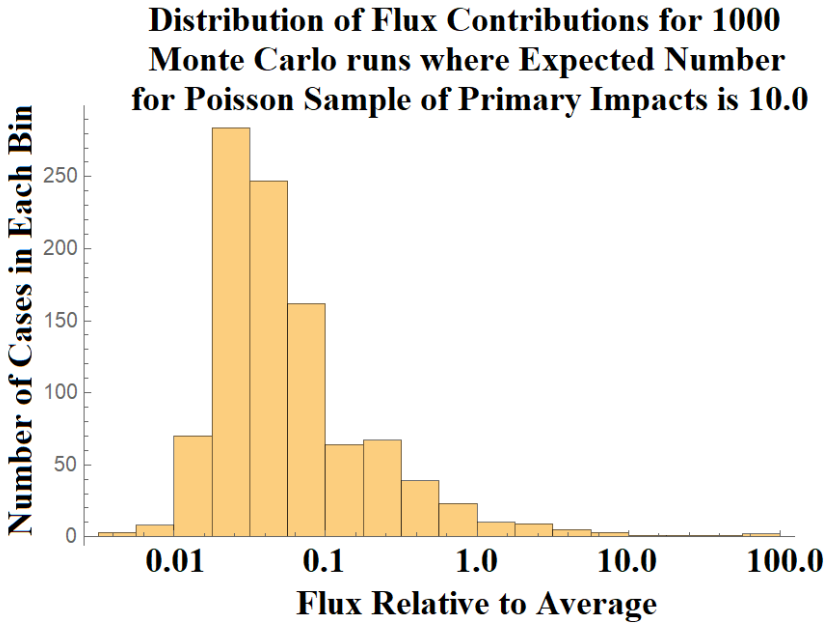

Figure 9.2-1. Range in Possible Flux Values Scaled to Average Descending Flux for an Average of 10.0 Primary Impacts Randomly Distributed Over the Surface of the Moon

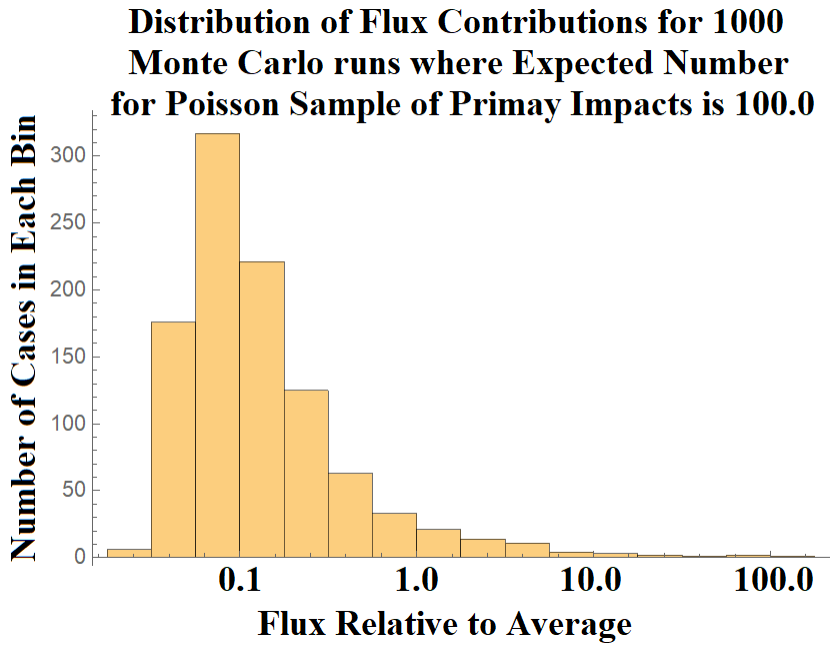

Figure 9.2-2. Range in Possible Flux Values Scaled to Average Descending Flux for an Average of 100.0 Primary Impacts Randomly Distributed Over the Surface of the Moon

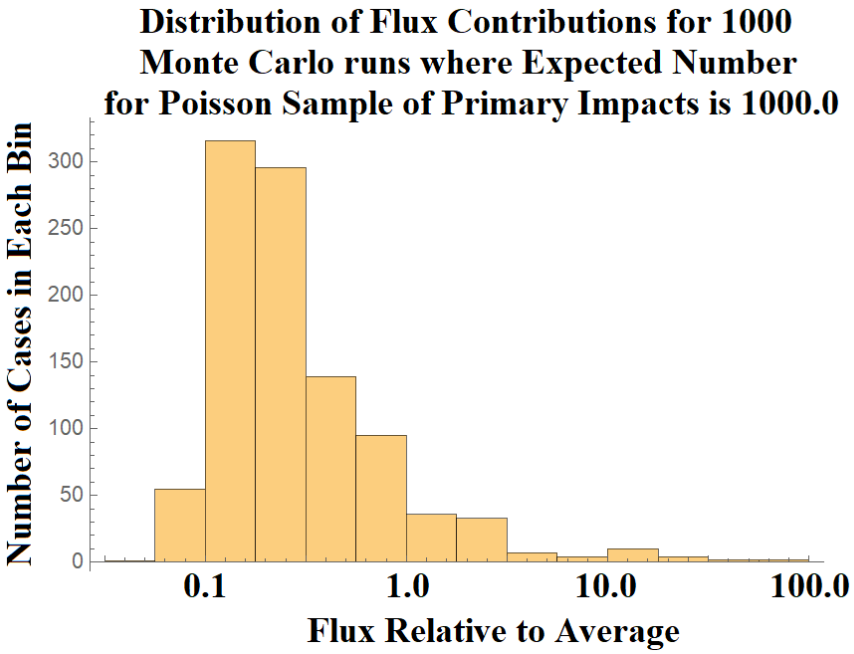

Figure 9.2-3. Range in Possible Flux Values Scaled to Average Descending Flux for an Average of 1000.0 Primary Impacts Randomly Distributed Over the Surface of the Moon

For the expectation value = 10.0 case, most of the sampled case have flux lower than the computed average value, but about 3% of the cases have primary impacts near the asset, giving fluxes higher than the average value. This skewed distribution is affecting the mean values, with a minority of cases giving flux much greater than the mean. For the expectation value = 100.0 case, about 6% of the cases have fluxes higher than the average. For the expectation value = 1,000.0 case, about 10% of the cases have flux higher than the average.

The average flux is driven by these rare close impacts, but only a small fraction of cases have higher-than-average flux. Interestingly, the more expected total number of primary impacts, the higher the chance of higher-than-average flux and lower the probability of much lower-than-average flux. This dramatic variability is more dynamic than what are typical for Poisson statistics. It is not clear that traditional average fluxes are the correct metric for computing risk in such a system. Note that the contribution of ascending flux from nearby primary impacts has not been included. The stochastic variability from this population is likely even more dynamic.

Finding 17: The stochastic nature of the primary impact flux location, combined with the strong dependence of the flux on distance from the asset, means that for any finite length of time, the number of secondaries impacting an asset may vary by several orders of magnitude from the average value.

Recommendation 15: Consider modifying the MeMoSeE model to use Monte Carlo methods in addition to or in lieu of analytic methods to compute the stochastic variability of the flux.

Recommendation 16: The manner in which the flux results are tabulated and reported in the DSNE should be reconsidered, perhaps to include mean, median, and extreme cases (such as 95% confidence levels for maximum flux) suitable for incorporation into a Probabilistic Risk Assessment.

10.0 Risk Model Sensitivity

An important aspect of how useful the MeMoSeE model will be in specifying lunar ejecta environments and their risk to lunar systems is the variability of the model outputs. This section examines sensitivity of the model outputs to the model inputs and assumptions.

10.1 Variability in Time and Space

In addition to the stochastic behavior described, the MeMoSeE model includes the effects of variable primary impactor fluxes at different regions of the Moon and at different times. These will lead to different ejecta fluxes for different mission scenarios. This raises questions about which scenarios should be included in the DSNE tables.

Tests with the MeMoSeE model indicate that temporal variations can vary up to a factor of 2. Different lunar latitudes/longitudes can give ejecta variations of up to a factor of 5, but averaging over local time, these will be reduced to a factor of 2.

However, these variations are mostly swamped by the stochastic behavior outlined in the prior sections, where the random variability can be orders of magnitude. As with the stochastic variations, the tables in the DSNE will need to include “average” and “worst-case” scenarios or split into percentiles. The time averages could include results from more “typical” missions (e.g., 7 days), rather than only a generic long-term average.

Finding 18: The ejecta flux can be non-uniform over different geographical regions of the Moon and at different times. Temporal variations are typically factors of 2, and variations with latitude/longitude are typically factors of 5, but closer to factors of 2 when averaged over local time. However, these variations are still orders of magnitude smaller than stochastic variations.

Recommendation 17: Reconsider choosing what is the “average” location/time on the Moon vs choosing several example locations for the DSNE (e.g., at different longitudes or use 7-day intervals rather than average 19 years).

10.2 Relative Contribution of Large Versus Small Impactors

MeMoSeE uses the equation from Table 1 of reference 20 to compute the total mass ejected at a speed of v or greater by an impacting particle:

$$M_{>v} = C_4 m_p \left(\frac{v}{v_p \sin\alpha}\right)^{-3\mu} \left(\frac{\rho}{\rho_p}\right)^{1-3\nu} \tag{10-1}$$

where

$$C_4 = \frac{3k}{4\pi} C_1^{3\mu} \tag{10-2}$$

In these equations, m_p is the mass of the projectile, v_p is its speed, and ρ_p is its density. The quantity α is the impact angle, measured from the local horizon, and ρ is the density of the regolith and ejected particles, which is assumed to be 3,100 kg m^{-3}. The quantities $\mu = 0.4$, $\nu = 0.4$, $k = 0.3$, and $C_1 = 0.55$ are material-specific constants for sand-fly ash (see Table 3 of reference 20); these values are not specified in reference 21, but are identified in reference 45. Particles with speeds less than 0.1 km s^{-1} are not included in the proposed DSNE edits [ref. 45], and so this is taken as the speed threshold for all calculations in this section. The total mass is partitioned into individual particles using a separate equation that does not depend on projectile properties.

From Eq. 10-1, it can be seen that the total mass of incoming particles is the key factor in determining the mass and number of ejected particles. As discussed in Section 7, the flux of incoming meteoroids is obtained using MEM 3, [ref. 12], which is proportional to Eq. A3 of reference 35. The flux of larger particles is derived from the flux of large objects onto the Earth's atmosphere [ref. 14], after accounting for the difference in gravitational focusing between the Earth and the Moon [ref. 15]. The two flux curves are presented in Figure 10.2-1; the solid blue curve presents the meteoroid flux obtained using MEM, while the dashed orange curve is the NEO flux derived from reference 14.

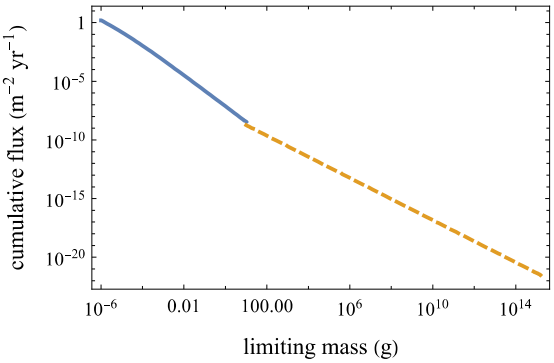

Figure 10.2-1. Flux of Particles of a Given Mass or Larger onto the Moon

While these sources provide the number flux of particles (f), the total incoming mass flux in the mass range (m_1, m_2) can be obtained as:

$$M_{1,2} = \left|\int_{m_1}^{m_2} \frac{df}{dm} m\, dm\right| \tag{10-3}$$

The absolute value of this integral is taken so that m_1 or m_2 can be greater. The MeMoSeE model includes primary impactors ranging from 110 μg in mass [ref. 26] to 1,000 m in diameter,

which, for an assumed NEO density of 3,000 kg m^{-3}, corresponds to a mass of 1.57×10^{12} kg. Figure 10.2-2 presents the mass flux of meteoroids lighter than $m_1 = 10$ g and NEOs heavier than $m_1 = 10$ g as a function of m_2, highlighting MeMoSeE's chosen limits. Again, the flux corresponding to meteoroids appears as a solid blue line and that of the NEO impacts appears as a dashed orange line. The mass shown is that of impacting objects that are between 10 g and the mass limit depicted on the ordinate axis. The nominal limits used by the MeMoSeE model are marked with solid black circles. The mass of a particle that hits the lunar surface an average of once per year is marked with an open circle, and the mass of a particle that cannot produce ejecta larger than 5 mm in diameter is marked with an open triangle.

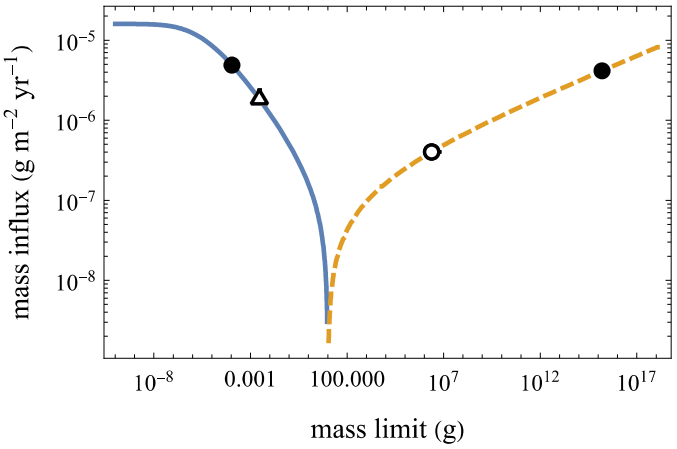

Figure 10.2-2. Mass Flux onto Lunar Surface from Meteoroid and NEO Impacts

Several pieces of information can be obtained from Figure 10.2-2. First, the current lower mass limit of 110 μg used by the MeMoSeE model does not capture most of the incoming meteoroid mass. If arbitrarily small particles are included in the mass flux calculation, then the total incoming mass would increase by 123%. However, these particles are unlikely to produce ejecta that are large enough to be hazardous. For large objects, the incoming mass continues to increase as the upper mass limit is raised. However, the upper mass limit used by the MeMoSeE model (i. e., 1.57×10^{15} g) is substantially larger than the maximum NEO mass that impacts the Moon annually (i.e., 2.38×10^{6} g). If the mass influx calculation is restricted to those objects that hit the Moon at least once per year on average, then a mass flux would be obtained that is about 40% lower than that obtained using MeMoSeE's nominal limits.

While Figure 10.2-2 characterizes the incoming mass, the amount of ejecta produced depends on the impactors' speeds, densities, and impact angle. So long as projectile speed, mass, and density are not correlated in the models of incoming particles, which is true if the high- and low-density populations in MEM are analyzed separately, then the estimated the total mass of ejecta produced is:

$$M_{>v} = C_4 m_p \left\langle \left(\frac{v}{v_p}\right)^{-3\mu} \right\rangle \left\langle \left(\frac{\rho}{\rho_p}\right)^{1-3\nu} \right\rangle \langle \sin^{3\mu} \alpha \rangle \qquad (10\text{-}4)$$

A MEM run using a "trajectory" in which the state vectors traced the position and motion of points on the lunar surface was performed. The outputs provide the speed and density distribution of two populations (i.e., high- and low-density) of meteoroids striking the Moon. The NEO speed distribution is taken from Moorhead [ref. 15] and the density is assumed to be 3,000 kg m^{-3}, following Brown et al. [ref. 14] and DeStefano [ref. 21].

For both meteoroids and NEOs, the angular term is computed as:

$$\langle \sin^{3\mu} \alpha \rangle = \frac{2\pi \int_0^{\frac{\pi}{2}} \cos^{3\mu} \phi \cdot \cos \phi \sin \phi}{2\pi \int_0^{\frac{\pi}{2}} \cos \phi \sin \phi} = \frac{5}{8} \tag{10-5}$$

where $\phi = \frac{\pi}{2} - \alpha$ is the central angle between the impactor's sub-radiant point and a given location on the Moon. This gives the impact angle raised to the power of 3μ, averaged over the lunar surface and expressed relative to the incoming flux. Figure 10.2-3 presents the results of ejected mass calculation for meteoroid (i.e., solid blue) and NEO (i.e., dashed orange) impacts. The mass shown is that produced by impacting objects that are between 10 g and the mass limit depicted on the ordinate axis. The nominal limits used by the MeMoSeE model are marked with solid black circles. The mass of a particle that hits the lunar surface an average of once per year is marked with an open circle, and the mass of a particle that cannot produce ejecta larger than 5 mm in diameter is marked with an open triangle.

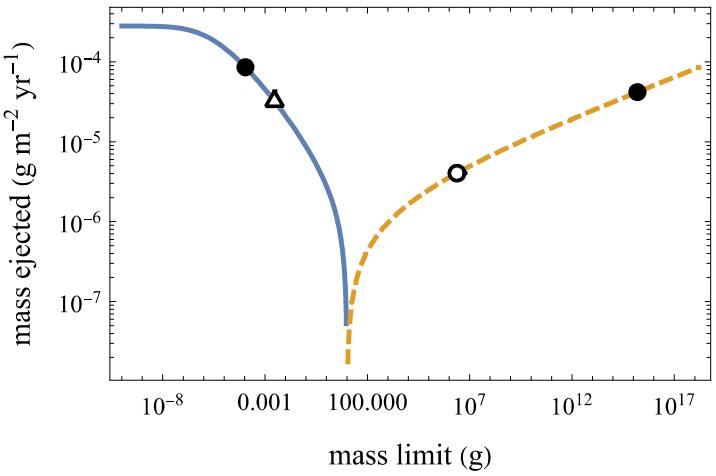

Figure 10.2-3. Mass of Particles Ejected from Lunar Surface Due to Meteoroid and NEO Impacts

It is apparent in Figure 10.2-3 that the mass of the ejected particles exceeds that of the primary impactors by an order of magnitude. This factor depends on the speed and density distribution of the incoming particles. The comparatively slow-moving NEOs excavate 10 times as much mass as impacts the Moon, while the fast, low-density meteoroid population excavates nearly 20 times their mass.

More importantly, the relative importance of meteoroids and NEOs in ejecta production can be assessed. Using MeMoSeE's nominal limits of 110 μg and 1.57×10^{12} kg, it is found that meteoroids are responsible for 54% of ejected particles. If particles larger than 2,400 kg (i.e., those too large to impact the Moon each year) are excluded, then the total ejected mass is 30% lower and 95% of it is produced by meteoroid impacts. Thus, the current upper mass limit for NEOs is conservative, at least on average, but the degree of conservatism is modest.

The MeMoSeE model does not appear to truncate the ejecta particle size distribution depending on the primary impactor size. Instead, the model allows small impacts to produce large particles. According to DeStefano [ref. 21], the fraction of ejected particles larger than a given size, x, is:

$$P_{>x} = e^{-\frac{1}{ax^b + cx^d}} \tag{10-6}$$

where x must be in units of mm, and the constants are $a = 0.0548$, $b = -1.015$, $c = 0.337$, and $d = -0.2518$ [ref. 21]. No upper limit is incorporated into Eq. 10-6, which is Equation 2.7 of reference 21. However, an upper limit of 10 mm is used to normalize the probability density function (Equation 2.8 of reference 21). Note that Eq. 10-6 contains no dependence on impactor properties, or the total amount of ejecta produced. Thus, according to the MeMoSeE model, 1.43% of the mass ejected by any impact above the 0.1 km s^{-1} minimum speed will be larger than 5 mm in diameter, regardless of the impactor size.

If arbitrarily small impactors are included in the ejected mass calculation, then the total ejected mass will be increased by 153%. Note this increase is larger than the 123% increase calculated for the total *incoming* mass. If the size distribution of ejected particles is independent of the incoming particle mass, then this would increase the total quantity of hazardous ejecta. However, conservation of energy dictates that the largest ejecta particle that can be lifted by an incoming dust particle is:

$$m_e = m_p \frac{v_p^2}{v_e^2} \tag{10-7}$$

where m_p is the mass of the incoming particle, v_p is its speed, and v_e is the speed of the ejected particle. As discussed in Section 10.5, ejected particles 5 to 10 mm in diameter are capable of damaging manmade assets. If the collision is completely inelastic and $m_e = 0.2$ g (i.e., the mass of a 5-mm-diameter particle with a density of 3,100 kg m^{-3}) is set, $v_p = 70$ km s^{-1}, and recall that $v_e = 0.1$ km s^{-1}, then $m_p = 4.1 \times 10^{-7}$ g, which is smaller than MeMoSeE's lower limit.

However, if it is assumed that the mass of the largest particle is constrained by Eq. 10-1, then an ejected particle of 0.2 g corresponds to an impactor mass of 2.9 mg. This is assuming a normal impact and that the impactor belongs to the low-density population in MEM, which is marked with an open triangle in Figures 10.2-2 and 10.2-3. This is larger than the 110 μg mass lower limit used by the MeMoSeE model, and indicates that the model may be overconservative in attributing part of the mass ejected by smaller particles to the hazardous ejecta flux.

Thus, if the maximum particle size is limited by the conservation of kinetic energy, the MeMoSeE model may be underestimating the quantity of hazardous ejecta by more than a factor of 2, and by not considering particles smaller than 110 μg. If the maximum particle size is limited by Eq. 10-1, then the MeMoSeE model is overestimating the quantity of hazardous ejecta by a factor of 3 to 4.

One practical way to limit maximum projectile size is to identify the size of impactor that has a 1% chance of hitting the Moon during a nominal mission time. For a 10-year lunar base mission, this corresponds to a mean time between impacts of 1,000 years. Alternatively, a Monte Carlo analysis with the full range of possible sizes might capture this effect without artificially limiting impactor size.

Finally, it is noted that references have been interpreted to "size" in references 21 and 26 as the diameter of a spherical particle. If these sizes are radii or some other measure, then the results identified in this section will change.

Finding 19: The MeMoSeE model may be overconservative in computing the quantity/mass of ejecta produced by including large NEO sizes that rarely impact the Moon.

Recommendation 18: Limit the maximum primary impactor size used to compute the ejecta or use a Monte Carlo technique to accurately incorporate large impactor effects.

Finding 20: The MeMoSeE model may produce estimates of the hazardous ejecta flux that are a factor of 3 to 4 too high because it assumes the mass of the largest particle ejected by an impact can exceed the total ejected mass predicted in reference 20.

Recommendation 19: Consider placing an upper limit on the ejected particle size determined from conservation of energy and/or the ejecta mass.

10.3 Sporadic Versus Shower Meteoroid Contribution to the Ejecta Flux

By using MEM, a sporadic meteoroid model, to compute the flux of incoming meteoroids, the MeMoSeE model excludes meteor showers from the impactor population. This mimics the approach taken by the NASA Meteoroid Environment Office, in which sporadic meteoroids are included in engineering models, and any short-term enhancements in the flux produced by these showers are provided separately in "forecasts." The reasoning behind this approach is that meteor showers produce a small fraction (i.e., a few percent) of hazardous particles on average, and thus do not merit inclusion in MEM. However, these showers can occasionally produce short-term enhancements of the flux that can be relevant during short periods of increased vulnerability (e.g., space walks).

However, meteor showers tend to be more heavily skewed toward large particles than the sporadic complex. Thus, it is possible that while showers contribute only a small portion of the *number* flux of meteoroids, they could contribute a more substantial fraction of the mass flux. To test this, an existing estimate of the mass flux of the Geminid meteor shower computed in Blaauw was used [ref. 26]. Table 2 of reference 46 gives this flux as 9.1×10^{-4} g km^{-2} hr^{-1} when the largest particles considered have a mass of 1 kg. After performing a unit conversion and dividing by 4 to convert this to the flux per unit lunar surface area, a value of 2.0×10^{-6} g m^{-2} yr^{-1} at the time of the shower's peak is obtained. This is 22% of the nominal mass influx. If a Geminid speed of 35 km s-1 and density of 2600 kg m^{-3} are used [ref. 46], then a mass production rate of 4.8×10^{-5} g m^{-2} yr^{-1} is obtained, which is 37% of the nominal rate. Thus, at the time of peak activity, the Geminid meteor shower could substantially increase the ejecta production rate (and indeed, this phenomenon appears to have been observed by LDEX [ref. 34]).

Reference 46 provides Geminid fluences (e.g., 271 g km^{-2}), which can be used to compute the contribution of this meteor shower when averaged over the course of a year (i.e., 6.8×10^{-8} g m^{-2} yr^{-1}). Thus, on average, the Geminid meteor shower constitutes 0.7% of the incoming mass and produce 1.3% of the ejected mass. These calculations do depend on the largest Geminid considered. If, for instance, Geminids as large as 100 kg in mass is included, then these Geminid rates will be a factor of 4 larger [ref. 46].

The small contribution of the Geminid stream to the overall ejecta production rate justifies their exclusion from an average environment description. The Geminids produce the greatest flux of hazardous meteoroids in a typical year [ref. 47] and have produced both large numbers of lunar impact flashes and spikes in lunar impact ejecta measured by LDEX [ref. 48]. If they are not capable of raising the average ejecta production rate by more than a few percent, then it is not likely that any other shower will.

While the analysis in this section concludes that the small contribution of Geminids justifies neglecting all meteor showers in MeMoSeE, there are some showers that might still be important, such as the daytime β Taurids that produced outbursts of meteoroids possessing sufficient impact energy to be detected by the Apollo seismometers left on the Moon in the 1970s [ref. 49].

Finding 21: The consideration of a single meteor shower, no matter how intense, is not sufficient to dismiss the contributions of meteor showers to ejecta production.

Recommendation 20: Developer should work with experts from NASA's Meteoroid Environment Office to reevaluate potential contributions from meteor showers to the ejecta environment.

10.4 Effect of Depth of Excavation on Soil Size Distribution Ejected from Crater

The MeMoSeE model assumes that comminution and agglutination in a single sporadic or NEO impact is sufficiently small to leave the regolith particle distribution unchanged, hence the *in situ* soil size distribution equals the ejecta particle sizes.

The lunar regolith constitutes the uppermost 10 meters of the maria and the upper most 30 meters of the lunar highlands. Sufficiently energetic sporadic meteoroids and NEOs will punch through the regolith into material with a different size distribution and launch that material as ejecta. Knowledge of the layers below the regolith comes from seismic studies. Figure 10.4-1 is a summary of the suspected layering based on sound speed measurements [ref. 3].

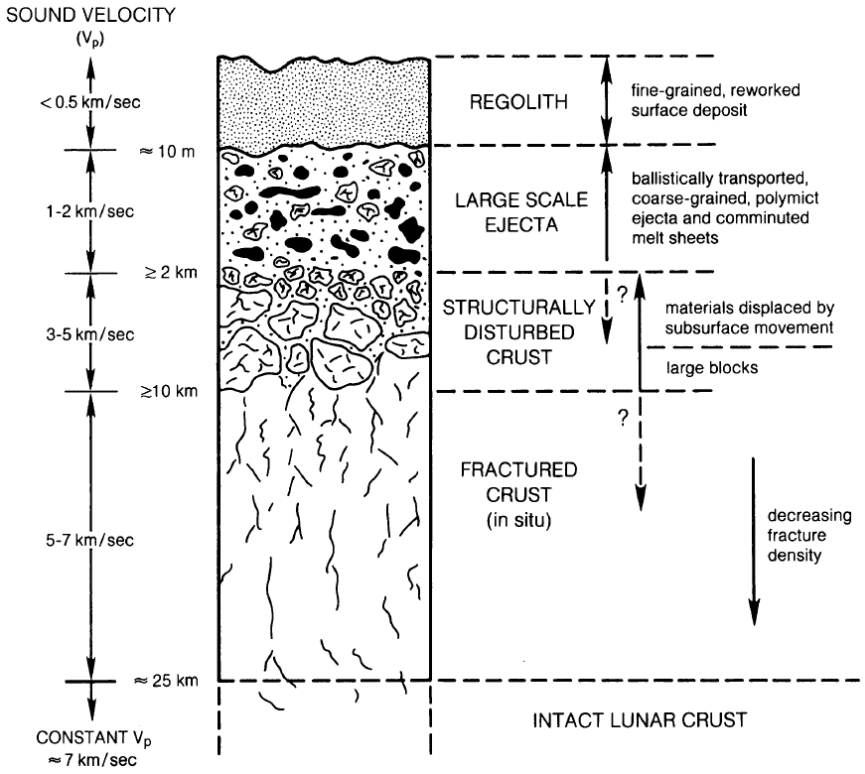

Figure 10.4-1. Schematic Cross-Section Illustrating Idealized Effect of Large-Scale Crater on Structure of Upper Lunar Crust [ref. 3]

The material between 10-m and 2-km depth has a sound speed more than 4 times larger than the regolith sound speed indicating larger particles and less porosity. However, the NESC assessment team is unaware of any estimates of the particle size distribution for these depths.

What follows in Subsection 10.4.1 is an overview of Apollo Program regolith particle size distribution measurements and how they vary between the Apollo landing sites. Subsection 10.4.2 is an estimate of the effect of the site variations on the lunar ejecta flux environment. Subsection 10.4.3 is an overview of the lunar crater dimension scaling, and Subsection 10.4.4 uses the dimension scaling to estimate the portion of the lunar ejecta flux calculation that is uncertain from the unknown size distribution for depths greater than 10 m.

10.4.1 Lunar Regolith Size Distribution

Figure 10.4-2 shows the distribution of particle sizes measured from four Apollo landing site samples.

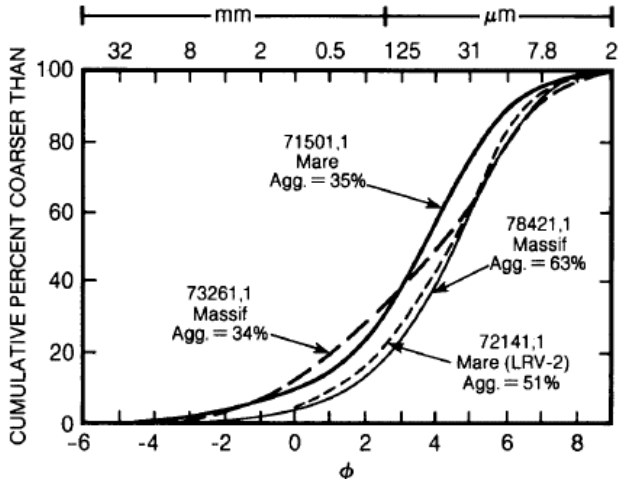

Figure 10.4-2. Cumulative Size-Frequency Diagram for Typical Lunar Surface Soil Samples [ref. 3]

The parameter φ (i.e., the Krumbein phi scale [ref. 50]) is defined as:

$$\varphi = -\log_2(d \text{ in mm}) \tag{10-8}$$

The corresponding diameters are listed across the top of Figure10.4-2. The regolith particle sizes are typically distributed with a normal probability density:

$$D(d) = \frac{1}{\sqrt{2\pi}\sigma}\exp[-(\varphi - M)^2/(2\sigma^2)] \tag{10-9}$$

Where M is the mean grain size, and σ is the standard deviation.

A number of researchers [refs. 3 and 51] have measured the parameters M and σ for various Apollo 17 samples and have characterized the sample ordered pairs (M, σ) as mature, submature, and immature as shown in Figure 10.4-3.

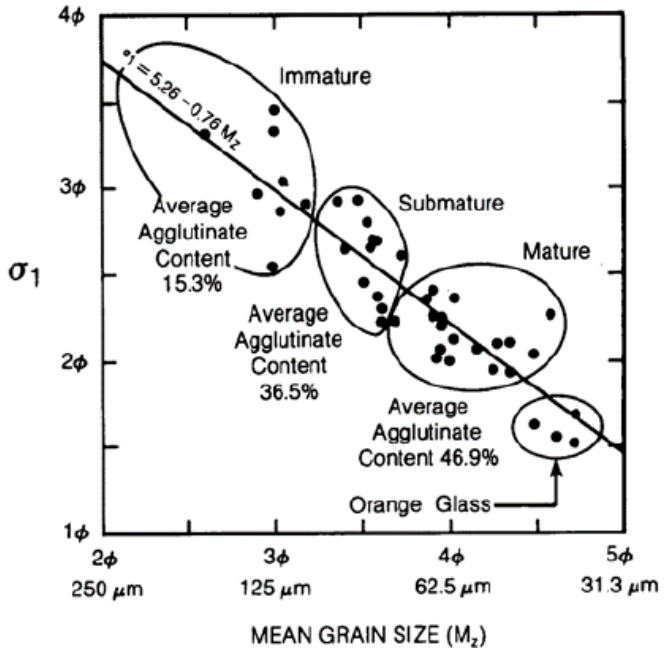

Figure 10.4-3. Relationship Between Grain Size, Sorting, and Agglutinate Content for 42 Apollo 17 Soils (ref. 52 as cited by ref. 3)

Maturity is a quantity roughly equivalent to age. Lunar soils change significantly over time, and a highly mature soil has the largest degree of comminution and melting [ref. 3]. Thus, the smallest regolith depths have the smallest mean grain size due to the large number of small impacts over time. Furthermore, the largest regolith depths have the largest mean grain size due to the smaller number of impacts that can penetration to 10-m depth.

However, the Apollo 16 core samples (i.e., 60-cm to 3-m core samples) showed no clear trend of change in mean grain size with depth. Reference 3 concluded that:

> *In summary, the analysis of regolith core samples has shown that regolith properties vary in a complex and not entirely predictable way with depth. A trend to coarser-grained samples with depth is present in some of the cores (e.g., Apollo 16), but there are exceptions* (e.g., Luna 24).

The MeMoSeE model uses the soils size distribution from Carrier [ref. 51]. This reference fit 4,500 points from 350 particle size analyses. These soil samples were obtained from seven lunar landing sites: Apollo 11, 12, 14, 15, 16, and 17; and Luna 24. Carrier recommended one soil size distribution, plotted as the gold solid curve on the righthand side of Figure 10.4-4. Note that this curve is close to the submature curve from reference 3 (center filled circle on the righthand side of Figure 10.4-4). Carrier plotted plus and minus one standard deviations, which are plotted in Figure 10.4-4 as the gold broken lines. These curves enclose the mature soil distributions, except at the largest particle diameters. The immature soil size distribution lies outside one standard deviation from Carrier's fit.

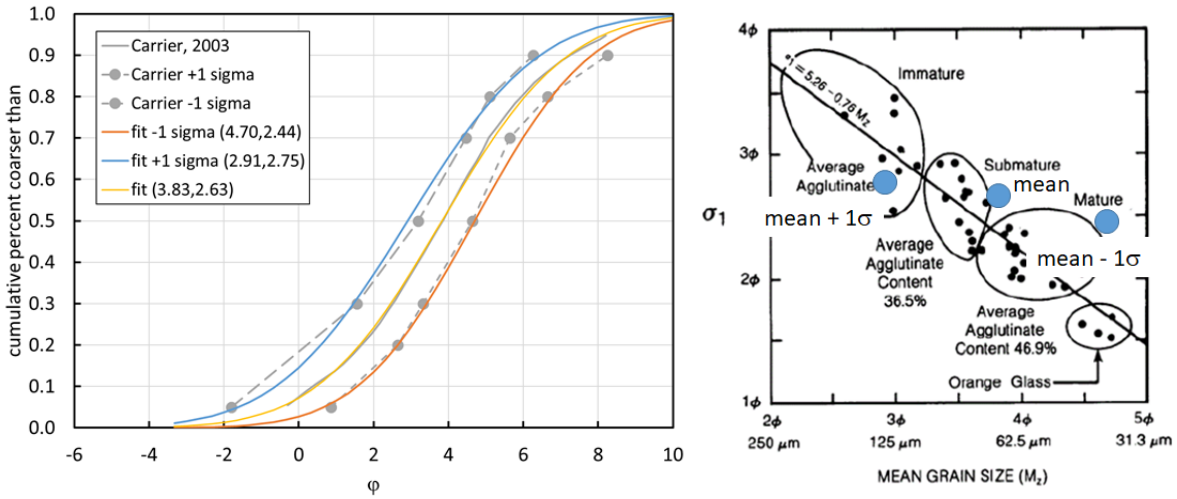

Figure 10.4-4. Comparison of Soil Size Distributions

An (M, σ) pair of (2.91, 2.75) provides a reasonable fit to the upper Carrier distribution, and a pair of (4.70, 2.44) provides a reasonable fit to the largest size soil particles in the lower Carrier distribution.

Finding 22: The MeMoSeE model uses a soil size distribution characteristic of a single submature soil.

10.4.2 Effect of Lunar Regolith Size Distribution on the Ejecta Flux

The MeMoSeE model procedure of using the same size distribution for all depths is considered reasonable because there is no clear trend of change in mean grain size with depth. However, the Apollo core samples show a range of size distribution parameters, hence a sensitivity study is warranted. This section is a preliminary sensitivity analysis using a simplified analysis that can be used as a verification artifact for the MeMoSeE model analysis.

The sensitivity analysis assumes the following:

1. The moon is a flat surface
2. No NEO contribution
3. Sporadics impact uniformly and normal to the lunar surface
4. Sporadics impact at 20.3 km/s
5. Sporadics flux onto the lunar surface is equal to the Grun flux onto a randomly tumbling flat sheet
6. All ejecta is launched at 45°
7. The soil-particle density is 3,100 kg/m^3
8. The soil bulk density is 1,500 kg/m^3
9. Housen's ejecta mass as function of ejection speed cumulative distribution with a coefficient of 0.018 and a slope of –1.23 (i.e., values for dry soils such as dry sand, lunar regolith, and dry terrestrial desert alluvium [ref. 53])

Figure 10.4-5 is the plot of the calculated variation in flux with soil size distribution parameters.

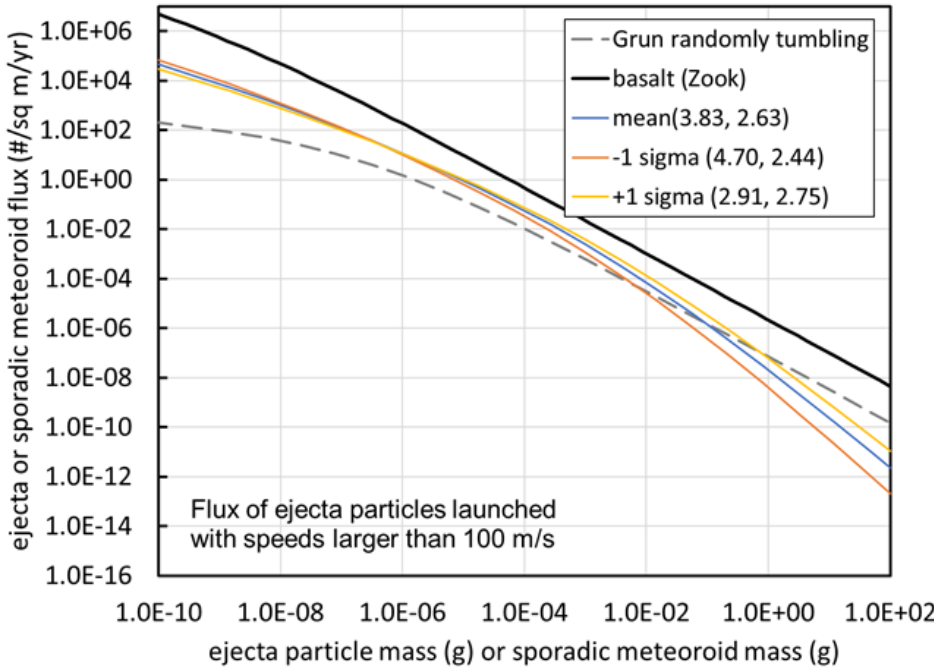

Figure 10.4-5. Ejecta Flux Distribution Sensitivity to Soil Size Distribution Parameters

The plotted Grun flux is the flux on a randomly tumbling flat sheet. The ejecta flux is the flux through an upwards facing flat sheet lying on the lunar surface. The solid black curve used the Gault and Shoemaker ejecta size relation and ejecta speed relation for basalt cratering. This curve should match the NASA SP-8013 ejecta model when summing all three speed bins.

The ordered pairs next to the mean and plus or minus one sigma legend entries list the mean and standard deviation (M,σ) of the soil size distribution.

Figure 10.4-5 shows that the ejecta flux relation is insensitive to the soil size distribution for ejecta particle masses less than 10 µg (i.e., diameters less than 183 µm). However, at the sizes of interest to spacecraft protection (i.e., 1 mm to 4.5 mm, or 2 mg to 150 mg), the –1 sigma flux is a factor of 0.48 to 0.24 smaller than the mean and the +1 sigma flux is a factor 1.6 to 2.6 larger than the mean. While perhaps not the largest uncertainty in the analysis, there appears to be a number of these smaller factors that should be accumulated to determine a worst-case flux.

Finding 23: A worst-case regolith particle size distribution can result in an ejecta flux that is 1.6 to 2.6 times larger (at the sizes of most interest to HLS) than the MeMoSeE flux calculated with the average regolith particle size distribution.

Recommendation 21: Perform a sensitivity study varying the soil size distribution parameters over the range of measured soil size distributions of the Apollo Program soil samples.

10.4.3 Crater Dimension Scaling

Holsapple's crater dimension scaling relations [ref. 44] are the basis of the present estimate of the maximum depth from which ejecta originates during an impact by sporadic meteoroids. Holsapple's crater volume relation for simple craters is:

$$\pi_V = K_1 \left\{ \pi_2 \left(\frac{\rho}{\delta}\right)^{\frac{6\nu-2-\mu}{3\mu}} + \left[K_2 \pi_3 \left(\frac{\rho}{\delta}\right)^{\frac{6\nu-2}{3\mu}} \right]^{\frac{2+\mu}{2}} \right\}^{\frac{-3\mu}{2+\mu}}, \tag{10-10}$$

where,

$$\begin{aligned} \pi_V &= \frac{\varrho V}{m} \\ \pi_2 &= \frac{ga}{U^2} \\ \pi_3 &= \frac{Y}{\varrho U^2} \end{aligned} \tag{10-11}$$

The variable V is the excavation crater volume, ρ is the lunar regolith bulk mass density, m is the impacting meteoroid mass, a is the impacting meteoroid radius, δ is the impacting meteoroid bulk mass density, U is the impact speed, Y is the lunar regolith strength. The parameter μ is the coupling parameter speed exponent and has the value 0.55. The parameter μ is weakly dependent on the Mie-Gruneisen equation of state parameters, but strongly dependent on the target porosity. Soils can have values around 0.41 while basalt has a value around 0.55. The parameter ν is the coupling parameter target density exponent and has the value 0.4 for all materials.

Figure 10.4-6 illustrates the cross section of a simple crater.

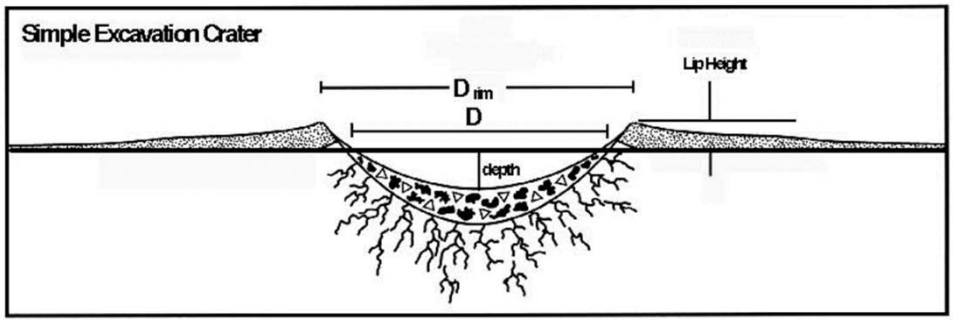

Figure 10.4-6. Dimensions of a Simple Crater [ref. 54]

The crater volume is the void between the plane of the original surface and the profile of the apparent crater. The depth of the crater is maximum vertical distance between the plane of original surface and the profile of the crater, and the crater diameter D is its diameter at the original surface as shown in Figure 10.4-6.

Holsapple's crater dimension scaling web site [ref. 55] lists the following relation between the apparent crater depth (i.e., the excavation depth by Holsapple) and the crater volume V for a simple crater in lunar regolith:

$$\text{depth} = 0.6\, V^{1/3} \tag{10-12}$$

and the following relation for the crater diameter D:

$$D = 1.1\, V^{1/3} \tag{10-13}$$

Holsapple does not list the maximum depth from which the ejecta originates. However, Holsapple indicates the ejecta volume is approximately 80% of excavation (i.e., apparent) volume. If the volume from which the ejecta originates has the same shape as the excavation volume, then the maximum depth the ejecta originates from is only 7% smaller than the excavation depth. Therefore, the maximum depth from which the ejecta originates is the same as the excavation depth.

Holsapple's crater dimension scaling web site [ref. 54] lists the following parameters for lunar regolith:

$$\begin{aligned} K_1 &= 0.14 \\ K_1 &= 0.75 \\ \rho &= 1{,}500 \text{ kg/m}^3 \\ Y &= 1.0\text{x}10^5 \text{ Pa} \\ \mu &= 0.4 \\ \upsilon &= 0.33 \end{aligned} \tag{10-14}$$

Finally, a comment about the assumption that all craters produced by sporadic meteoroids and NEOs are simple. This is true for sporadic meteoroids which has been defined as 10 g and smaller. However, it is not true for the upper end of the size range of NEOs considered. The Holsapple's web calculator was used to obtain the Table 10.4-1 asteroid diameters at the transition from simple to complex craters for two impact speeds and two impact angles.

Table 10.4-1. NEO Diameter at Transition from Simple to Complex Craters

Impact speed km/s	Asteroid diameter (m)	Impact angle (measured from surface normal) degrees
15	420	0
15	490	45
40	290	0
40	330	45

Thus, the cratering relations for simple craters should not be used for NEOs larger than 200 m.

10.4.4 Contribution to Ejecta Flux from Impacts Excavating to Depths Larger than 10 m

Finally, the depth of penetration into the lunar regolith by sporadic meteoroids and NEOs was calculated. The excavation depth is independent of the projectile density because Holsapple chose $\nu = 1/3$. Thus, the excavation depth by the maximum mass sporadic meteoroid (i.e., 10 g) is a function of impact speed and angle. Figure 10.4-7 is a plot of the calculated excavation depths for meteoroids traveling at approximately the average and maximum speed (i.e., 20 and 70 km/s, respectively).

The excavation depths are within the regolith at the maria and the highlands, and the Apollo lunar core samples.

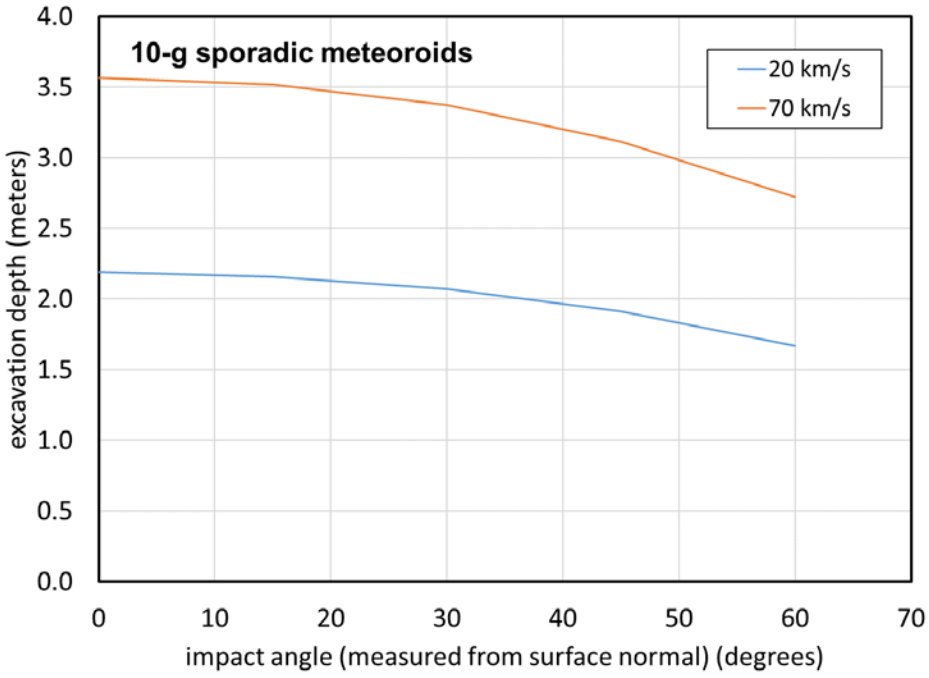

Figure 10.4-7. Excavation Depth into Lunar Regolith by Sporadic Meteoroids

The crater dimension relations can be used to estimate the NEO mass that will excavate the lunar regolith to the bottom of the regolith layer. Any NEO that excavates deeper than this is no longer cratering regolith, hence the ejecta scaling relations using regolith material parameters no longer apply. Figure 10.4-8 is a plot of the results for impact speeds near the average and maximum NEO impact speeds, and for impact angles near the worst case and the average impact angle on a sphere.

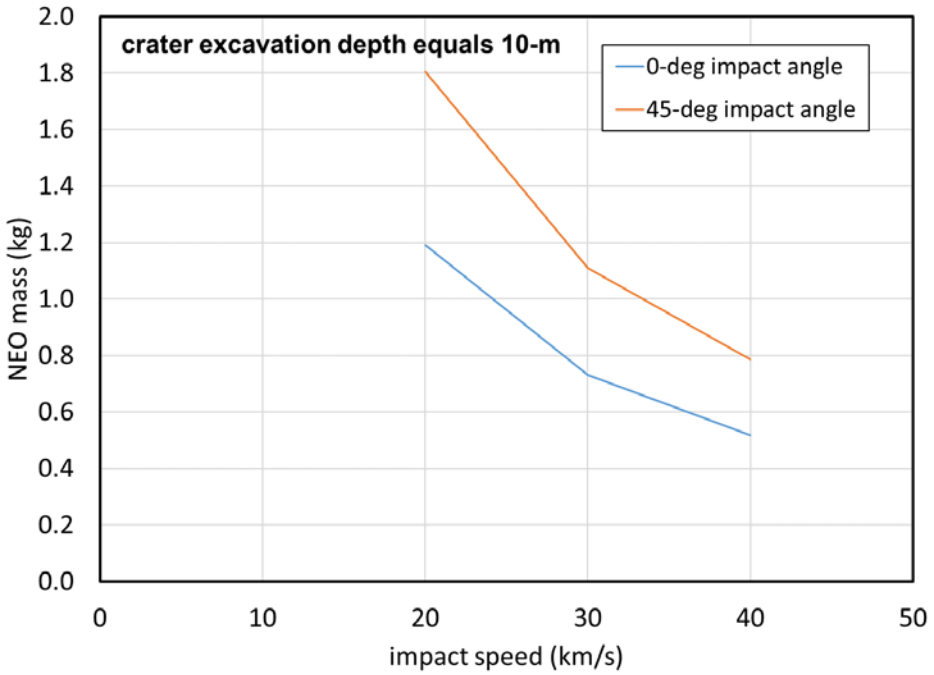

Figure 10.4-8. NEO Mass that Will Excavate to Bottom of Regolith 10 m thick Resulting in a 37-m-Diameter Crater

The masses are in the range of 0.5 kg to 1.8 kg (i.e., 6.8 cm to 10.5 cm), nowhere near the maximum 1.57×10^{12} kg for a 1-km-diameter NEO considered by the NEO environment model. Thus, the NEOs in the range of 1 m to 1 km are cratering into bedrock material and different material parameters should be used in the ejecta mass scaling relation.

Finding 24: Ejecta mass scaling used by MeMoSeE for impacts by NEOs 1 m to 1 km in diameter uses soil as the target material, but basalt is more appropriate because the impactor will push through the soil layer and contact the bedrock layer below.

Recommendation 22: Use basalt as the target material for NEO impacts in the 1 m to 1 km diameter range.

Figure 10.4-9 shows an example of a lunar bench crater [ref. 54] where the impactor has penetrated the regolith. The crater in the regolith is 140 m in diameter. In the center of the crater is a smaller crater in the basalt bedrock[2]. The area between the two crater rims is the exposed basalt bedrock and is roughly flat, forming the bench mentioned in name of the crater morphology. Typically, these types of craters are searched for to estimate the regolith thickness. Note the large blocks surrounding the crater from the excavation of the basalt bedrock. These blocks are not described by the regolith soil size distribution. However, this crater must have had a large amount of ejecta from the regolith and the bedrock. Not until the crater in the maria is substantially deeper than 10 m will the ejecta be mostly composed of basalt.

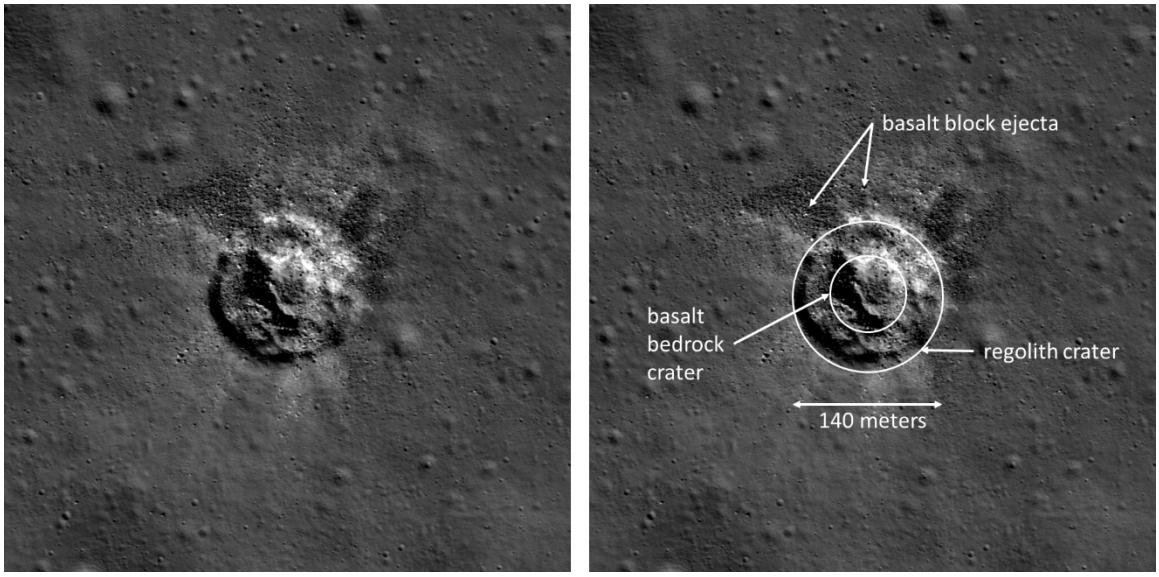

Figure 10.4-9. Example of Bench Crater in Lunar Crater Plato [ref. 56]

Figure 10.4-10 is a plot of the contribution of the NEO flux to the creation of the lunar ejecta flux. The ratio plotted along the y-axis is the ratio of the ejecta flux created by sporadic and NEO impacts with masses less than 1 kg (gray curve), 100 kg (orange curve), 10^7 kg (gold curve), or 10^{12} kg (blue curve), but larger than 10^{-7} kg to the ejecta flux created solely by the sporadic flux between 10^7 kg to 10^{-7} kg.

[2] Bedrock is called basalt here, even though this is typical of the maria and not the anorthosite of the lunar highlands at the lunar south pole. The effect of the different material properties on cratering is not large. Typically, the two materials are lumped together under the heading of hard rock and a single set of material parameters using in crater scaling. [ref. 55]

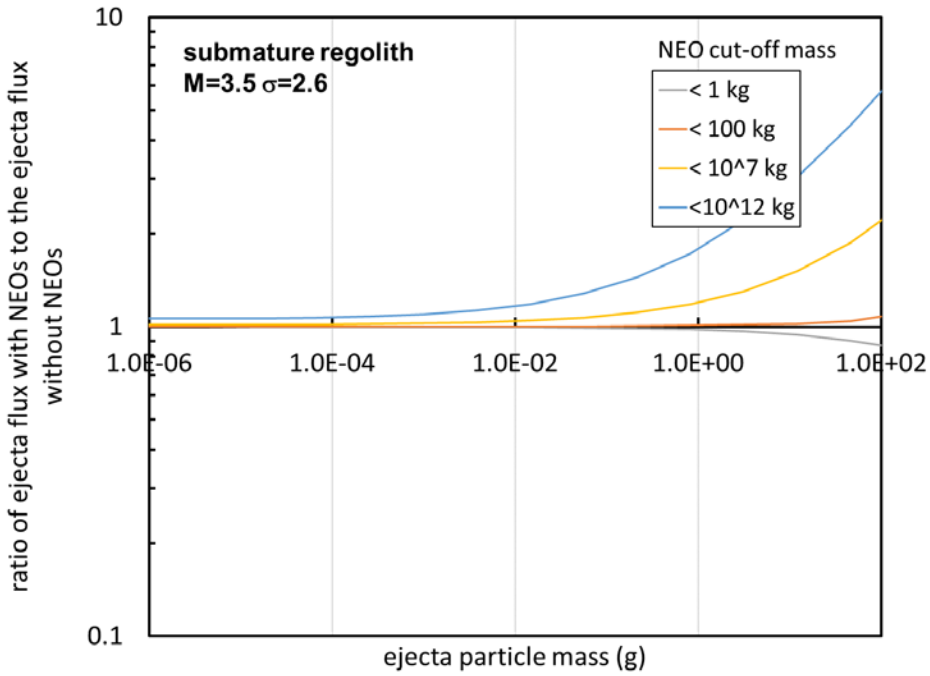

Figure 10.4-10. Contribution to Ejecta Flux from Impacts by Sporadic and NEOs with Masses Less than 1 kg, less than 100 kg, and less than 10^7 kg

The mass cut-off at 1 kg is around the mass of a sporadic or NEO that will excavate to 10-m depth, which is also close to the transition between the Grun flux curve for sporadics and the NEO flux curve. The grey curve shows that about 15% of the flux of 100 g ejecta particles comes from sporadics larger than 1 kg when there is no contribution from NEOs.

The blue curve shows that the MeMoSeE model procedure of including 1-km-diameter asteroid impacts of Moon increases the ejecta flux of 100 g particles by a factor of about 6 for the assumptions of this simplified analysis. This is a substantial addition to the ejecta flux based on the assumptions about the ejecta particle size distribution.

Furthermore, the mean time between occurrences of impacts of the Moon by 1-km asteroids is large. An estimate of the mean time using the results by Ivanov [ref. 56] is plotted in Figure 10.4-11. The probability per year of an NEO impact with the Earth is plotted along the y-axis and the diameter of the NEO is plotted along the x-axis.

The filled squares on point are the data used by Brown [ref. 14] to calculate his NEO flux used in the MeMoSeE model, which range in diameters from 100 cm to 8 m. The red broken line is a curve with slope –2.7, where the Brown flux mass exponent is cubed to convert to diameter. The probability of impact per year is about 3×10^{-7} per year or a mean time between occurrences of 3.33×10^6 years. Ivanov [ref. 56] lists the impact rate on the Earth as 20 times larger than the impact rate on the Moon, hence the mean time between impacts of the Moon by 1-km-diameter NEOs is 6.67×10^7 years.

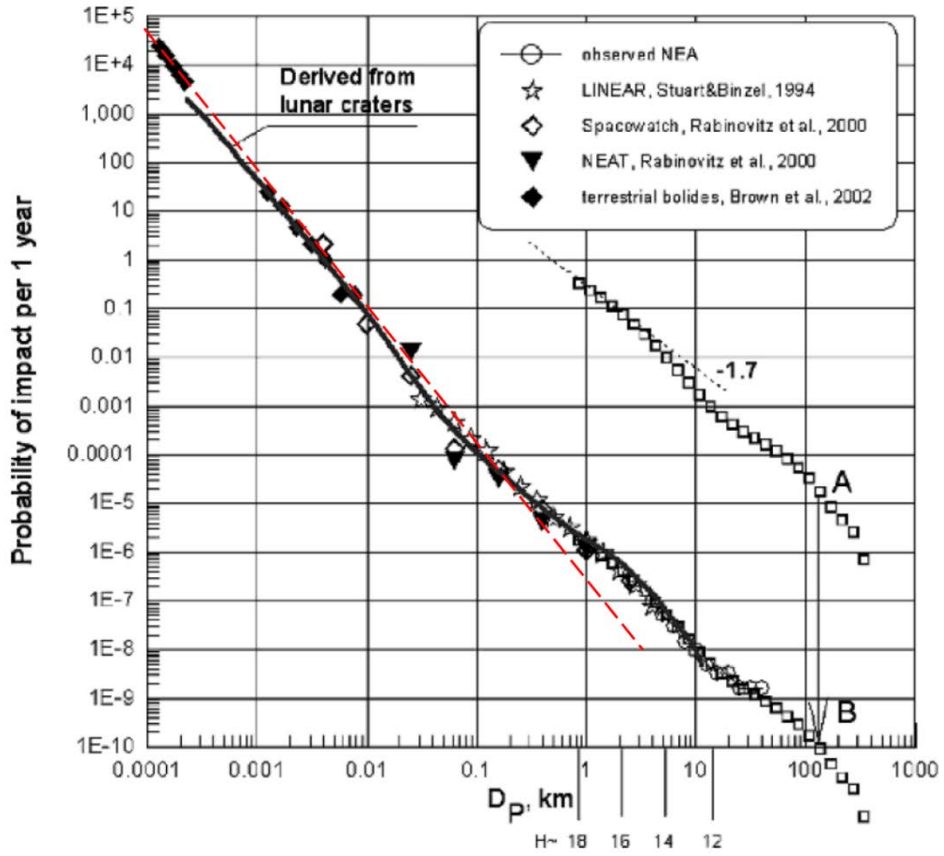

Figure 10.4-11. Ivanov's Estimate of Probability of a NEO Impact with Earth as a Function of Diameter of NEO [ref. 57]

Ivanov's estimate of the probability of occurrence of an impact on the Moon by a 1-km-diameter NEO deviates from Brown's extrapolation. Ivanov estimates the mean time between occurrences as is once every 10 million years, which is six times smaller, but still a large number.

Clearly, averaging this flux over 66 million years to obtain a yearly flux is not appropriate.

The open rectangles in Figure 10.4-11 is the distribution of asteroid diameters in the main belt expressed as a probability. Ivanov translated this curve from point A to point B and obtained good agreement with the NEO size distribution. Ivanov then concluded that the shape of the NEO probability curve at the largest diameters is due to the distribution of the asteroid sizes in the main belt that are perturbed into Earth crossing orbits. Thus, the data do not justify a power law curve, and extrapolating from 10 cm to 1 km by a power-law is not warranted.

10.5 Ejecta Impact Risk Versus Sporadic Meteoroid Impact Risk

Engineers will ultimately use the MeMoSeE model output to evaluate the risk of an HLS failure by lunar ejecta. This section uses the model output to calculate a spacecraft's impact risk by lunar ejecta to preview what the HLS engineers can expect.

Section 10.5.1 presents results from Apollo and Constellation Programs using the 1969 ejecta environment model. These results indicate that the lunar ejecta risk is 5% or less of the total penetration risk from sporadic meteoroids and lunar ejecta while on the lunar surface. Section 10.5.1 documents reasons to think that the HLS risk of penetration by lunar ejecta risk calculated

with MeMoSeE model will be a smaller fraction of the total meteoroid and ejecta risk than that calculated with the Apollo lunar ejecta environment model.

Section 10.5.2 should be preliminary HLS results. However, all three HLS designs are competition-sensitive, and any estimates of ejecta impact risk are not publishable. Therefore, the Constellation Program Altair lunar lander is used as a surrogate. This subsection presents results for the previous sporadic meteoroid and ejecta models and the current sporadic meteoroid model with the MeMoSeE ejecta model. As expected, the MeMoSeE model results are a smaller fraction of the total sporadic meteoroid and ejecta risk than the previous models.

Risk assessments generally develop two numbers, the probability of loss of crew (LOC) and the probability of loss of mission (LOM). The analysis of Section 10.5 uses failure criteria appropriate to LOC.

Section 10.5.3 contains some thoughts on the importance of lunar ejecta to the Artemis Base Camp mission.

Section 10.5.4 is a summary of the importance of lunar ejecta to the xEMU.

10.5.1 Overview of Prior Results and Consequences for the MeMoSeE Model

What follows is a discussion of the proposition that the NASA SP-8013 model specifies more flux than the MeMoSeE ejecta model. The first part is an overview of spacecraft MMOD impact-risk results from the prior ejecta model to establish a baseline for comparison with the MeMoSeE model. The second part is a discussion of the variability of the baseline results with the spacecraft construction, and the relative separation of the ejecta and sporadic meteoroid flux equations. The third and final part combines the second part with the different assumed lunar surface geologies and the different ejecta mass scaling relations to predict how the MeMoSeE model results will differ from the prior results.

MMOD analysts evaluated the risk of lunar ejecta impact risk for two prior spacecraft, the Apollo Lunar Module and the Constellation Altair lunar lander. In each case, analysts used the Zook lunar ejecta environment [ref. 57] as simplified for NASA SP-8013 [ref. 2]. Eardley and Lang in reference 58 calculated the Apollo Lunar Module impact risk for the its various components. Eardley and Lang found that ejecta accounted for 4% of the on-surface meteoroid/ejecta impact risk. However, for some components the ejecta was 15% to 50% of the total risk. Similarly, Bjorkman and Christiansen [ref. 59] found for the Constellation Altair lunar lander that ejecta accounted for 5.4% of the total on-surface meteoroid/ejecta impact risk. The single sheet components had ejecta risks ranging from 1.6% to 5.2% of the total component meteoroid/ejecta impact risk, and components protected by a meteor bumper [ref. 60] had ejecta risks ranging from 12% to 37% of the total component meteoroid/ejecta impact risk. The reason for ejecta's small contribution to single sheet penetration risk is twofold. First, the basalt ejecta travel so slowly that 5- to 10-mm-diameter ejecta particles are required to perforate spacecraft components. Second, the flux of larger basalt ejecta particles is so much smaller than the flux of small meteoroids that perforate at a factor of 20 or more in impact speed, that the relative contribution to the risk is small. However, when a meteor bumper protects the component, it acts as a low-pass filter and prevents most of the high-speed meteoroids from perforating the spacecraft, leaving just a few meteoroid perforations roughly equal to the number of ejecta penetrations. Thus, protecting a component with a meteor bumper does not change the number of

penetrations by ejecta, but does reduce the number of penetrations by sporadic meteoroids to the point that ejecta penetrations become significant.

The result that ejecta may contribute 50% of the component risk is specific to the Apollo Lunar Module and the NASA SP-8013 [ref. 2] environment and may or may not apply to other spacecraft or other ejecta environments. Figure 10.5-1 illustrates the variability of the ejecta contribution to the total risk. One computes the relative risk from Figure 10.5-1 with the assumption all NASA SP-8013 ejecta particles travel at the average speed of 0.1 km/s, and all Meteoroid Engineering Model, release 2 (MEMR2) [ref. 61] sporadic meteoroids travel at the average speed of 22.3 km/s. Furthermore, it is assumed all sporadic meteoroid trajectories are normal to the upwards facing flat sheet lying on the lunar surface. The graph on the left is a plot of the ballistic limit curve of a single sheet of aluminum 0.1791 cm thick (the red curve) and the ballistic limit curve of a meteor bumper and its rear wall (i.e., a geometry often referred to as a Whipple shield) with the same total thickness. A ballistic limit curve separates the space of impact-speed and projectile-diameter pairs that perforate the shield (i.e., those lying above the curve) from those pairs that are stopped by the shield (i.e., those lying below the curve). These particular curves apply to projectiles that impact at 90° to a flat sheet pointing upwards. The graph on the right is the cumulative flux of MEMR2 sporadic meteoroids (red curve) and NASA SP-8013 ejecta (green curve) with diameters larger than the value plotted on the x-axis. The penetrating flux is determined by reading across the ballistic limit plot starting at the critical diameter that perforates at the impact speed and then reading down the cumulative flux plot to obtain the cumulative number of penetrations per square meter per year.

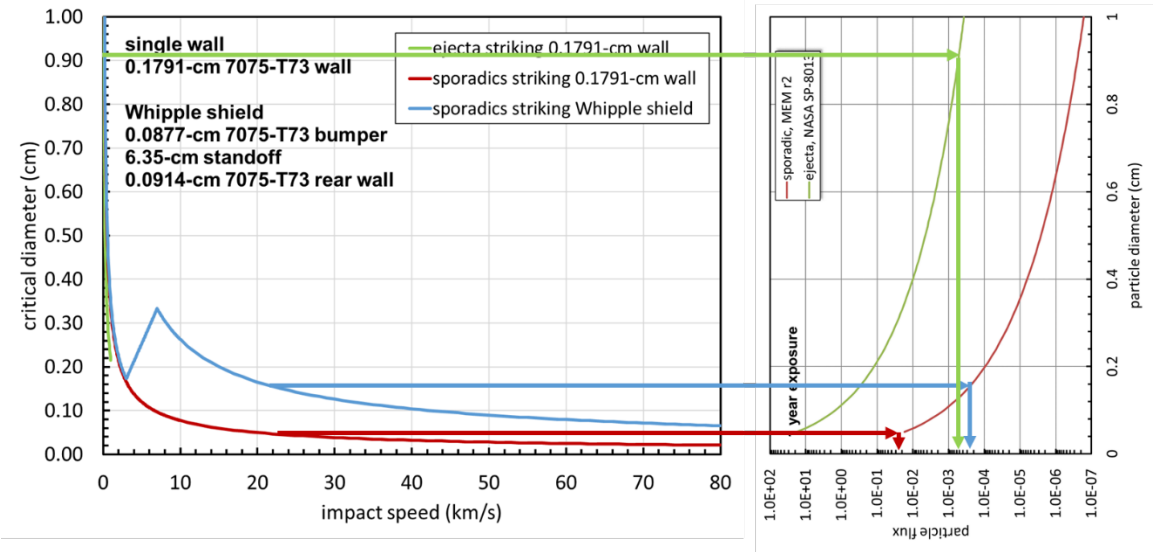

Figure 10.5-1. How to Calculate Penetrating Flux for Single Speed and Single Impact Angle Ejecta and Sporadic Meteoroid Environments

In Figure 10.5-1, the set of green arrows give the ejecta single-wall penetration flux, which is within a few percent of the ejecta Whipple shield penetration flux. The set of red arrows gives the sporadic single-wall penetration flux. The set of blue arrows gives the sporadic Whipple shield penetration flux. In this example, ejecta accounted for 62% of the total number of Whipple shield penetrations, while ejecta accounted for only 2% of the total number of single-sheet penetrations. The relative positions of the curves in Figure 10.5-1 illustrate two important points:

1. Ejecta will always be a small fraction of the total number of single-wall penetrations provided the ejecta flux is not vastly larger than the sporadic meteoroid flux (i.e., three orders of magnitude or larger than the sporadic meteoroid flux).
2. Ejecta can be a small or large contribution to the total number of Whipple shield penetrations. If the Whipple shield is optimal, then ejecta will be nearly all of the penetrations. If the ejecta environment model is changed so that the ejecta flux is decreased to the point that it is near the sporadic meteoroid flux, or the sporadic meteoroid model changed so that the sporadic meteoroid flux is increased to values near the ejecta flux, then the sporadic meteoroids will be nearly all the penetrations.

Lastly, it is important to remember the Apollo and Constellation designs were for sortie missions with a single-use lunar lander. The Artemis Program intends to develop reusable spacecraft and to establish the Artemis base camp at the lunar South Pole where the HLS could be exposed to the lunar ejecta environment for months. These two features (i.e., reusability and polar location) of the Artemis Program will drive the HLS design towards using meteor bumpers. Thus, the Apollo and Constellation Altair lunar landers are a low-side estimation of the importance of lunar ejecta impact risk to the HLS.

With this as background, there are two conclusions as to how the MeMoSeE model ejecta environment affects MMOD impact-risk assessment results. First, DeStefano based the MeMoSeE model on the scaling of the total mass ejected for a cratering flow governed by a coupling parameter. Figure 10.5-2 is a plot from reference 55 in Gault et al. [ref. 9] results for impacts of basalt (i.e., the blue triangles, fitted with the black curve) which Zook and Cour-Palais used to develop the NASA SP-8013 ejecta model.

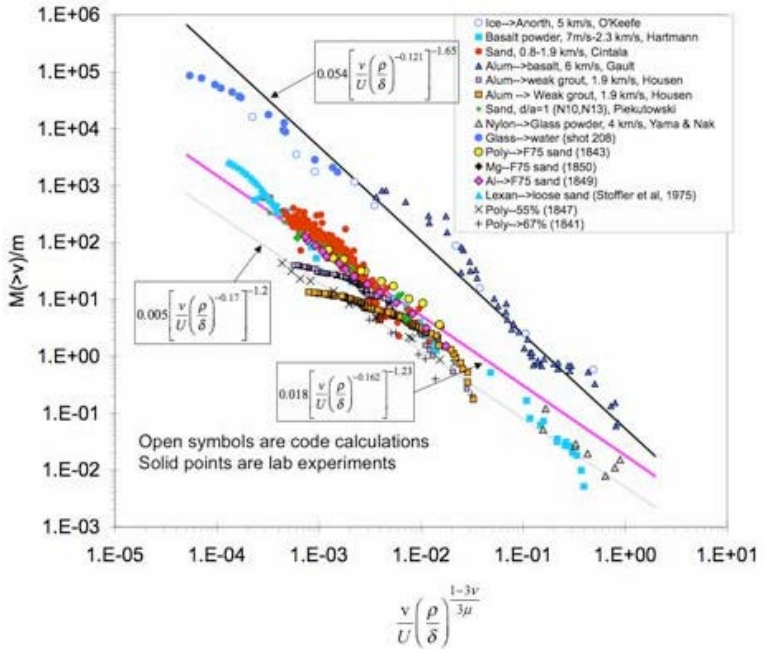

Figure 10.5-2. Scaled Ejection Mass Versus Ejection Speed for Various Geological Materials [ref. 55]

The magenta curve in Figure 10.5-2 fits the test data from the 1970s to the present for soil impacts. Note that the excavated mass is significantly smaller for the craters in soil. Consequently, the MeMoSeE ejecta flux will be smaller than the NASA SP-8013 ejecta flux.

Hence, the conclusion that less flux combined with smaller particles will result in less risk of penetration than the NASA SP-8013 ejecta environment. Second, because of the Apollo Program, it is known that a fine soil layer to a depth of 5 m to 10 m in the lunar maria, and a depth of 20 m to 30 m in the lunar highlands covers the lunar surface. The distribution of soil particle diameters is restricted to a small range with an average particle size of 80 μm to 100 μm. Thus, the maximum mass ejecta particle ever likely to strike a spacecraft is smaller than expected if the lunar surface were solid basalt. Therefore, it is concluded that the MeMoSeE lunar eject environment requires larger impact speeds to penetrate spacecraft components than the larger particles from the NASA SP-8013 environment.

10.5.2 Application of the MeMoSeE model to the HLS Sortie Mission

Figure 10.5-3 is a plot to scale of the two spacecraft for which there are results using the NASA SP-8013 environment (i.e., Apollo and Constellation Altair lunar modules) and the three HLS bidder's spacecraft concepts for which results are desired using the MeMoSeE environment (i.e., HLS National Team, HLS Dynetics, and HLS SpaceX). However, at the time of this analysis, the HLS contract was in competition, hence the designs were competition sensitive and not available for this report. This evaluation uses the Altair minimum requirements spacecraft and the lunar lander with the HVIT-recommended shielding as a surrogate. Considering the discussion in Section 10.5.1, it is expected that the Altair single-wall tends to generalize to the HLS spacecraft. However, the Whipple shield results do not generalize to the HLS because the results depend on the shield standoff, which may or may not be similar to the HLS standoffs.

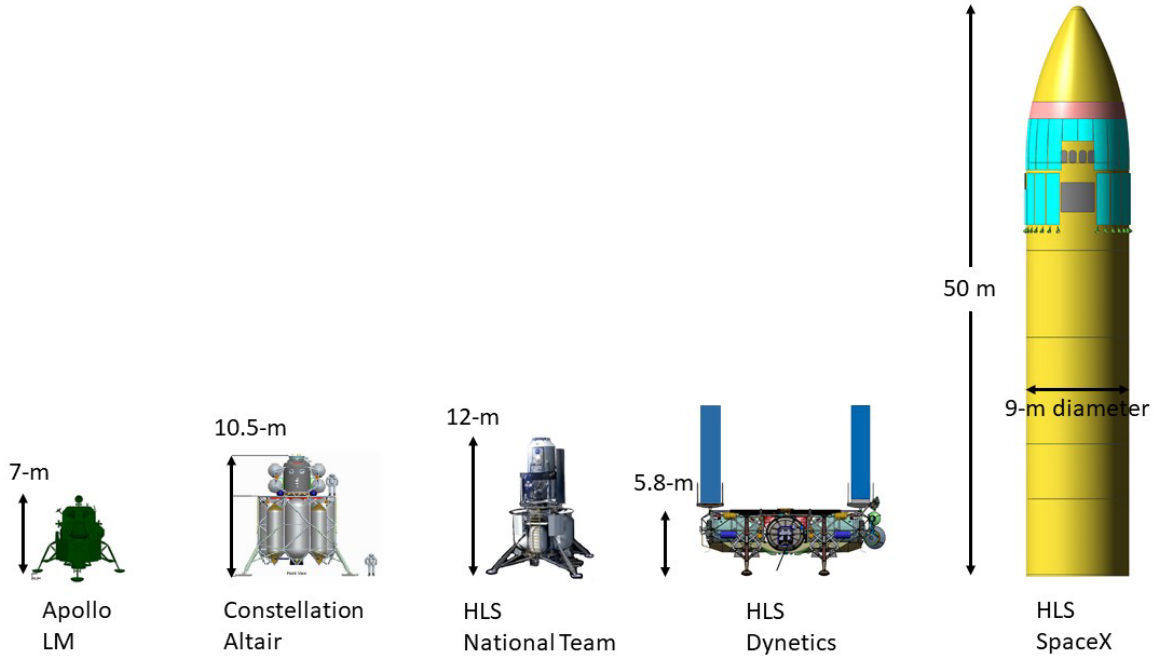

Figure 10.5-3. Apollo Lunar Lander, and Constellation and HLS Program Crewed Lunar Lander Concepts

The Altair meteoroid and ejecta impact risk was assessed using Bumper. NASA has used Bumper to evaluate spacecraft MMOD risk since 1987 [ref. 62]. A detailed description of the Bumper algorithm is not given here. In general, Bumper uses:

1. A triangular and rectangular surface-element geometry model of the spacecraft to keep track of the orientation of its various regions relative to the impinging meteoroid and ejecta trajectories.
2. Ballistic limit equations (BLEs) to calculate the particle diameter required to damage the spacecraft component given the particle's impact speed and impact angle.
3. The surface element model to calculate the portions of the spacecraft shadowed from the particle trajectory by other portions of the spacecraft.

Figure 10.5-4 is a render of the Altair surface element model created for the 2010 MMOD impact risk assessment [ref. 59]. The model includes the Altair ascent module and tanks, and the descent module tanks, but does not include the landing gear. The landing gear are assumed to be robust structures resistant to meteoroid and eject impact, and do not shadow significant portions of the spacecraft when it is on the lunar surface. Therefore, this analysis excludes the landing gear to simplify calculations.

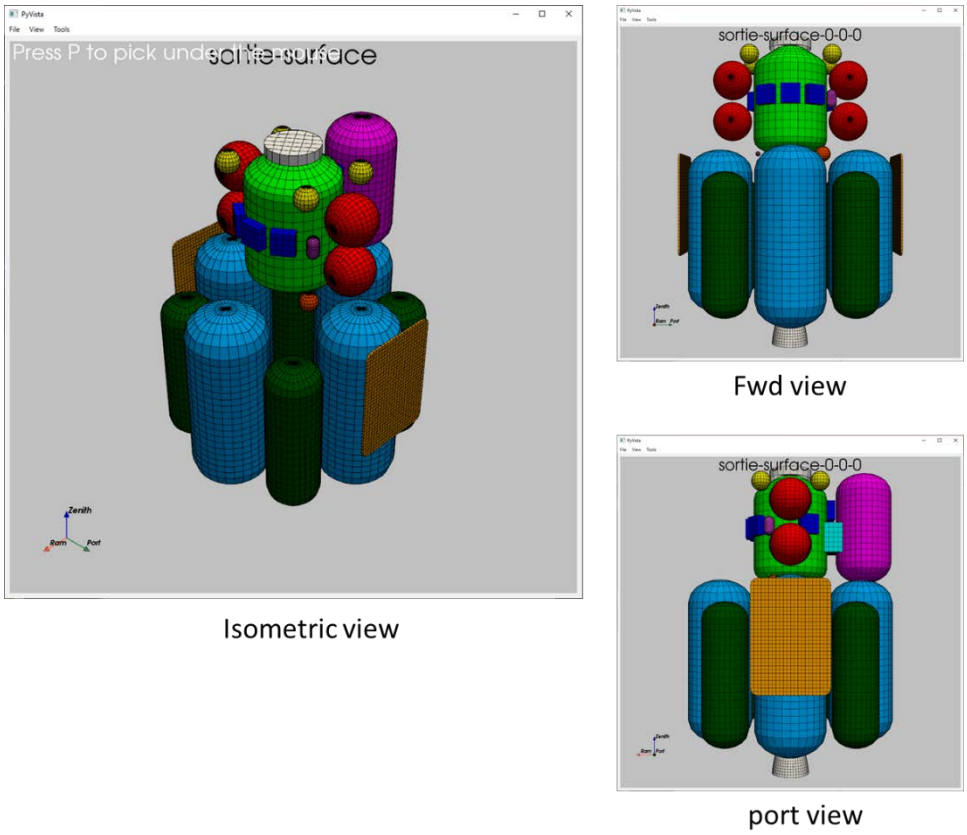

Figure 10.5-4. Altair Surface Element Model Constructed for Bumper MMOD Impact Risk Assessment

The left-hand-side of Figure 10.5-5 is a render of the ascent module including labels of the various components assessed. The right-hand-side of Figure 10.5-5 is a schematic diagram of the component wall thicknesses and materials. Note that the crew cabin is the only double wall

construction (i.e., Whipple shield). All the other components are single-wall construction. The crew module wall is a 2.54-cm-thick aluminum honeycomb with composite face sheets. However, this standoff distance will reduce the effectiveness of the honeycomb as a Whipple shield.

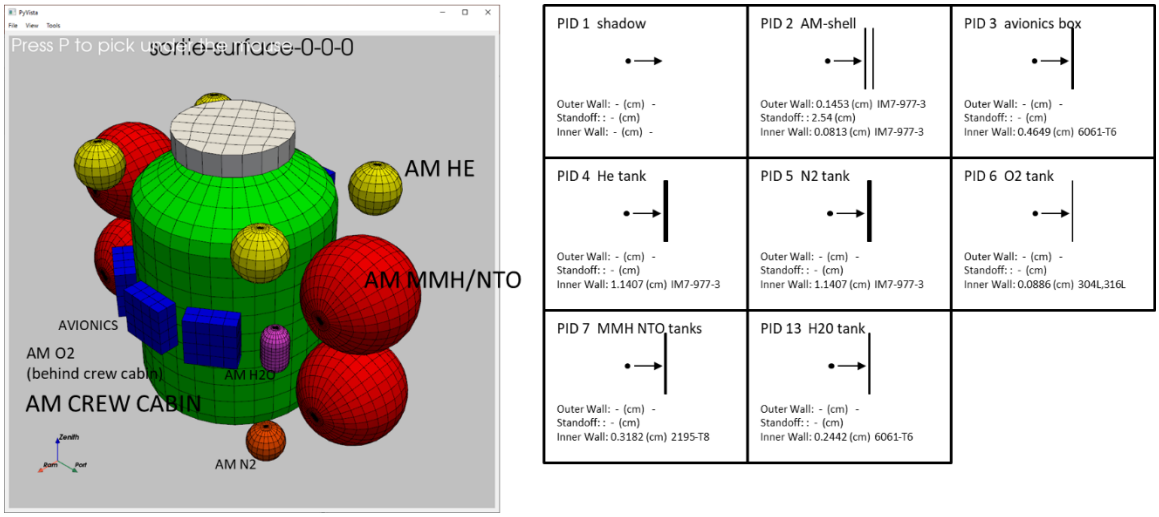

Figure 10.5-5. Altair Ascent Module Wall Construction

Figure 10.5-6 is a similar plot for the descent module. The descent module render is on the left and wall construction of the descent module is on the right.

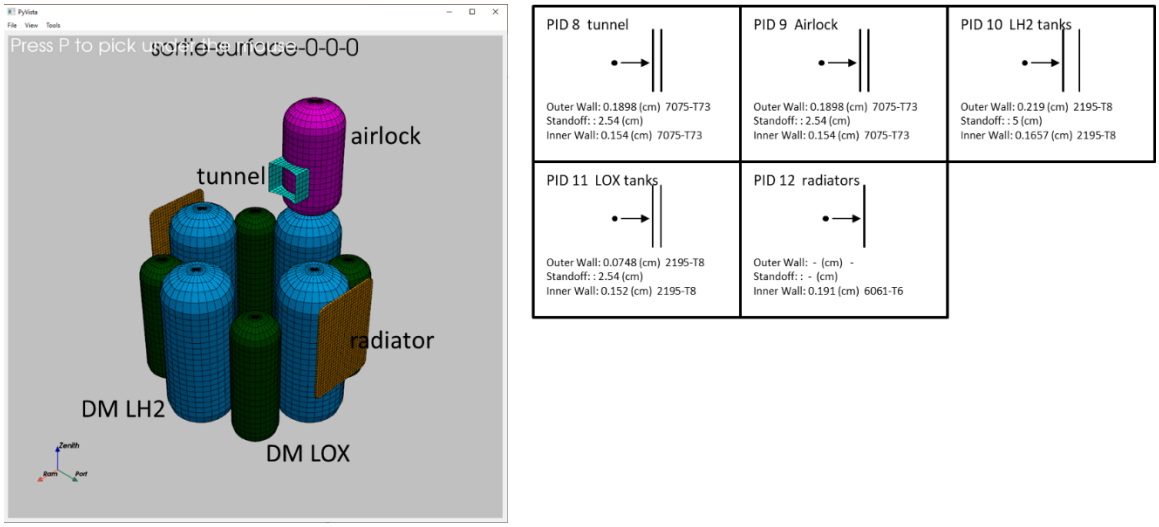

Figure 10.5-6. Altair Descent Module Wall Construction

The descent module tanks use honeycomb materials for the walls. The only single-wall component in the descent module are the radiators.

The assessments that follow use the same HLS sortie mission lunar stay. The lunar stay starts on November 14, 2024 and runs for 5.8 days. The Altair lander is located at the lunar south pole at the HLS design reference mission site 01 [ref. 63]. The Altair lander is oriented so that its x-axis is pointing east. The axis labeled “ram” in the render is the Altair x-axis.

Figure 10.5-7 is a rendering of the number of penetrations per square meter per year contouring the Altair geometry model. The sporadic and ejecta contours are on two different scales. The

number of ejecta penetrations is much smaller than the number of sporadic meteoroid penetrations. The two renderings used different color-map scales, else the ejecta penetration contours would render as all dark blue, making it difficult to tell where the ejecta penetrations occur.

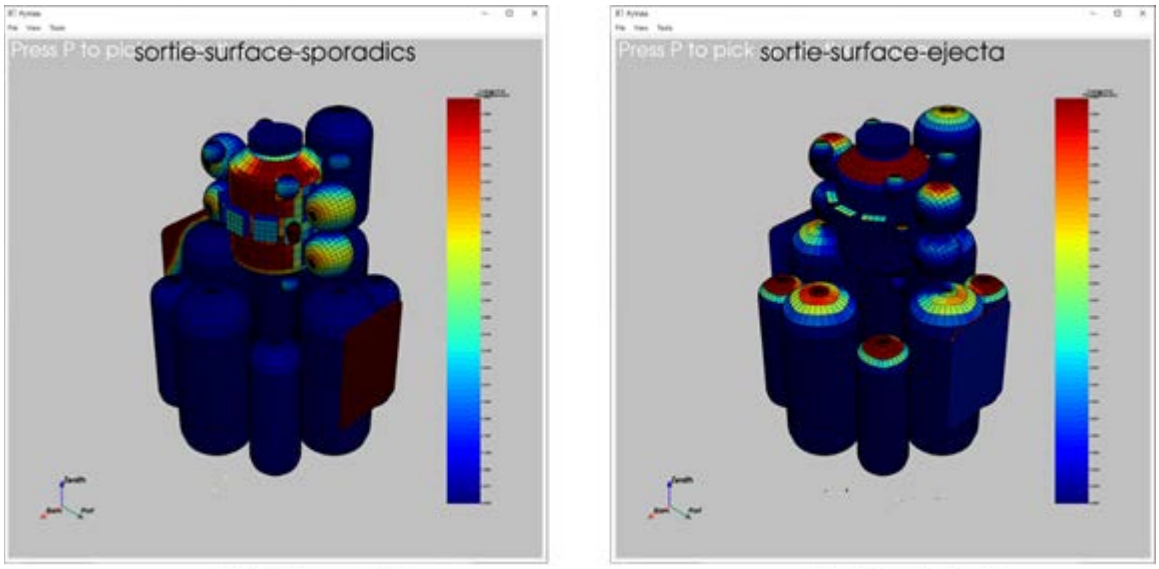

Figure 10.5-7. Penetrations per Square Meter per Year by Sporadic Meteoroids and Lunar Ejecta

Figure 10.5-7 shows that the majority of the MEM 3 [ref. 64] penetrating sporadic meteoroids come from one direction along the horizon, and that the MeMoSeE penetrating ejecta come from above. If the sporadic meteoroid flux is averaged over 19 years, then the penetrations are spread uniformly around the circumference of the crew cabin. Thus, while there might be a preferred landing orientation for sortie missions that minimizes impact risk, long-duration base-camp missions have no preferred orientation. Another feature of Figure 10.5-6 is that the descent module Whipple-shield-protected tanks have less risk of penetration per unit area by sporadic meteoroids than the single-wall construction crew cabin and ascent module tanks, as expected.

While not shown in Figure 10.5-7, the location of the peak number of penetrations makes one complete rotation around the circumference of the crew cabin during the lunar month. Thus, the number of penetrations of the crew cabin varies with the landing date because of the shadowing provided by the air lock and tanks.

Figure 10.5-8 is a histogram comparing the relative number of penetrations by sporadic meteoroids and lunar ejecta for the same mission, but with two different sets of environments. The histogram on the left uses the MEMR2 sporadic meteoroid environment and the NASA SP-8013 ejecta environment. The histogram on the right uses the MEM 3 sporadic meteoroid environment and the MeMoSeE lunar ejecta environment.

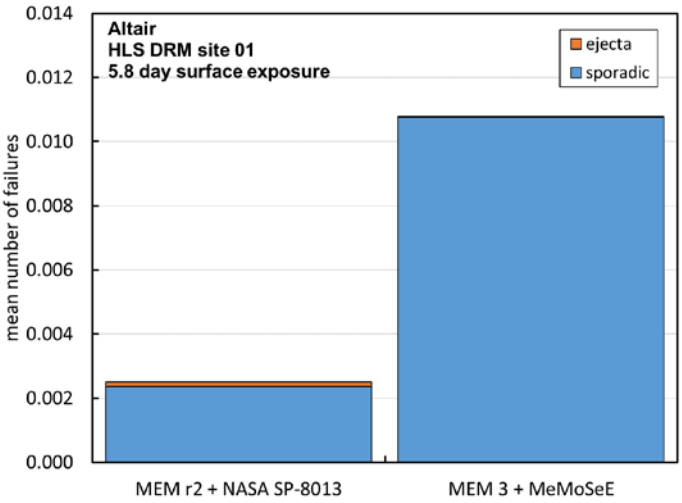

Figure 10.5-8. Total Number of Penetrations Due to Ejecta and Sporadic Meteoroid Impacts Calculated with Two Environment Sets

The blue fractions of the Figure 10.5-8 histogram are the number of penetrations due to sporadic meteoroids during 5.8 days of exposure of the Altair minimum functionality vehicle. The orange fractions are the mean number of penetrations due to ejecta impacts. The NASA SP-8013 ejecta model number of penetrations is a small fraction of the MEMR2 sporadic meteoroid model number. However, as anticipated, the MeMoSeE ejecta number of penetrations is smaller than the NASA SP-8013 ejecta number of penetrations. The relative contribution to the total number of failures is smaller not only due to the smaller number of ejecta penetrations but also due to the larger number of MEM 3 sporadic meteoroid penetrations. While the MEM 3 flux is smaller than MEMR2, the mass densities are a factor of 3.5 larger leading to more penetrations.

The histograms in Figures 10.5-9 and 10.5-10 illustrate the effect of adding the HVIT-recommended Whipple shields to two Altair components. Figure 10.5-9 shows the changes in the results from adding Whipple shields to the ascent module shell and the ascent module monomethylhydrazine and nitrogen tetroxide (MMH/NTO) tanks when evaluated using the MEMR2 sporadic meteoroid environment and the NASA SP-8013 lunar ejecta environment. Figure 10.5-10 shows the changes from adding Whipple shields when evaluated with the MEM 3 ejecta environment and the MeMoSeE lunar ejecta environment.

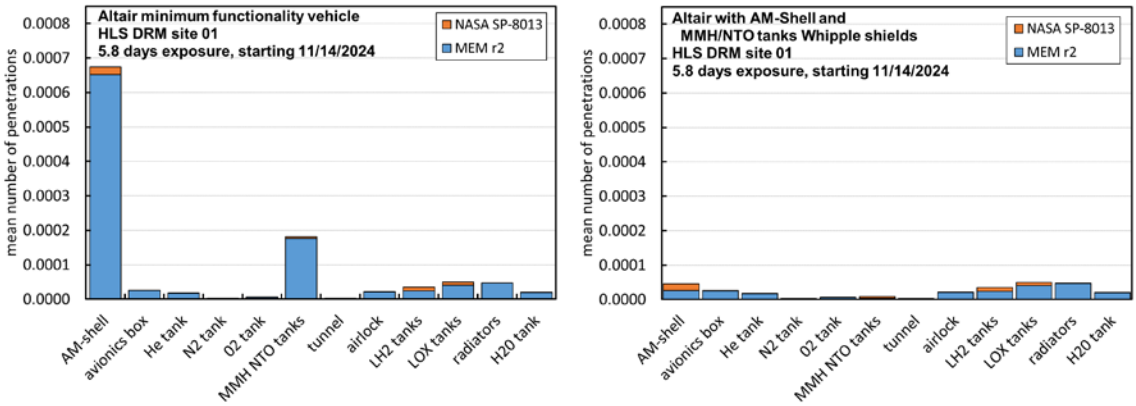

Figure 10.5-9. Number of Penetrations by Component, with and without Whipple Shields, Evaluated with NASA SP-8013 Lunar Ejecta Environment and MEMR2 Sporadic Meteoroid Environment

The Figure 10.5-9 histogram on the left shows the component mean number of failures for sporadic meteoroids (blue) and for ejecta (orange). The Altair ascent model shell and the propellant tanks mean number of penetrations is decreased significantly by the Whipple shield, but only the number of penetrations by sporadic meteoroids was decreased, not the number of penetrations by lunar ejecta. This resulted in roughly equal numbers of penetrations by sporadic meteoroids and lunar ejecta for the two Whipple shield protected components.

Finding 25: Multi-walled shields are optimized for protection against fast meteoroids, but may provide minimal enhanced protection against slow, high-density ejecta over single-walled shields. Switching from single-wall to multi-wall shield designs will decrease the sporadic (and therefore the total) risk, but will not necessarily reduce the ejecta risk. Therefore, some of the proposed multi-wall shielding designs for HLS have a significant fraction of their risk contribution from ejecta.

Figure 10.5-10 contains plots similar to Figure 10.5-9, only for the MEM 3 sporadic meteoroid number penetrations, and for the MeMoSeE lunar ejecta number of penetrations. The number of penetrations by lunar ejecta are so small in this plot they are barely visible.

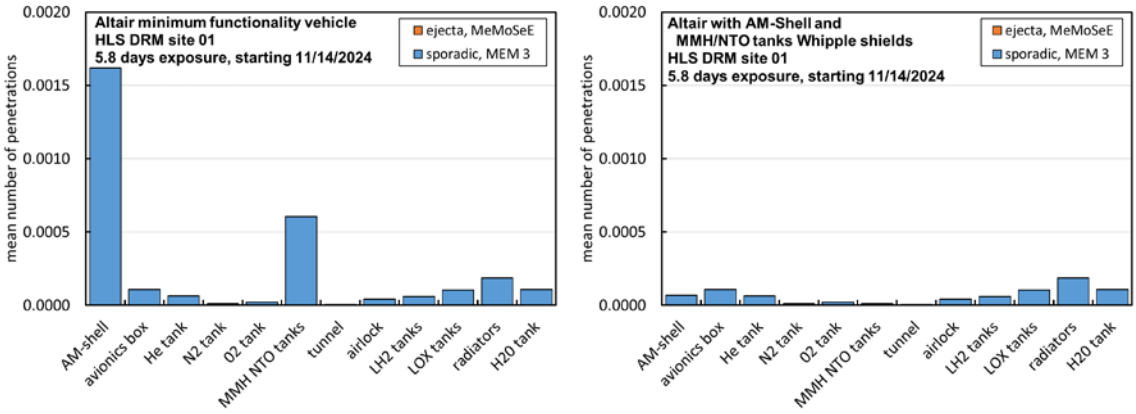

Figure 10.5-10. Number of Failures by Component, with and without Whipple Shields, Evaluated with MeMoSeE Lunar Ejecta Environment and MEM 3 Sporadic Meteoroid Environment

Table 10.5-1 lists the sum of the above results for reference.

Table 10.5-1. Summary of Results with and without Shields for Two Sets of Environments

Altair lunar lander configuration assessed	NASA SP-8013 lunar ejecta number of penetrations as a fraction of the total MEMR2 sporadic meteoroid and lunar ejecta number of penetrations	MeMoSeE lunar ejecta number of penetrations as a fraction of the total MEM 3 sporadic meteoroid and lunar ejecta number of penetrations
Minimum functionality vehicle	4.8%	0.04%
With HVIT recommended shields	17.5%	0.14%

Note that the MeMoSeE contribution to the Altair lunar lander total ejecta and meteoroid impact risk is 2 orders of magnitude smaller than the NASA SP-8013 contribution to the risk. This is a combination of the larger MEM 3 sporadic meteoroid impact risk and the smaller MeMoSeE lunar ejecta impact risk.

The second anticipated feature was a typical MeMoSeE ejecta penetration would require a larger impact speed than the typical NASA SP-8013 ejecta penetration. The reason for thinking this is the regolith particles are smaller and faster on average that basalt crater ejecta particles. The hypothesis was tested by modifying the Bumper program to output the number of penetrations per environment speed bin. Figure 10.5-11 is a plot of the results.

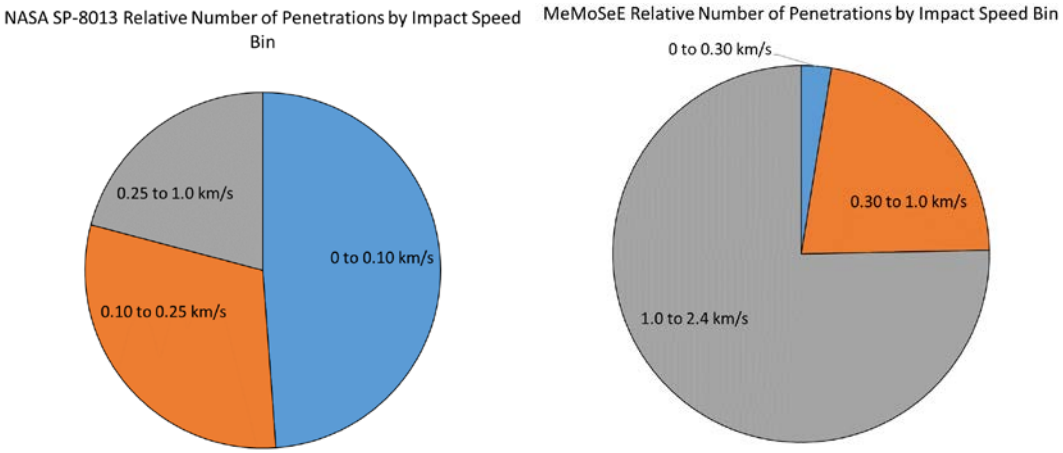

Figure 10.5-11. Relative Number of Penetrations per Bumper Speed Bin for Two Ejecta Environments

NASA SP-8013 results in half of the penetrations occurring for speeds between 0 and 0.1 km/s, and essentially none of the penetrations occurring for speeds larger than 1 km/s. However, the MeMoSeE model results in three quarters of the penetrations occurring for speeds between 1 and 2.4 km/s.

10.5.3 Lunar Ejecta Penetration Risk and HLS at Artemis Base Camp

If the HLS makes longer stays on the lunar surface, then more meteoroid shielding is required. If the HLS design uses more Whipple shields to decrease the sporadic meteoroid penetration risk, then the lunar ejecta penetration risk becomes more important. Hence, it is anticipated that the lunar ejecta environment is important to HLS designs for the Artemis Base Camp mission.

10.5.4 xEMU Lunar Ejecta Penetration Risk

Though not discussed, preliminary studies [ref. 65] indicate that the xEMU risk of penetration by lunar ejecta is nearly equal to the sporadic meteoroid penetration risk using the Apollo lunar ejecta environment model. This is due to the limited effectiveness of the thermal-meteoroid garment as a Whipple shield due to the small thickness of the garment.

10.6 Number of MeMoSeE Speed Bins Required for Converged Calculations of Mean Number of Failures

The calculated number of spacecraft penetrations varies with the number of MeMoSeE impact speed bins. Currently, the MeMoSeE model uses three logarithmically spaced speed bins. The question arises whether three speed bins provide a converged answer, and if not, then is the non-converged answer an overestimate or an underestimate of the risk? If three bins are an overestimate of the risk and the increased risk is acceptable to the HLS Program, then the MeMoSeE model is suitable for spacecraft design. If three bins are an underestimate of the risk,

then MeMoSeE needs more speed bins, or the MeMoSeE developers need to create a factor that designers can apply to its results to arrive at an appropriately conservative design.

A preliminary analysis of the time required to do a convergence study with the MeMoSeE model indicated that it was prohibitive. A typical MeMoSeE model run takes 72 hours. If results with 2, 4, 6, … 50 bins are desired, then a total of 650 MeMoSeE runs are needed. Running 20 serial jobs on a workstation at a time results in a total wall clock time of 98 days.

Therefore, it was opted to use the Zook ejecta environment to make the convergence study. The NASA SP-8013 environment cannot be used because it is a three speed-bin model developed from a fit to the published three bins output from the Zook model. However, the Zook model can be used to calculate the fluxes corresponding to any number of speed bins. The Zook model was coded in MathCAD with the modification of using the coupling parameter relation for cumulative ejecta mass launched with speed, v, or larger. Figure 10.6-1 is a comparison of the Zook model (blue curve) ejecta mass relation and the coupling parameter relation (orange curve).

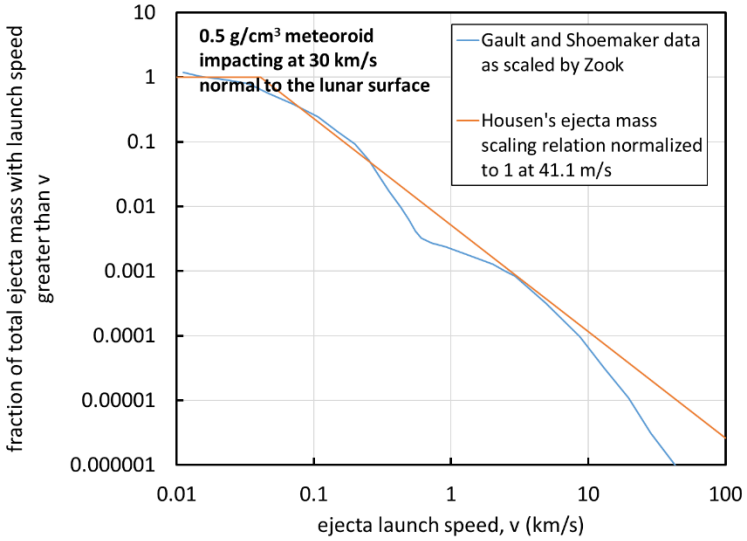

Figure 10.6-1. Zook Function G(v) Scaled to Sporadic Meteoroid Impact Conditions Assumed by Zook in His Model Compared with Function used in Author's MathCAD Analysis

The Zook model does not use the coupling parameter relation precisely. The coupling parameter relation uses cumulative ejecta mass M(>v) normalized by meteoroid mass m, while the Zook model uses the cumulative ejecta mass M(>v) normalized to the excavated crater mass ρV, where ρ is the regolith density and V is the apparent crater volume. The Zook model ejecta mass relation and excavated crater mass relation do not use a consistent coupling parameter, so the excavated crater mass was treated as a free parameter and adjusted the coefficient of the orange curve in Figure 10.6-1 until agreement with published Zook ejecta flux curves was obtained.

Figure 10.6-2 compares the published Zook flux curves (the solid lines) with the flux curves calculated with the MathCAD implementation of the Zook model. The agreement, while not exact because of the different cumulative ejecta mass relations used, is acceptable.

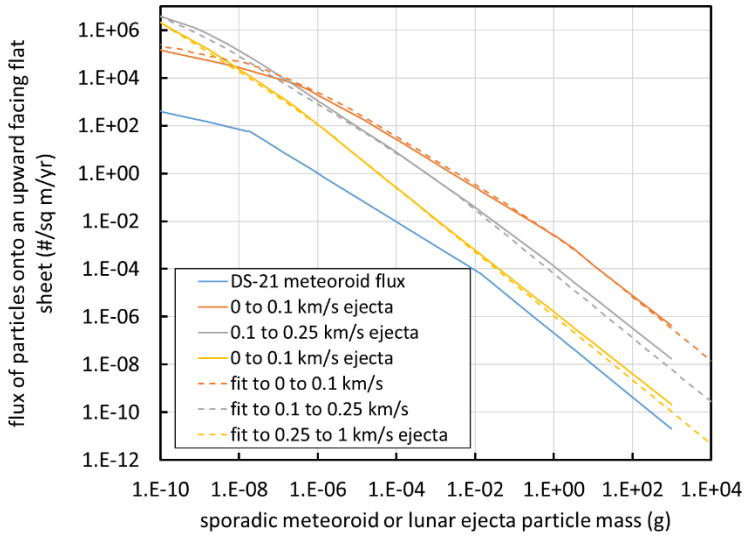

Figure 10.6-2. Comparison of Published Zook Ejecta Flux Curves and MathCAD Implementation of Zook Model

With the ejecta flux equations in hand, the number of penetrations μ was calculated during exposure time Δt of a single sheet of 6061-T6 aluminum 1 mm thick and surface area A, lying on the lunar surface pointing up. Though not specified in the Zook model, it was assumed a 45° ejecta launch angle and a 45° impact angle.

First, consider the mean number of impacts by particles with mass m for the i^{th} speed bin with speeds between v_i and v_{i+1}:

$$\mu_i = A\Delta t\{F(m, v_i) - F(m, v_{i+1})\} \tag{10-15}$$

where F is the Zook ejecta model flux and m is the ejecta particle mass.

Now the desired mean number of perforations is approximately the mean number of impacts of mass m filtered by the BLE for critical diameter $d_c = B(v, \vartheta)$, where $m = \rho\, \pi/6\, d_c^3$ and ρ is the mass density of the ejecta particles (about 3.1 g/cm^3).

The ballistic limit thickness equation for a single sheet of aluminum is:

For $\varrho_p/\varrho_t < 1.5$

$$t = 9.43 d_c^{\,19/18} BHN^{-0.25} \left(\frac{\varrho_p}{\varrho_t}\right)^{0.5} \left(\frac{V\cos\vartheta}{C_t}\right)^{2/3} \tag{10-16}$$

For $\varrho_p/\varrho_t \geq 1.5$

$$t = 9.43 d_c^{\,19/18} BHN^{-0.25} \left(\frac{\varrho_p}{\varrho_t}\right)^{2/3} \left(\frac{V\cos\vartheta}{C_t}\right)^{2/3} \tag{10-17}$$

where

$$
\begin{aligned}
BHN &= \text{Brinell hardness number} \\
C_t &= \text{speed of sound in the target (km/s)} \\
d_c &= \text{critical projectile diameter (cm)} \\
t &= \text{target thickness (cm)} \\
\varrho_p &= \text{projectile density (g/cm}^3\text{)} \\
\varrho_t &= \text{target density (g/cm}^3\text{)} \\
\vartheta &= \text{impact angle measured from target normal} \\
V &= \text{impact speed (km/s)}
\end{aligned}
\tag{10-18}
$$

This can be solved for the BLE $d_c = B(v, \vartheta)$.

Therefore, the mean number of perforations is approximately:

$$
\begin{aligned}
\mu_i &= A\Delta t\{F(m_i, v_i) - F(m_i, v_{i+1})\} \\
m_i &= \rho \frac{\pi}{6}\left[B\left(v_{avg,i}, \frac{\pi}{4}\right)\right]^3
\end{aligned}
\tag{10-19}
$$

Where m_i is the typical perforating ejecta mass for the speed bin computed with a weighted average impact speed. In what follows, linearly spaced speed bins are used with an average impact speed of:

$$
v_{avg,i} = \frac{v_i + v_{i+1}}{2} \tag{10-20}
$$

And logarithmically spaced speed bins with a log average impact speed of:

$$
v_{avg,i} = 10^{\frac{\log v_i + \log v_{i+1}}{2}} \tag{10-21}
$$

Figure 10.6-3 is a plot of the two sets of results. The x-axis is the number of speed bins used between 0.01 km/s and 1 km/s. The y-axis is the ratio or the result for $1 \le n \le 50$ bins divided by the result for 50 bins, the fully converged answer. The red curve is the plot of the linearly spaced speed bins results and the broken blue curve is the plot of the logarithmically spaced speed bins results.

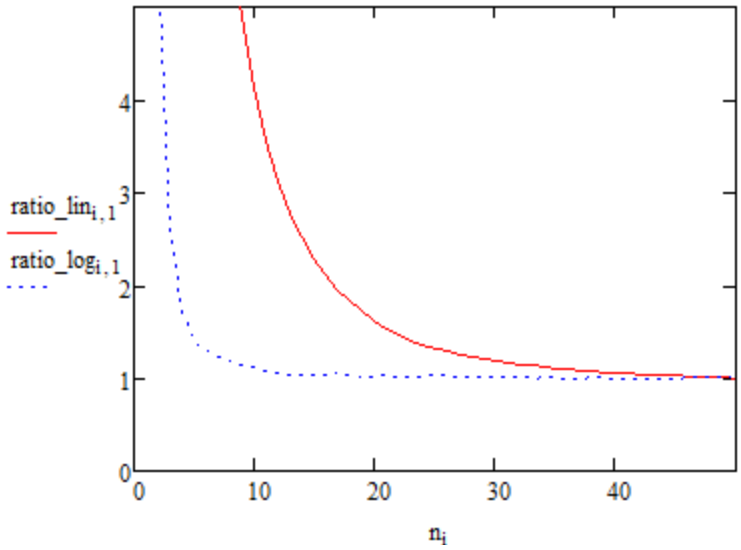

Figure 10.6-3. Ratio of Convergence (μ_n/μ_{50}) as a Function of Speed Bin Spacing and Number of Speed Bins

The following is concluded from Figure 10.6-3 for the MeMoSeE model:

1. Uses logarithmically spaced speed bins, thus the Bumper number of penetrations calculations will converge faster than if MeMoSeE used linearly spaced speed bins.
2. Uses three speed bins and their results are a factor of 1.43 overestimate of the penetration risk, hence the Bumper penetration risk estimates using MeMoSeE will lead to conservative spacecraft designs.

Table 10.6-1 lists the number of bins required for better than a factor of 1.43 convergence.

Table 10.6-1. Ratio of Convergence as a Function of Speed Bin Spacing and Number of Speed Bins

Ratio of convergence, μ_n/μ_{50}	Number of linearly spaced speed bins	Number of logarithmically spaced speed bins
1.10	36	8
1.05	42	11
1.01	48	39

Finding 26: The MeMoSeE model use of three ejecta velocity bins overestimates penetration risk by a factor of 1.4. Three bins are conservative and therefore are suitable for an engineering model.

11.0 MeMoSeE Software Review

Source code for the MeMoSeE model was provided to the NESC assessment team in January 2021. The last revision to the source was time-stamped August 5, 2020. The team was unable to find a version number in the source or the output to further identify the software under review.

11.1 Software Issues

The NESC assessment team conducted a review of the MeMoSeE source code and identified a number of issues, which will be summarized in the following sections.

11.1.1 MeMoSeE Intel c++ Compiler Error

The MeMoSeE software does not compile with the Intel c++ compiler.

The Intel c++ compiler threw a compilation error on a typo. A `cout` statement in `ImpactSites_and_ROI::getDbeta` in the file *lunarEjecta_SecondaryFluxData.cpp*

```
double ImpactSites_and_ROI::getDbeta(double D0, double D1) // D's in units of circumference (2*Pi*rm)
{
        double D = (D0 + D1) / 2.; // units of circ (2pi*rm)
        // use
https://en.wikipedia.org/wiki/Spherical_trigonometry#Napier's_rules_for_right_spherical_triangles
        cout "getDbeta: = " << atan2(tan(ROI_radius/radius), sin(2.*PI*D + ROI_radius/radius)) / DtoR <<
endl;
        return atan2(tan(ROI_radius/radius), sin(2.*PI*D + ROI_radius/radius));

}
```

should have a `<<` operator between the `cout` and the string "`getDbeta = "`.

This indicates that the operating code was edited without testing before distribution to the NESC assessment team.

Finding 27: The MeMoSeE software does not compile with the Intel c++ compiler.

11.1.2 MeMoSeE Array Out of Bounds Error

The MeMoSeE software does not run when compiled debug with intel c++ compiler due to an array out of bounds error.

The MeMoSeE software throws an array out of bounds runtime error when compiled debug using the Intel c++ compiler. The release executable compiles with less error checking and runs to completion. Accessing arrays out of bounds can lead to unexpected results.

The error occurs in `lunarEjecta_FractalIntegration::h_evalLevel_reduce` in the file *lunarEjecta_FractalIntegration.cpp*. The problem is that `h_renormReduce` is trying to access `reducedSum[-1]` when `levelCur=0`. Print statements were added to the release executable and checked the values of `reducedSum[-1]` for about 30 seconds of output. The variable `reducedSum[-1]` was zero except for when it was not a number (NaN). NaNs are problematic so logic was added to bypass the out of bounds array call. The original call:

```
        // renormalize and reduce previous levels
            reducedSum[levelCur] += h_renormReduce(levelCur - 1, dx, dy);}
```

was changed to:

```
        // renormalize and reduce previous levels
        // mdb fix: added the if statement to preclude the out of bounds error.
        if (levelCur > 0)
        {
                reducedSum[levelCur] += h_renormReduce(levelCur - 1, dx, dy);}
        else
        {
        /* Don't increment reducedSum when levelCur=0 because h_renormReduce is out of
   bounds.*/
                reducedSum[0] = reducedSum[0];

        }
```

The debug executable now runs to completion.

Finding 28: The MeMoSeE software has an array out of bound error. It would not run when compiled in debug mode with the Intel c++ compiler after fixing the compilation error. Modification of the source code is required before the executable will run.

11.1.3 Number of Ejecta Particles Per Unit Ejecta Mass

After reading the MEM igloo files and before reading the NEO igloo files, the MeMoSeE software writes the following to screen:

```
Output type = MassLimitedIglooIntegratedFlux
```

This indicates that the output igloo files are not in a format that the Bumper MMOD impact-risk analysis tool can use. The MeMoSeE software outputs a mass flux while Bumper requires a number flux.

To convert the mass flux to a number flux, the number of ejecta particles per unit mass are required.

To solve for the number of particles per unit mass, the following equation, equivalent to Eq. 2.9 in reference 21, is required:

$$N_{ej}(d) = \int_d^{\infty} \frac{1}{m(x)} P_{Moon}(x)\, dx \qquad (11\text{-}1)$$

where Eq. 2.8 in reference 21 defines P_{Moon}. The differential $P_{Moon}dx$ is the fraction of a unit mass of ejecta that has diameters in the range x to $x + dx$. To determine the number of particles with diameters in the range x to $x + dx$, divide the fraction by the ejecta particle mass $m(x)$. The function $m(x)$ has the units of mass in kilograms for ejecta particles with diameters x in units of millimeters. Performing the integration from the diameter of a 1-microgram ejecta particle gives 7.387×10^7 ejecta particles per kg of ejecta composed of ejecta particles with 3,100 kg/m^3 mass density. However, dividing the DSNE Table 3.4.8.3-2 in reference 1 by the MeMoSeE output in the file NESCtest_secondaryEjecta.txt created the by example submitted to the NESC assessment team for review gives approximately 3.5×10^7 ejecta particles per kilogram of ejecta, indicating the analyst created the DSNE table with a different function for P_{Moon}.

The MEMoSeE analyst presented a third function during the February 24th teleconference, which integrated to 3.14×10^7 ejecta particles per kg of ejecta.

Finding 29: The MeMoSeE software does not provide the number flux required by the Bumper MMOD risk tool. One must multiply the MeMoSeE result by the number of ejecta particles per unit mass to convert the reported mass flux to a number flux.

Recommendation 23: In order for Bumper (and the DSNE) to use the MeMoSeE output, a preferred method of converting the MeMoSeE output to the number of ejecta particles per unit mass should be provided and documented in the algorithm document reference 21.

11.1.4 The Exponent of Alternate Zenith Angle Distribution

Equation 2.29 in reference 21 defines the alternate distribution zenith angle function as:

$$F(\alpha) = (1 - \cos\alpha)^{1/a} \cos^a \alpha$$

Equation 2.30 in reference 21 defines the exponent a as:

$$a^2 = \frac{\cos \alpha_{max}}{2\sin^2(\alpha_{max}/2)}$$

A review of the MEMoSeE source code showed that the exponent a occurs at two locations in the code as the function `a_power`. According to the source comments in the function `a_power` the developer first entered the function `a_power` as a^2 and later corrected it to a. However, the correction was made at one location and not both. The source snippets below illustrate the error.

`lunarEjecta_Assembly` template class in *lunarEjecta_Assembly.h*

```
	// a = cos(a_max) / (1 - cos(amax)), converted to half sin to avoid subtraction of
possible close #'s
	double a_power(double impactZenith, double x) {
		double alpha_max = HH_zenithGeneral(impactZenith, x); // in units of
radians
		return sqrt(cos(alpha_max)/2.) / sin(alpha_max / 2.);
		//return cos(alpha_max) / (2. * sqr(sin(alpha_max / 2.))); // forgot the
sqrt...
	}
```

and

`lunarEjecta_FractalIntegration` class in file *lunarEjecta_FractalIntegration.cpp*.

```
// a = cos(a_max) / (1 - cos(amax)), converted to half sin to avoid subtraction of
possible close #'s
// x = \beta - \beta_i
double lunarEjecta_FractalIntegration::a_power(double impactZenith, double x) {
	double alpha_max = HH_zenithGeneral(impactZenith, x); // in units of radians
	return cos(alpha_max) / (2. * sqr(sin(alpha_max / 2.)));
}
```

When the `a_power` function is corrected in the `lunarEjecta_FractalIntegration` class the DSNE table changes to the values shown in Figure 11.1-1 plotted as the gray curve. The orange curve plots the original values listed in the DSNE.

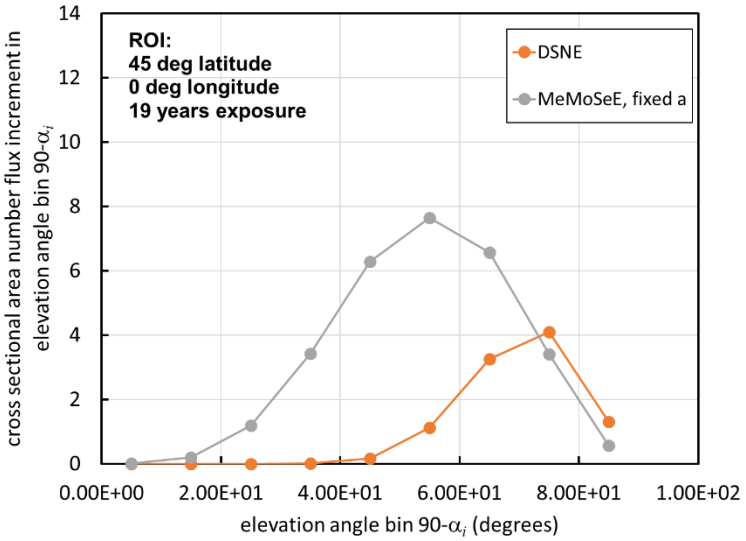

Figure 11.1-1. Effect on DSNE Table from Correcting a_power

Correcting `a_power` has doubled the flux and decreased the elevation angle of the most probable flux from 75° to 55°.

Finding 30: The MeMoSeE software does not implement the alternative zenith angle function Eq. 2.29 of reference 21 in the software correctly. The developer implemented the exponent "a" as "a" at one place in the code and as "a squared" at a second place.

11.1.5 Dependence of Ejecta Mass Flux on Regolith Bulk Density

A review of the MeMoSeE code showed that the software uses ejecta particle mass density for the regolith bulk density in the relation for cumulative ejecta mass with speeds larger than v distribution. The screen output confirms this with the listing:

```
Regolith Density Model: DSNE
  lowDensity = 2886.79 kg/m^3
  avgDensity = 3100 kg/m^3
  highDensity = 3129.63 kg/m^3
```

Figure 11.1-2 is from the DSNE and it lists bulk densities in the first three meters of the regolith between 1,500 kg/m^3 and 2,000 kg/m^3.

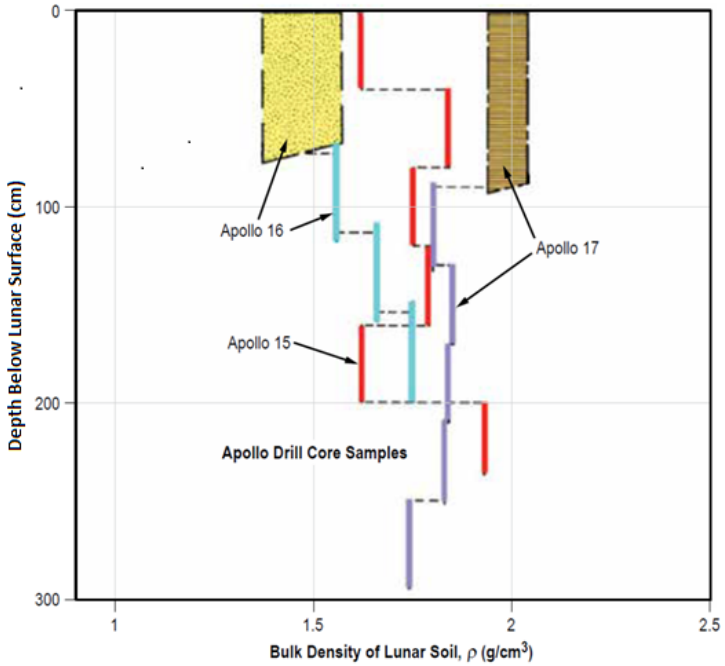

Figure 11.1-2. In Situ Bulk Density of Regolith based on Drill Core Samples from Apollo 15, 16, and 17 Missions
The abrupt increases and decreases result from different layers at different depths (Lunar Sourcebook 1991). DSNE Figure 3.4.2.3.1-1 [ref. 1]

The bulk density of 2,000 kg/m^3 can be calculated from the ejecta particle density using the porosity listed in *lunarEjecta_Regolith.cpp*. The code listing below shows how to calculate the bulk density:

```
double H_compH11RegDensFactor(int lowHighDens){
        double dens = 0.0;
        double porosity = 0.0;
        switch(lowHighDens){
                case 0: // low density regolith
                        dens = RegolithProperties->getlowDensity();
                        break;
                case 1: // high density regolith
```

```
                        dens = RegolithProperties->gethighDensity();
                        break;
                case 2: // average density regolith
                        dens = RegolithProperties->getavgDensity();
                        break;
                default:
                        cerr << "ERROR: H_compH11RegDensFactor invalid density type
selection\n";
        }
        porosity = RegolithProperties->getHH11_porosity();
        return pow(dens*(1.0-porosity), -(3.*RegolithProperties->getHH11_nu()-1.));

}
```

Figure 11.1-3 illustrates the effect on the DSNE table of correcting the regolith bulk density plotted as the blue curve.

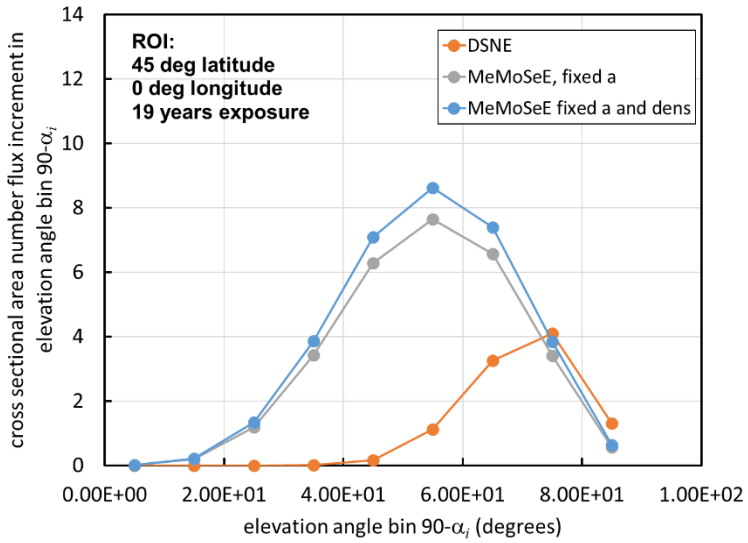

Figure 11.1-3. Effect of Correcting Regolith Bulk Density on DSNE Table

The change increases the flux by ~10% for all elevation angles.

Finding 31: The MeMoSeE software uses the ejecta particle density for the regolith bulk density in the distribution of ejecta mass launched with speeds larger than v (Table 1 in reference 20).

11.1.6 Equation 2.113 for v_{min}

Equation 2.112 and Eq. 2.113 in reference 21 for $x_{min}^2 = (v_{min}/v_{esc})^2$ produce different results yet are nominally equal. The following example for 800-km distance of travel shows the difference.

$r_m := 1737.1 \quad km$

$$x(D) := \left(\tan\left(\frac{D}{2 \cdot r_m}\right)\right)^2 \cdot \left(\csc\left(\frac{D}{2 \cdot r_m}\right) - 1\right) \qquad \text{Eq. 2.112}$$

$$y(D) := \frac{\tan\left(\frac{D}{2 \cdot r_m}\right)}{\tan\left(\frac{\pi}{4} - \frac{D}{4 \cdot r_m}\right)} \qquad \text{Eq. 2.113}$$

Check that Eq. 2.112 produces a different answer from Eq. 2.113.

$x(800) = 0.186$ $\qquad \frac{800}{2 \cdot r_m} = 0.23$

$y(800) = 0.296$

The author could derive Eq. 2.112 from Eq. 2.111, but could not derive Eq. 2.113 from Eq. 2.112, indicating that Eq. 2.113 has a typo. Equation 2.115 for the optimum ejection angle (nominally derived from Eq. 2.113) appears to be correct, though.

These equations are the limits of integration (i.e., the integral is over a non-rectangular region). One such boundary for D=800-km is illustrated below.

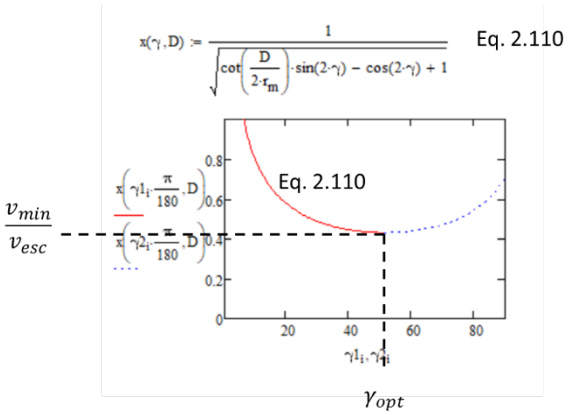

A search of the code did not turn up Eq. 2.113, at least in an easily recognizable form. If Eq. 2.113 is not used in the code, then the MeMoSeE developer should consider deleting the equation from the algorithm document. If it is the code, then the developer will need to replace it with the correct equation.

Finding 32: It is not clear how Equation 2.113 in reference 21 was derived, nor how it is used in the program.

11.1.7 Fractal Integration

The fractal integration generates NaNs. The software developer included debug print statements in the `computeSecondaryFlux()` function in lunarEjecta_Assembly.h. Table 11.1-1 contains the MeMoSeE debug output results. When uncommented, the print statements listed NaNs for some of the results. For example, when i_sitedist=0, k_impactHorzAngle == 9, l_impactAzm == 0, j_siteAzm == 0, D0 = 0.000145, and D1 = 0.001047.

Table 11.1-1. MeMoSeE Debug Output Results

	0	1	2	3	4	5	6	7	8	9	10	11
0	0.00717798	0.00021132	9.47728e-06	0	0	0	0	0	0	0	0	0
1	0.0262453	0	0	0	0	0	0	0	0	0	0	0
2	0.0323964	0	0	0	0	0	0	0	0	0	0	0
3	0.0282051	0	0	0	0	0	0	0	0	0	0	0
4	0.0197941	0	0	0	0	0	0	0	0	0	0	0
5	0.011848	0	0	0	0	0	0	0	0	0	0	0
6	0.00520186	0	0	0	0	0	0	0	0	0	0	0
7	0.00119268	0	0	0	0	0	0	0	0	0	0	0
8	5.34103e-05	-nan(ind)	-nan(ind)	-nan(ind)	-nan(ind)	1.69843e-14	4.39513e-16	0	0	0	0	0

The algorithm needs correction so that it calculates the correct real value. NaNs can propagate throughout the calculation corrupting the results.

Finding 33: The MeMoSeE software fractal integration generates NaN values.

11.1.8 Dependence of Ejecta Mass Flux on Launch Speed

A sensitivity test varying the MeMoSeE input parameters revealed unexpected results from changing the parameter SecvMin in the input parameters file parameters_lat45_NESCtest.txt. Figure 11.1-4 cross plots the results of two calculations: one with SecvMin = 100 m/s, and the other with SecvMin = 30 m/s. The points on the curve are the average speed for the speed bin. There are 12 speed bins, each with linearly spaced bin boundaries between SecvMin and 2.67 km/s.

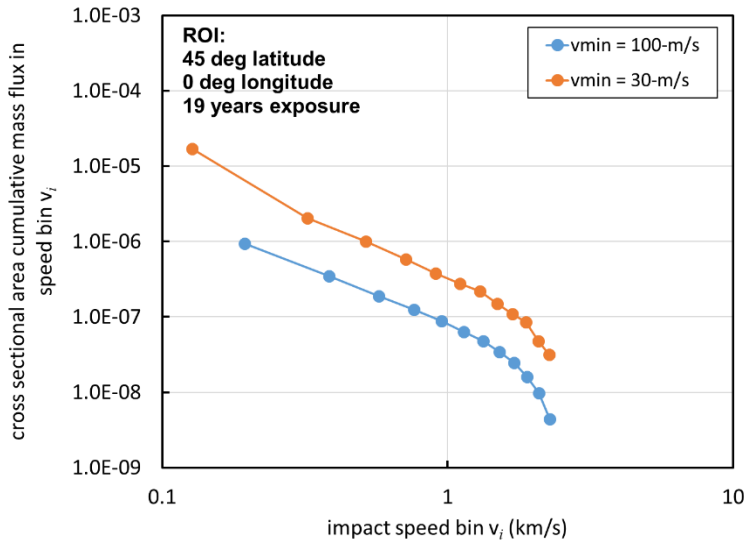

Figure 11.1-4. Cumulative Mass Flux for Launch Speeds Larger than v Calculated for Two Values of SecvMin

The SecvMin = 30-m/s curve should extend the SecvMin = 100-m/s curve to smaller speeds, not shift all flux values to larger values for speeds larger than 100-m/s.

Figure 11.1-5 shows that there are similar issues with the values of mass flux as a function of range in the flux_vs_D.txt file output. Adding flux traveling between 30 m/s and 100 m/s should not add flux beyond the range flux traveling at 100-m/s can travel. A 100-m/s particle can travel no further than 6.1 km hence the flux should be unchanged beyond 6.1 km.

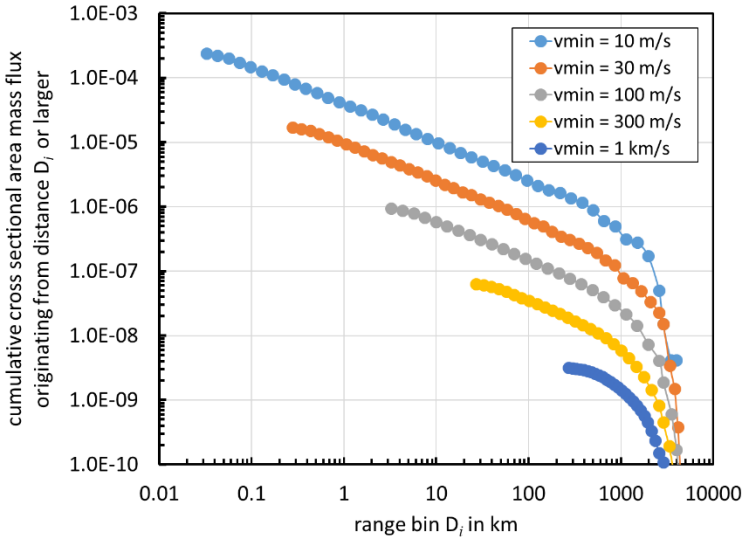

Figure 11.1-5. Cumulative Mass Flux from Ranges Larger than D Calculated for Five Values of SecvMin

This error is crucial and means the software implementation of the MeMoSeE algorithm under review is flawed. It is not clear currently whether this is an issue with the algorithm or the software implementation of the algorithm.

Finding 34: The MeMoSeE software does not compute the dependence of ejecta mass flux on minimum launch speed correctly. It is not clear whether this is an issue with the algorithm or the software implementation of the algorithm. This is a crucial error and the reviewed version of MeMoSeE should not be used for HLS design.

11.1.9 MeMoSeE Defaults to Runtime Initialization Value of Zero

The MeMoSeE software never sets the sporadic-meteoroid impact angle variable to the value of the impact angle within the scope of the integration. Therefore, it defaults to the runtime initialization value of zero.

The integration occurs when the function evalBins calls the function evalIntegral. The parameter definitions and the variable initialization for both functions are:

```
void lunarEjecta_AdaptiveMesh::evalBins(double D0,
                                        double D1,
                                        double new_x_azm, // = beta - beta_i, units of
rads
                                        double new_Dbeta, // units of rads
                                        double new_mu,
                                        double new_imp_zenith,
                                        double new_excZone)
{
       int i, j;

       double xMin, xMax, yMin, yMax;

              x_azm = fmod(new_x_azm + 2.*PI, 2.*PI); // force in 0 to 2PI
              Dbeta = new_Dbeta;
              mu = new_mu;
              excZone = new_excZone;
```

```
double lunarEjecta_FractalIntegration::evalIntegral(double new_x_azm,
                                                    double new_Dbeta,
                                                    double new_mu,
                                                    double new_imp_zenith,
                                                    double new_excZone)
{
	double curError = 10.*epsError;

	x_azm = new_x_azm;
	Dbeta = new_Dbeta;
	mu = new_mu;
	imp_zenith = new_imp_zenith;
	excZone = new_excZone;
```

If the global scope variable imp_zenith is not defined before the call to evalIntegral, which uses the parameter imp_zenith in the evalIntegral parameter list, then the functions called by evalIntegral only have the runtime initialization value for imp_zenith that is zero.

The function evalIntegral only calculates with the parameter imp_zenith in the functions HH_AzmDist and a_power.

To get imp_zenith passed to HH_AzmDist and a_power as a global variable, then the following statement must be added to evalBins before the call to evalIntegral:

```
	imp_zenith = new_imp_zenith;
```

Finding 35: The MeMoSeE software never sets the sporadic-meteoroid impact angle variable to the impact angle within the scope of the integration, which defaults to the runtime initialization value of zero.

Recommendation 24: Correct the software issues identified in the Findings before the reviewed version can be used for DSNE updates.

11.1.10 MeMoSeE Calculations of the MEM Elevation Angles Do Not Agree with the Values in the MEM 3 Igloo File

MeMoSeE calculates the sporadic meteoroid approach direction elevation angle in the template class `lunarEjecta_Assembly` with the method `computeSecondaryFlux()` in the file *lunarEjecta_Assembly.h*. The code used to calculate the elevation angle is

```
	for (k_impactHorzAngle = 0; k_impactHorzAngle < Nk; ++k_impactHorzAngle)
	{
		impactHorzAngle = PI/2. * k_impactHorzAngle / double(Nk-1.);
```

Table 11.1-2 compares the approach-direction elevation angle listed in the MEM 3 igloo file with the valued computed by the modified code, which results in difference values.

Table 11.1-2. Comparison of Approach-Direction Elevation Angles

Elevation angle in MEM 3 igloo file	Elevation angle computed by MeMoSeE
86.4650	90.000
82.0966	84.706
77.2564	79.412
72.3279	74.118
67.3687	68.824
62.3954	63.529
57.4145	58.235
52.4290	52.941
47.4405	47.647
42.4500	42.353
37.4582	37.059
32.4653	31.765
27.4716	26.471
22.4774	21.176
17.4828	15.882
12.4879	10.588
7.4928	5.2941
2.4976	0

There is no reason to use different values. The formula used by MEM 3 to calculate the bin average elevation angle is:

$$\sin \varphi_{avg} = \frac{1}{2}(\sin \varphi_1 + \sin \varphi_2) \qquad (11\text{-}2)$$

The revised MeMoSeE code is:

```
for (k_impactHorzAngle = 0; k_impactHorzAngle < Nk; ++k_impactHorzAngle)
{
        //impactHorzAngle = PI/2. * k_impactHorzAngle / double(Nk-1);
        phi1 = PI / 2. * double(k_impactHorzAngle) / double(Nk);
        phi2 = PI / 2. * double(k_impactHorzAngle + 1) / double(Nk);
        impactHorzAngle = asin(0.5*(sin(phi1) + sin(phi2)));
```

Finding 36: When MeMoSeE calculates the values for the sporadic meteoroid approach direction elevation angle, it does not get the same values as the MEM 3 igloo file.

Recommendation 25: Use the MEM 3 algorithm for averaging elevation angles.

11.1.11 Software Verification-Test Results

The NESC assessment team was not able to locate any software verification test results for review. MeMoSeE is class D software per NPR 7150.2C, which requires the software project to have test plans, procedures and verification test results documents.

Observation 5: The NESC assessment team was unable to locate any software verification-test results.

11.1.12 Sensitivity Test Results

The NESC assessment team was unable to locate results from tests of the sensitivity of the flux to the algorithm and its inputs. In particular, the review team was interested in sensitivity test results for

- Variations in the alternative zenith angle function parameters and form
- Convergence with number of MEM igloo flux files

- Variation in results resulting from time integrations typical of sortie missions and not lunar base missions

Sensitivity tests of the zenith angle function developed for and unique to MeMoSeE are especially desirable due to the number of alternative functions developed by the planetary science community during the past sixty years.

Observation 6: The NESC assessment team was unable to locate any software sensitivity-test results.

11.1.13 Software Documentation

NPR 7150.2C outlines a waterfall development plan for NASA class D software. A minimum set of documents for a small software project like MeMoSeE is

- A software design document – composed of the user and software requirements and a listing of the software components and their required function.
- The source – and a software user manual.
- The software verification document – composed of the plan, procedures, and test results.
- The software configuration management document – composed of the plan for operations, maintenance, and retirement. The maintenance plan needs to include the requirements for version control and change board to approve changes to the version of the code used to produce the DSNE tables.

The NESC assessment team was provided for review an MeMoSeE algorithm document [ref. 21] (the business logic), the source, and a user manual. Typically, the developer uses the business logic to develop the requirements and the design. Section 2.2 of reference 21 contains a start at the development of the design from the business logic. However, while Section 2.2 provides the order in which MeMoSeE will loop through the parameters, it does not list the section of reference 21 that is executed in each loop.

Observation 7: The MeMoSeE algorithm document [ref. 21] Section 2.2 is a list of seven loops with no work done in any but the first loop.

At the minimum, a traceability matrix between the section of reference 21 and the source procedure will aid maintenance of the code. A reference to the applicable 2eference 21 section could even be included in the source comments for each procedure.

Further review of the algorithm document [ref. 21] did not find any equation for the computation of the ejecta mass flux at the region of interest (ROI) from the ejecta mass flux increment launched from the site of the sporadic meteoroid or NEO impact site. A review of the source found the following code in `void computeSecondaryFlux()` of lunarEjecta_Assembly.h, which appears to be the calculation of the flux increment at the ROI.

```
// at this point, we can get specific MEM fluxes for high and low densities, and NEO's
// units of (kg/m^2/yr)
MEM_massfluxLo = MEM_normLo * siteSA / ImpactSitesROILoc->getROI_SA() * MEMLatDataLo-
>getFlux_atAngleVelLat(impactHorzAngle/DtoR, impactAzm/DtoR, impactSpeed, siteLat);
MEM_massfluxHi = MEM_normHi * siteSA / ImpactSitesROILoc->getROI_SA() * MEMLatDataHi-
>getFlux_atAngleVelLat(impactHorzAngle/DtoR, impactAzm/DtoR, impactSpeed, siteLat);
```

```
NEO_massflux   = NEO_norm   * siteSA / ImpactSitesROILoc->getROI_SA() * NEOLatData-
>getMassFluxNEO_atAngleVelLat(impactHorzAngle/DtoR, impactAzm/DtoR, impactSpeed,
siteLat);
```

Where the surface area ROI_SA the launched flux increment lands on is defined in `ImpactSites_and_ROI::ImpactSites_and_ROI` of lunarEjecta_SecondaryFluxData.cpp as

```
// compute ROI surface area
ROI_radius = 2. *  radius * sin(Dmin/2.); // 0.5*d_lat/2.0
ROI_SA = PI * sqr(ROI_radius);

SA_check += ROI_SA;//2.*ROI_SA;

// cout << " ROI radius = " << ROI_radius << " m" << endl;
// cout << " ROI SA = " << ROI_SA << " m^2" << endl;
cout << " Total surface area = " << SA_check << " m^2" << endl;
```

None of these formulae appear in reference 21.

Observation 8: The MeMoSeE algorithm document is missing the formula for the computation of the ejecta mass flux from the ejecta mass increment for a single impact.

All of these flux increments are summed over the loops listed in Section 2.2 of reference 21 in procedure `computeSecondaryFlux()` of lunarEjecta_Assembly.h to obtain the total flux at the ROI. Again, this formula does not appear in the algorithm document [ref. 21], though Section 2.2 of reference 21 appears to be a start.

Observation 9: The MeMoSeE algorithm document is missing the formula for the computation of the ejecta mass flux from the sporadic mass flux.

12.0 Findings, Observations, and NESC Recommendations

12.1 Findings

The following findings were identified by the assessment team during the course of this study:

F-1. The DSNE tables provide the information necessary for Bumper micrometeoroid and orbital debris (MMOD) risk assessments.

F-2. The NEO flux appears to be implemented incorrectly in the MeMoSeE model (e.g., a meteoroid flux that is partially shielded by the Moon is rescaled using a NEO flux that contains no such shielding).

F-3. It is not clear that the 10-gram boundary between the cometary and asteroid populations used in MeMoSeE is an appropriate boundary. Observations and research indicate that the transition occurs at masses between 2 and 4 orders of magnitudes larger (1 to 100 kilograms).

F-4. The MeMoSeE model's assumed NEO impact angles of incidence with respect to the Moon's surface resemble the MEM high-density population but should more closely resemble the low-density meteoroid population in MEM.

F-5. The MeMoSeE model adequately accounts for the LADEE ejecta particle size distribution measured from lunar orbit.

F-6. The MeMoSeE model and the LADEE data are both consistent with a lunar impact ejecta yield of ~10.

F-7. The MeMoSeE model ejecta angular distribution does not reproduce LADEE measurements.

F-8. The MeMoSeE model's ejecta speed distribution shape differs from the exponential distribution determined from LADEE observations.

F-9. The LADEE data are more consistent with the Housen and Holsapple [ref. 20] formula over the Koschny and Grun [ref. 22] formula. This provides confidence in the modeling approach adopted for MeMoSeE.

F-10. The MeMoSeE model focuses on particles ejected during the impact excavation phase and does not account for jetted material expelled at low angles to the target's surface and high velocities during the contact/compression phase.

F-11. The lunar resurfacing rate of ~80,000 years modeled with MeMoSeE is comparable with statistics derived from LROC NAC temporal observations.

F-12. The LROC temporal image pairs (before/after observations) reveal secondary surface disturbances that are significantly larger (i.e., 1 m to 30 m in diameter) than the secondary impacts modeled in MeMoSeE (<0.01 m).

F-13. Monte Carlo techniques have been used to compute fluxes for reference cases that can be compared with the MeMoSeE algorithm for consistency.

F-14. The flux of ascending ejecta (i.e., striking the asset "from below") is not included in the MeMoSeE model.

F-15. The detailed effect of the ascending component of the ejecta on an asset is dependent on the detailed shape and size of that asset.

F-16. Ascending ejecta particles from nearby primary impacts can strike an asset with speeds greater than escape velocity, adding to the overall MMOD risk.

F-17. The stochastic nature of the primary impact flux location, combined with the strong dependence of the flux on distance from the asset, means that for any finite length of time, the number of secondaries impacting an asset may vary by several orders of magnitude from the average value.

F-18. The ejecta flux can be non-uniform over different geographical regions of the Moon and at different times. Temporal variations are typically factors of 2, and variations with latitude/longitude are typically factors of 5, but closer to factors of 2 when averaged over local time. However, these variations are still orders of magnitude smaller than stochastic variations.

F-19. The MeMoSeE model may be overconservative in computing the quantity/mass of ejecta produced by including large NEO sizes that rarely impact the Moon.

F-20. The MeMoSeE model may produce estimates of the hazardous ejecta flux that are a factor of 3 to 4 too high because it assumes the mass of the largest particle ejected by an impact can exceed the total ejected mass predicted in reference 20.

F-21. The consideration of a single meteor shower, no matter how intense, is not sufficient to dismiss the contributions of meteor showers to ejecta production.

F-22. The MeMoSeE model uses a soil size distribution characteristic of a single submature soil.

F-23. A worst-case regolith particle size distribution can result in an ejecta flux that is 1.6 to 2.6 times larger (at the sizes of most interest to HLS) than the MeMoSeE flux calculated with the average regolith particle size distribution.

F-24. Ejecta mass scaling used by MeMoSeE for impacts by NEOs 1 m to 1 km in diameter uses soil as the target material, but basalt is more appropriate because the impactor will push through the soil layer and contact the bedrock layer below.

F-25. Multi-walled shields are optimized for protection against fast meteoroids, but may provide minimal enhanced protection against slow, high-density ejecta over single-walled shields. Switching from single-wall to multi-wall shield designs will decrease the sporadic (and therefore the total) risk, but will not necessarily reduce the ejecta risk. Therefore, some of the proposed multi-wall shielding designs for HLS have a significant fraction of their risk contribution from ejecta.

F-26. The MeMoSeE model use of three ejecta velocity bins overestimates penetration risk by a factor of 1.4. Three bins are conservative and therefore are suitable for an engineering model.

F-27. The MeMoSeE software does not compile with the Intel c++ compiler.

F-28. The MeMoSeE software has an array out of bound error. It would not run when compiled in debug mode with the Intel c++ compiler after fixing the compilation error. Modification of the source code is required before the executable will run.

F-29. The MeMoSeE software does not provide the number flux required by the Bumper MMOD risk tool. One must multiply the MeMoSeE result by the number of ejecta particles per unit mass to convert the reported mass flux to a number flux.

F-30. The MeMoSeE software does not implement the alternative zenith angle function Eq. 2.29 of reference 21 in the software correctly. The developer implemented the exponent “a” as “a” at one place in the code and as “a squared” at a second place.

F-31. The MeMoSeE software uses the ejecta particle density for the regolith bulk density in the distribution of ejecta mass launched with speeds larger than v (Table 1 in reference 20).

F-32. It is not clear how Equation 2.113 in reference 21 was derived, nor how it is used in the program.

F-33. The MeMoSeE software fractal integration generates NaN values.

F-34. The MeMoSeE software does not compute the dependence of ejecta mass flux on minimum launch speed correctly. It is not clear whether this is an issue with the algorithm or the software implementation of the algorithm. This is a crucial error and the reviewed version of MeMoSeE should not be used for HLS design.

F-35. The MeMoSeE software never sets the sporadic-meteoroid impact angle variable to the impact angle within the scope of the integration, which defaults to the runtime initialization value of zero.

F-36. When MeMoSeE calculates the values for the sporadic meteoroid approach direction elevation angle, it does not get the same values as the MEM 3 igloo file.

12.2 Observations

O-1. The radius of the Moon used in MeMoSeE when calculating the escape velocity is 1737.1 km versus the traditionally accepted mean lunar radius of 1737.4 km.

O-2. The model name "Meteoroid Model of Secondary Ejecta" does not accurately and unambiguously describe the environment modeled and the acronym (MeMoSeE, pronounced "mimosa") is difficult to type and unclear how to pronounce.

O-3. The documentation uses the term "secondary ejecta." This term can be ambiguous, as it can be confused with other phenomena on the Moon.

O-4. The NEO input population is not modeled to the same level of detail as the meteoroid population and is instead a global average.

O-5. The NESC assessment team was unable to locate any software verification-test results.

O-6. The NESC assessment team was unable to locate any software sensitivity-test results.

O-7. The MeMoSeE algorithm document [ref. 21] Section 2.2 is a list of seven loops with no work done in any but the first loop.

O-8. The MeMoSeE algorithm document is missing the formula for the computation of the ejecta mass flux from the ejecta mass increment for a single impact.

O-9. The MeMoSeE algorithm document is missing the formula for the computation of the ejecta mass flux from the sporadic mass flux.

12.3 NESC Recommendations

The following NESC Recommendations are directed to the developer of the MeMoSeE model:

R-1. Use 1737.4 km for the geometrically averaged lunar radius. ***(O-1)***

R-2. Consider changing the model name and acronym to those that emphasize accuracy and ease of use (e.g., Lunar Ejecta Engineering Model (LEEM)). ***(O-2)***

R-3. Use the terms "secondaries," "secondary environment," or "ejecta" in place of "secondary ejecta." ***(O-3)***

R-4. Calculate the meteoroid-to-NEO flux scaling using the meteoroid flux on a flat plate sitting on the lunar surface and facing local zenith as compared to the NEO flux onto the lunar surface per unit surface area. ***(F-2)***

R-5. Developer should work with experts from NASA's Meteoroid Environment Office to identify an appropriate mass boundary between the cometary and asteroidal populations. ***(F-3)***

R-6. The NEO angular distribution should be corrected by extracting impact angles from an appropriate dynamical model of asteroids and comets.***(F-4)***

R-7. The presence of ejecta detected at altitudes above the lunar surface suggests that it might be appropriate to consider extending MeMoSeE to also cover objects in low lunar orbit and provide an appropriate altitude limit where the model is applicable. ***(F-5)***

R-8. Include LADEE ejecta angular distributions inferred from plume measurements into the MeMoSeE model. ***(F-7)***

R-9. Incorporate LADEE ejecta speed distributions into the MeMoSeE model and compare with current speed distribution assumptions. ***(F-8)***

R-10. Incorporate jetted material expelled during the impact contact/compression phase into the MeMoSeE model. ***(F-10)***

R-11. Consider modifying the MeMoSeE model to account for the clustering of secondary particles impacting the surface. ***(F-12)***

R-12. Use the Monte Carlo flux calculation results provided to verify MeMoSeE flux calculations. ***(F-13)***

R-13. Include ascending ejecta flux in the MeMoSeE model. ***(F-14, F-15)***

R-14. Include high-velocity (i.e., ≥ escape velocity) particle flux in the DSNE tables if ascending ejecta are added to the model. ***(F-16)***

R-15. Consider modifying the MeMoSeE model to use Monte Carlo methods in addition to or in lieu of analytic methods to compute the stochastic variability of the flux. ***(F-17)***

R-16. The manner in which the flux results are tabulated and reported in the DSNE should be reconsidered, perhaps to include mean, median, and extreme cases (such as 95% confidence levels for maximum flux) suitable for incorporation into a Probabilistic Risk Assessment. ***(F-17)***

R-17. Reconsider choosing what is the "average" location/time on the Moon vs choosing several example locations for the DSNE (e.g., at different longitudes or use 7-day intervals rather than average 19 years). ***(F-18)***

R-18. Limit the maximum primary impactor size used to compute the ejecta or use a Monte Carlo technique to accurately incorporate large impactor effects. ***(F-19)***

R-19. Consider placing an upper limit on the ejected particle size determined from conservation of energy and/or the ejecta mass. ***(F-20)***

R-20. Developer should work with experts from NASA's Meteoroid Environment Office to reevaluate potential contributions from meteor showers to the ejecta environment. ***(F-21)***

R-21. Perform a sensitivity study varying the soil size distribution parameters over the range of measured soil size distributions of the Apollo Program soil samples. ***(F-22, F-23)***

R-22. Use basalt as the target material for NEO impacts in the 1 m to 1 km diameter range. ***(F-24)***

R-23. In order for Bumper (and the DSNE) to use the MeMoSeE output, a preferred method of converting the MeMoSeE output to the number of ejecta particles per unit mass should be provided and documented in the algorithm document reference 21. ***(F-29)***

R-24. Correct the software issues identified in the Findings before the reviewed version can be used for DSNE updates. ***(F-27, F-28, F-30, F-31, F-32, F-33, F-34, F-35)***

R-25. Use the MEM 3 algorithm for averaging elevation angles. ***(F-36)***

12.4 Potential NESC Constraints

The assessment team identified a set of recommendations as potential NESC constraints including recommendations R-4, R-6, R-13, R-14, R-18, R-23, and R-24. These recommendations should be addressed and implemented in a revised version of MeMoSeE before the lunar ejecta model output is used to update the DSNE lunar ejecta design environments.

13.0 Alternative Viewpoint(s)

There were no alternative viewpoints identified during the course of this assessment by the NESC team or the NRB quorum.

14.0 Other Deliverables

No unique hardware, software, or data packages, outside those contained in this report, were disseminated to other parties outside this assessment.

15.0 Lessons Learned

No lessons learned were identified by this assessment.

16.0 Recommendations for NASA Standards and Specifications

No recommendations for NASA standards and/or specifications were identified as a result of this assessment.

17.0 Definition of Terms

Finding	A relevant factual conclusion and/or issue that is within the assessment scope and that the team has rigorously based on data from their independent analyses, tests, inspections, and/or reviews of technical documentation.
Observation	A noteworthy fact, issue, and/or risk, which may not be directly within the assessment scope, but could generate a separate issue or concern if not addressed. Alternatively, an observation can be a positive acknowledgement of a Center/Program/Project/Organization's operational structure, tools, and/or support provided.
Problem	The subject of the independent technical assessment.
Recommendation	A proposed measurable stakeholder action directly supported by specific Finding(s) and/or Observation(s) that will correct or mitigate an identified issue or risk.

18.0 Acronyms and Nomenclature

ALaMO	Automated Lunar and Meteor Observatory
AM	Ascent Module
ARC	Ames Research Center
au	Astronomical Unit
BLE	Ballistic Limit Equation
CNEOS	Center for Near Earth Object Studies
DHRZ	Distal High Reflectance Zone
DLRZ	Distal Low Reflectance Zone
DM	Descent Module
DRM	Design Reference Mission
DSNE	Design Specification for Natural Environments
ESD	Exploration Systems Development
GSFC	Goddard Space Flight Center
H_2O	Water
He	Gaseous Helium
HLS	Human Landing System
HTC	Halley-type Comet
HVIT	Hypervelocity and Impact Technology group
JFC	Jupiter-family Comet
JSC	Johnson Space Center
LADEE	Lunar Atmosphere Dust and Environment Explorer
LaRC	Langley Research Center
LDEX	Lunar Dust Experiment
LEEM	Lunar Ejecta Engineering Model
LH_2	Liquid Hydrogen
LM	Apollo Lunar Module
LOC	Loss of Crew
LOM	Loss of Mission
LOX	Liquid Oxygen
LRO	Lunar Reconnaissance Orbiter
LROC	Lunar Reconnaissance Orbiter Camera
MEM	Meteoroid Engineering Model
MEM 3	Meteoroid Engineering Model, version 3
MEMR2	Meteoroid Engineering Model, release 2
MeMoSeE	Meteoroid Model of Secondary Ejecta
MMH/NTO	Monomethylhydrazine and Nitrogen Tetroxide
MMOD	Micrometeoroid and Orbital Debris
MSC	Manned Spacecraft Center
MSFC	Marshall Space Flight Center
N_2	Gaseous Nitrogen
NAC	Narrow Angle Camera
NAN	Not a Number
NEA	Near Earth Asteroid
NEO	Near Earth Object
NESC	NASA Engineering and Safety Center
O_2	Gaseous Oxygen
OCC	Oort-cloud Comet
ORDEM	Orbital Debris Engineering Model
PHRZ	Proximal High Reflectance Zone
PLRZ	Proximal Low Reflectance Zone

ROI	Region of Interest
SME	Subject Matter Expert
WAC	Wide-Angle Camera
xEMU	Exploration Extravehicular Mobility Unit

19.0 References

1 Roberts, B.: *Cross-Program Design Specification for Natural Environments (DSNE): Revision G*, SLS-SPEC-159, 2019.

2 Cour-Palais, B. G.: *Meteoroid Environment Model- 1969 [Near Earth to Lunar Surface]*, Technical Report NASA/SP–8013, March 1969.

3 Lunar Source Book. edited by Grant H. Heiken, David T. Vaniman, Bevan M. French, Cambridge University Press, 1991. https://www.lpi.usra.edu/publications/books/lunar_sourcebook/, accessed on May 15, 2021.

4 Szalay et al.: "Dust Phenomena Relating to Airless Bodies," *Space Science Reviews*, 214(5), 1-47, 2018. http://doi.org/10.1007/s11214-018-0527-0

5 Orrok, G. T.: *The meteoroid environment of project Apollo. Technical Report*, NASA/CR–117188, Bellcomm, Inc., January 1963.

6 Morse, M. L.; and Bays, J. K.: *The Apollo Spacecraft: A Chronology*, Technical Report NASA/SP–4009, May 1973.

7 Miller, B.: "NASA studies hazards of lunar impact particles," *Aviation Week and Space Technology*, January 14, 1963, pp. 54-55, 57, 59.

8 Anon.: *MSC Engineering Criterion Bulletin*, Technical Report EC-1, 1963.

9 Gault, D. E.; Shoemaker, E. M.; and Moore, H. J.: *Spray Ejected from the Lunar Surface by Meteoroid Impact*, Technical Report NASA TN D-1767, N April 1963.

10 Whipple, F. L.: "On meteoroids and penetration," *J. Geophys. Res.*, 68(17):4929–4939, 1963.

11 Zook, H. A.: "The Problem of Secondary Ejecta Near the Lunar Surface," *In Transactions of the 1967 National Symposium on Saturn V/Apollo and Beyond, volume I*, pages EN–8. American Astronautical Society, 1967.

12 Moorhead: *NASA Meteoroid Engineering Model (MEM) Version 3*, NASA/TM–2020-220555, 2020.

13 Moorhead et al.: NASA's "Meteoroid Engineering Model 3 and its ability to replicate spacecraft impact rates," *Journal of Spacecraft and Rockets*, 57:1, 160-176, 2020.

14 Brown et al.: "The flux of small near-Earth objects colliding with the Earth," *Nature*, 420:6913, 294-296, 2002.

15 Moorhead: Internal memo: OSMA/MEO/Lunar-001, 2020.

16 Jones, J.; Campbell, M.; and Nikolova, S.: "Modelling of the sporadic meteoroid sources," *Proceedings of the Meteoroids 2001 Conference*, Kiruna, Sweden, 2001.2001, 575, 2001. https://ui.adsabs.harvard.edu/abs/2001ESASP.495..575J

17 Jones, J.: *Meteoroid Engineering Model – Final Report*, SEE/CR-2004-400, NASA Marshall Space Flight Center, 2004.

18 Kikwaya, J.-B.; Campbell-Brown, M.; and Brown, P. G.: "Bulk density of small meteoroids." *Astronomy and Astrophysics*, Vol. 530: p. A113. DOI: 10.1051/0004-6361/201116431, 2011. https://ui.adsabs.harvard.edu/abs/2011A&A...530A.113K.

19 Moorhead et al.: “A Two-Population Sporadic Meteoroid Bulk Density Distribution and Its Implications for Environment Models,” *Monthly Notices of the Royal Astronomical Society*, 472(4), 3833-3841. https://doi.org/10.1093/mnras/stx2175., 2017
20 Housen; and Holsapple: “Ejecta from impact craters,” *Icarus*, 211:1, 856-875, 2011. https://doi.org/10.1016/j.icarus.2010.09.017
21 DeStefano, A. M.: *Lunar Impact Ejecta Benchmark and Models*, NASA EV44. January 27, 2021.
22 Koschny, D.; and Grün, E.: “Impacts into Ice–Silicate Mixtures: Ejecta Mass and Size Distributions.” *Icarus*, Vol. 154(2): p. 402-411, 2001. DOI: https://doi.org/10.1006/icar.2001.6708 https://www.sciencedirect.com/science/article/pii/S0019103501967089.
23 Rival, M., Mandeville, J. Modeling of Ejecta Produced upon Hypervelocity Impacts. *Space Debris* **1,** 45–57 (1999). https://doi.org/10.1023/A:1010021403591.
24 The Moon Factsheet, https://nssdc.gsfc.nasa.gov/planetary/factsheet/moonfact.html
25 Coltheart, M.; and Freeman, R.: “Case alternation impairs word identification.*” Bulletin of the Psychonomic Society*, 1974. Vol. **3**(2): p. 102-104. DOI: 10.3758/bf03333407 https://doi.org/10.3758/BF03333407.
26 Blaauw: The Mass Index and Mass of the Geminid Meteoroid Stream as Determined With Radar, Optical And Lunar Impact Data,” *Planetary and Space Science*, 143, 83-88, 2017. https://doi.org/10.1016/j.pss.2017.04.007
27 Zolensky, M.; Bland, P.; Brown, P. G.; and Halliday, I.: “Flux of Extraterrestrial Materials,” *Meteorites and the Early Solar System II*, pages 869–888, Jan 2006.
28 Hughes, D. W.: “Comets and Asteroids,” *Contemporary Physics*, 35(2):75–93, 1994. doi: 10.1080/0010751940822445
29 Horányi et al.: “A Permanent, Asymmetric Dust Cloud Around the Moon,” *Nature*, 522(7), 324-326, 2015. http://doi.org/10.1038/nature14479.
30 Szalay et al.: “Impact Ejecta and Gardening in the Lunar Polar Regions.” *Journal of Geophysical Research: Planets*, 124(1), 143–154, 2019. http://doi.org/10.1029/2018JE005756
31 Pokorný, P.; Janches, D.; Sarantos, M.; Szalay, J. R.; Horanyi, M.; Nesvorny, D.; and Kuchner, M. J.: “Meteoroids at the Moon: Orbital Properties, Surface Vaporization, and Impact Ejecta Production,” *Journal of Geophysical Research: Planets*, 124(3), 752–778, 2019. http://doi.org/10.1029/2018JE005912
32 Krüger, H.; Krivov, A. V.; Sremčević, M.; and Grün, E.: Impact-Generated Dust Clouds Surrounding the Galilean Moons. *Icarus*, 164(1), 170–187, 2003. http://doi.org/10.1016/S0019-1035(03)00127-1
33 Bernardoni, E. A.; Szalay, J. R.; and Horanyi, M.: “Impact Ejecta Plumes at the Moon.” *Geophysical Research Letters*, 46(2), 534–543, 2019. http://doi.org/10.1029/2018GL079994
34 Szalay; and Horanyi: “Lunar meteoritic gardening rate derived from in situ LADEE/LDEX measurements,” *Geophysical Research Letters*, 43(1), 4893–4898, 2016. http://doi.org/10.1002/2016GL069148
35 Grün et al.: “Collisional Balance of the Meteoritic Complex,” *Icarus*, 62:2, 244-272, 1985. https://doi.org/10.1016/0019-1035(85)90121-6
36 Carrier, D.: *The Four Things You Need to Know About the Geotechnical Properties of Lunar Soil*, Lunar Geotechnical Institute, 2-9, 2005.

37 Suggs et al.: “The Flux of Kilogram-Sized Meteoroids From Lunar Impact Monitoring,” *Icarus*, 238, 23-36, 2014. https://doi.org/10.1016/j.icarus.2014.04.032
38 Robinson, M. S.; Boyd, A. K.; Denevi, B. W.; Lawrence, S. J.; McEwen, A. S.; Moser, D. E.; Povilaitis, R. Z.; Stelling, R. W.; Suggs, R. M.; Thompson, S. D.; and Wagner, R. V.: “New Crater on the Moon and a Swarm of Secondaries,” *Icarus* 252, 229–235, 2015. https://doi.org/10.1016/j.icarus.2015.01.019
39 Speyerer, E. J.; Povilaitis, R. Z.; Robinson, M. S.; Thomas, P. C.; and Wagner, R. V.: “Quantifying crater production and regolith overturn on the Moon with temporal imaging,” *Nature* 538, 215–218, 2016. https://doi.org/10.1038/nature19829
40 Melosh, H. J.: *Impact Cratering: A Geologic Process*,” Oxford University Press, ISBN: 978-0195104639, 1989.
41 Vickery, A. M.: “The Theory of Jetting: Application to the Origin of Tektites,” *Icarus* 105, 441–453, 1993. https://doi.org/10.1006/icar.1993.1140
42 Sugita, S.; and Schultz, P. H.: “Spectroscopic characterization of hypervelocity jetting: Comparison with a standard theory,” *Journal of Geophysical Research: Planets*, 104(E12), 30825-30845, 1999.
43 Wakita, S.; Johnson, B. C.; Denton, C. A.; and Davison, T. M.: “Jetting during oblique impacts of spherical impactors,” *Icarus*, 360, 114365, 2021.
44 Holsapple: “The Scaling of Impact Processes in Planetary Sciences,” *Annual Reviews of Earth and Planetary Sciences*, 21, 333-373, 1993. https://doi.org/10.1146/annurev.ea.21.050193.002001
45 DeStefano: Untitled document (proposed changes to *The Design Specification for Natural Environments*), 2020.
46 Borovička et al.: “Material properties of transition objects 3200 Phaethon and 2003 EH1,” In: *Icy Bodies of the Solar System*, 218-222, 2010. https://doi.org/10.1017/S174392131000178X
47 Moorhead et al.: “Meteor Shower Forecasting in Near-Earth Space,” *Journal of Spacecraft and Rockets*, 56:5, 1531-1545, 2019. https://doi.org/10.2514/1.A34416
48 Szalay et al.: “Activity of the 2013 Geminid Meteoroid Stream at the Moon,” *Monthly Notices of the Royal Astronomical Society*, 474:3, 4225-4231, 2018. https://doi.org/10.1093/mnras/stx3007
49 F. K. Duennebier, Y. Nakamura, G. Latham, and H. J. Dorman. Meteoroid storms detected on the moon. Science, 192:1000, Jun 1976.
50 Wikipedia, *Grain Size*, https://en.wikipedia.org/wiki/Grain_size , accessed on May 15, 2021.
51 Carrier: “Particle Size Distribution of Lunar Soil,” *Journal of Geotechnical and Geoenvironmental Engineering*, 129:10, 956-959, 2003. https://doi.org/10.1061/(ASCE)1090-0241(2003)129:10(956)
52 McKay D. S.; Fruland R. M.; and Heiken G. H.: “Grain Size and Evolution of Lunar Soils,” *Proc. Lunar Sci. Conf. 5th*, pp. 887–906, 1974.
53 Holsapple, K. A.; and Housen, K. R.: “Gravity or Strength? An Interpretation of the Deep Impact Experiment,” paper no. 1068, *Lunar and Planetary Science XXXVII*, 2006.
54 Bench Crater in Plato. http://lroc.sese.asu.edu/posts/446
55 Holsapple, K. A.: *Impact and Explosion Effects*. http://keith.aa.washington.edu/craterdata/scaling/index.htm. accessed on May 15, 2021.

56 Ivanov, B.: “Size-Frequency Distribution Of Asteroids And Impact Craters: Estimates Of Impact Rate,” in: Adushkin V., Nemchinov I. (eds) *Catastrophic Events Caused by Cosmic Objects*, Springer, Dordrecht, 2008. https://doi.org/10.1007/978-1-4020-6452-4_2
57 Zook, H. A.: “The Problem of Secondary Ejecta Near the Lunar Surface,” in *Transactions of the 1967 National Symposium on Saturn V/Apollo and Beyond, volume I*, pages EN–8. American Astronautical Society, 1967.
58 Eardley, C. J.; and Lang, E. A.: *Lunar Module Analysis for Meteoroid Hazard*, TIR 580-S-8034, General Electric Apollo Support Department, 2-Feb-68.
59 Bjorkman, M. D.; and Christiansen, E. L.: *Altair LDAC-2 MM Impact Risk Assessment*, Report JSC-65834. November 19, 2010.
60 Whipple: “Meteorites and Space Travel,” *The Astronomical Journal*, 52, 131, 1947.
61 Moorhead, A. V.; Koehler, H. M.; and Cooke, W. J.: *NASA Meteoroid Engineering Model Release 2.0*, NASA/TM−2015-218214. October 1, 2015.
62 Coronado, A. R., Gibbins, M. N.; Wright, M. A.; and Stern, P. H.: *Space Station Integrated Wall Design and Penetration Damage Control: Users Guide for Design Analysis Code BUMPER*, NASA/CR−179169 and NTIS number N88-10070, July 1987.
63 Cragg, Scott; Price, Greg; and Burke, Laura: Presentation charts (MSFC/EV42), HLS Design Reference Mission, Undated, but circa 9/21/2020.
64 Moorhead, A. V.: “Meteoroid Engineering Model (MEM) 3: NASA’s Newest Meteoroid Model,” *First International Orbital Debris Conference*., Sugarland, TX., Paper no. 6054. December 9, 2019.
65 Bjorkman, M. D.: “An Astronaut’s Risk of Experiencing a Critical Impact from Lunar Ejecta during Lunar EVA,” paper prepared for the *1st International Orbital Debris Conference*, 2019 (Unpublished manuscript).

REPORT DOCUMENTATION PAGE

Form Approved
OMB No. 0704-0188

1. REPORT DATE *(DD-MM-YYYY)*	2. REPORT TYPE	3. DATES COVERED *(From - To)*
01/26/2022	Technical Memorandum	

4. TITLE AND SUBTITLE
Review of the MeMoSeE Lunar Meteoroid Ejecta Model

5a. CONTRACT NUMBER

5b. GRANT NUMBER

5c. PROGRAM ELEMENT NUMBER

6. AUTHOR(S)
Minow, Joseph; Matney, Mark; Bjorkman, Michael; Kendall, Jordan; Moorhead, Althea; Sarantos, Menelaos; Speyerer, Emerson; Squire, Michael; Szalay, Jamey

5d. PROJECT NUMBER

5e. TASK NUMBER

5f. WORK UNIT NUMBER
869021.01.23.01.01

7. PERFORMING ORGANIZATION NAME(S) AND ADDRESS(ES)
NASA Langley Research Center
Hampton, VA 23681-2199

8. PERFORMING ORGANIZATION REPORT NUMBER
NESC-RP-20-01576

9. SPONSORING/MONITORING AGENCY NAME(S) AND ADDRESS(ES)
National Aeronautics and Space Administration
Washington, DC 20546-0001

10. SPONSOR/MONITOR'S ACRONYM(S)
NASA

11. SPONSOR/MONITOR'S REPORT NUMBER(S)
NASA/TM-20220000562

12. DISTRIBUTION/AVAILABILITY STATEMENT
Unclassified - Unlimited
Subject Category Space Transportation and Safety
Availability: NASA STI Program (757) 864-9658

13. SUPPLEMENTARY NOTES

14. ABSTRACT
The NASA Engineering and Safety Center (NESC) Lunar Meteoroid Ejecta Model Review assessment team was tasked with reviewing the proposed lunar ejecta model Meteoroid Model of Secondary Ejecta (MeMoSeE), developed at Marshall Space Flight Center, and to review the model inputs to the SLS-SPEC-159 Cross-Program Design Specification for Natural Environments document to be used by NASA's Exploration Systems Development and Artemis Programs for future lunar surface system design. This report contains the outcome of the NESC assessment.

15. SUBJECT TERMS
Meteoroid Model of Secondary Ejecta; NASA Engineering and Safety Center; Lunar Meteoroid Ejecta Model; Design Specification for Natural Environments

16. SECURITY CLASSIFICATION OF:			17. LIMITATION OF ABSTRACT	18. NUMBER OF PAGES	19a. NAME OF RESPONSIBLE PERSON
a. REPORT	b. ABSTRACT	c. THIS PAGE			STI Help Desk (email: help@sti.nasa.gov)
U	U	U	UU	99	19b. TELEPHONE NUMBER *(Include area code)* (443) 757-5802